POLITECNICO DI TORINO

Collegio di Ingegneria Chimica e dei Materiali

Corso di Laurea Magistrale

in Ingegneria Chimica e dei Processi Sostenibili

Tesi di Laurea Magistrale

Particulate matter analysis from engine outlet in heavy duty vehicles: a study of soot reactivity, morphology and ash-to-soot ratio from the outlet of 6-cylinder and 8-cylinder diesel engines

Relatore

prof. Samir Bensaid

Candidato

Tayisiya Vlasenko

Luglio 2023

Riassunto della Tesi di Laurea Magistrale (Sessione Luglio 2023)
"**Analisi del particolato in uscita dai motori dei veicoli pesanti"**
Candidato: Tayisiya Vlasenko
Relatore: Samir Bensaid

Introduzione e obiettivi

Il principale rischio per la salute ambientale in Europa è l'inquinamento atmosferico e il trasporto stradale rappresenta uno dei principali responsabili [A1] [A2]. Le normative Euro VI stabiliscono attualmente i limiti delle emissioni dei veicoli diesel in Europa [A3]. Risulta tuttavia necessario continuare a perfezionare i sistemi di trattamento dei gas di scarico per raggiungere standard più rigorosi, attesi nel prossimo futuro, e per migliorare la qualità dell'aria nelle città. Nel contesto del settore automobilistico, i motori pesanti contribuiscono in modo significativo alle emissioni e, di conseguenza, all'impatto sulla salute. La combustione all'interno del motore produce emissioni di scarico contenenti diversi prodotti, tra i quali le particelle solide (PM). Il particolato di scarico è definito come un materiale filtrabile che può essere ottenuto dalla diluizione e dal raffreddamento dei gas di scarico. Include una frazione solida ed eventuali liquidi che si condensano sulla superficie della particella durante il raffreddamento. La composizione di base comprende una frazione carboniosa, comunemente nota come fuliggine, una frazione incombustibile etichettata come cenere, una frazione organica volatile (VOF) ed eventuali altre impurità [A4].

Un componente chiave alla riduzione delle emissioni di particolato all'interno dei veicoli pesanti è il filtro antiparticolato diesel (DPF). Il particolato si accumula all'interno del filtro: la fuliggine viene eliminata periodicamente durante il normale uso del veicolo tramite una procedura chiamata rigenerazione, durante la quale l'innalzamento della temperatura permette di ossidare la parte carboniosa. La rigenerazione avviene quando la perdita di pressione generata dal filtro supera una determinata soglia. Le ceneri d'altro canto, in quanto incombustibili, si accumulano nel filtro e possono essere eliminate solo tramite la pulizia del filtro [A5].

Per ottimizzare il DPF e le sue strategie di rigenerazione, è innanzitutto importante comprendere la quantità di cenere generata e le proprietà della fuliggine. Ad esempio, la reattività all'ossidazione della fuliggine durante i diversi modi operativi. In questo campo sono state condotte un'ampia serie di ricerche scientifiche, che hanno evidenziato la necessità di impiegare più modelli per studiare un miglioramento delle prestazioni del DPF. Come primo passo verso lo sviluppo di modelli validi è dunque rilevante comprendere quale tipo di particolato può essere adatto a simulare le emissioni in condizioni stradali reali e il tipo di particolato che il DPF può incontrare in vari punti della mappa del motore. Ed è all'interno di questo contesto che il seguente lavoro di ricerca si posiziona: lo scopo principale è legato ad un dettagliato studio del particolato da diverse angolazioni. I principali punti di investigazione si possono riassumere nelle seguenti domande di ricerca.

1. Qual è il rapporto ceneri/fuliggine nei motori diesel per veicoli pesanti in diverse condizioni operative?
2. La reattività all'ossidazione della fuliggine è simile o diversa per diversi motori e condizioni operative?
3. Quali tecniche sperimentali sono più adatte per caratterizzare le ceneri?
4. In che modo i metodi di raccolta e manipolazione dei campioni influiscono sui risultati finali e qual è il modo migliore per ottenere dati affidabili in termini di reattività ossidativa, rapporto ceneri/fuliggine e composizione delle ceneri?

Apparato sperimentale e metodologia

Per rispondere a tali domande, una vasta gamma di campioni di particolato sono stati collezionati dalle celle motore durante diversi cicli operativi. Il particolato è stato collezionato su una serie di filtri con l'ausilio dell'apparato sperimentale presentato in Figura 1. I campioni di particolato sono stati raccolti su filtri mediante un sistema di diluizione a flusso parziale (PFDS). Ciò significa che una piccola parte del gas di scarico in uscita dal motore è stata convogliata in un tunnel di diluizione dove è stata raffreddata e filtrata. Il filtro in questione ha lo scopo di trattenere il particolato solido per poi essere analizzato. I campioni vengono prelevati prima del sistema di post-trattamento. Caratteristiche come la concentrazione di fuliggine nel flusso di scarico e la concentrazione del numero di particelle sono state valutate rispettivamente con un micro sensore di fuliggine (MSS) e un misuratore di particelle aerodinamiche (APC). Diversi filtri, per via delle loro proprietà intrinseche risultano più adatti a diverse parti della ricerca. Sono stati adoperati filtri in fibra di vetro rivestita di Teflon (Pallflex TX40HI20), in Teflon (Teflo2µm) ed in quarzo (Pallflex Tissuquartz). In addizione, due campioni sono stati collezionati raschiando i depositi accumulati sulle pareti del silenziatore all'uscita del motore, in quanto presenti in quantità più grandi e non risultano contaminati dai filtri di raccolta del particolato. Nella ricerca sono stati utilizzati diversi motori, un sei cilindri Euro V (550 CV) e un otto cilindri Euro VI (650 CV) con sistema di iniezione XPI. È stato analizzato anche un campione di un motore a 5 cilindri (360 CV). I carburanti adoperati erano diesel a bassissimo tenore di zolfo (ULSD). In tutti i motori, il sistema di ricircolo dei gas esausti (EGR), non era attivo. Una descrizione dettagliata di tutti i campioni in raccolti è presentata in Tabella 1.

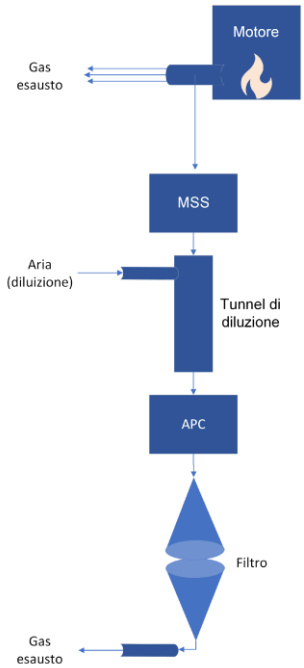

Figura 1: Apparato sperimentale con tunnel di diluizione (PFDS) accoppiato con un micro sensore di fuliggine (MSS), un contatore di particelle aerodinamiche (APC) e un portafiltro contenente il filtro per ogni campionamento

Tabella 1: Dettagliata descrizione dei campioni collezionati con informazioni relative al motore del veicolo, concentrazione in peso di ceneri nell'olio lubrificante e combustibile adoperato, dove B0 identifica un combustibile tradizionale e B7 un combustibile fossile con 7% di biocarburante, nello specifico Esteri metilici di olio di colza (RME)

Nome campione	**Motore (n° cilindri)**	**Lubricant oil (%ceneri)**	**Combusitibile**	**Filtro**	**Descrizione**
"STD"	6	1	B0	Fibra di vetro	Collezionato durante un ciclo di durabilità del motore. Il campione è stato collezionato su due filtri, per ognuno il tempo di raccolta è stato di 3h.
"900 rpm"	6	1	B0	Fibra di vetro	Alternazione di funzionamento a 900 rpm e pieno carico con spegnimenti del motore, ogni pochi secondi.
"1700 rpm"	6	1	B0	Fibra di vetro	Alternazione di funzionamento a 1700 rpm e pieno carico con spegnimenti del motore, ogni pochi secondi.
"2300 rpm"	6	1	B0	Fibra di vetro	Alternazione di funzionamento a 2300 rpm e pieno carico con spegnimenti del motore, ogni pochi secondi.
"Oil consumption"	6	1	B7	Fibra di vetro	Ciclo di analisi del consume di olio lubrificante. Il collezionamento è durato 4h.
"Pipe 5-cylinder"	5	-	-	-	Deposito raschiato dall'ingresso del silenziatore.
"Pipe 8-cylinder"	8	1.9	B7	-	Deposito raschiato dall'ingresso del silenziatore. L'area di interesse è stata pulita in precedenza e il deposito è stato collezionato in seguito a 3 giorni operativi.
"Pressure sweep 1h"	8	1.9	B7	Quarzo	Graduale diminuzione di velocità da 1800 a 860 [rpm] in 1h.
"Pressure sweep 2h"	8	1.9	B7	Quarzo	Graduale diminuzione di velocità da 1800 a 860 [rpm] in 1h. ciclo ripetuto due volte per un campionamento totale di 2h.
"Pressure sweep warm"	8	1.9	B7	Quarzo	Graduale diminuzione di velocità da 1800 a 860 [rpm] in 1h, iniziando il collezionamento con un motore già scaldato.
"Pressure sweep Teflon"	8	1.9	B7	Teflon	Graduale diminuzione di velocità da 1800 a 860 [rpm] in 1h.
"Soot loading"	8	1.9	B7	Quarzo	Test a 1600 [rpm] e 600 [Nm] per 1h.
"Soot regeneration"	8	1.9	B7	Quarzo	Test a 1800 [rpm] e pieno carico. Condizioni simili al funzionamento durante la rigenerazione del DPF.

In seguito, tali campioni sono stati studiati tramite numerose analisi di caratterizzazione come sintetizzato in Figura 2. In particolare, sono state condotte una serie di analisi termogravimetriche (TGA) per lo studio della reattività della fuliggine e per misurare il rapporto tra la parte carbonica e quella di ceneri residua alla fine dell'analisi. Un'altra parte della ricerca si è concentrata sulla riduzione della contaminazione dei campioni da parte dei filtri utilizzati per la raccolta del particolato e sullo sviluppo di una tecnica di estrazione per ridurre tali contaminazioni. Per stimare i parametri cinetici della reattività di ossidazione della fuliggine è stato utilizzato MATLAB.

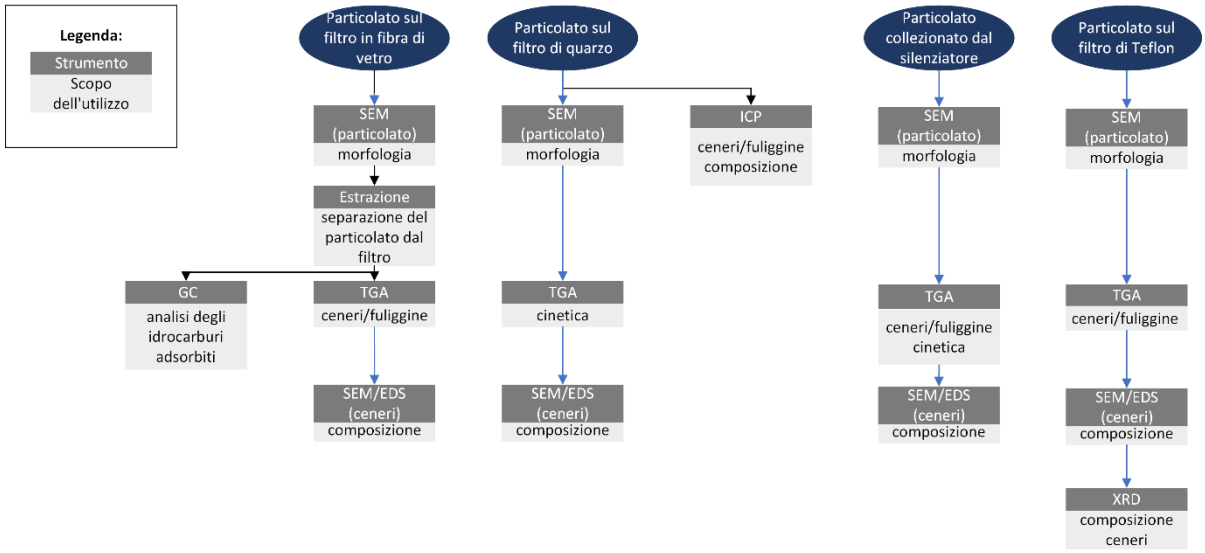

Figura 2: Rappresentazione sintetica delle tecniche di caratterizzazione tra cui spettroscopia a dispersione di energia (EDS), gascromatografia liquida (GC), plasma accoppiato induttivamente (ICP), microscopia elettronica a scansione (SEM), analisi termogravimetrica (TGA) e diffrazione a raggi-X (XRD), utilizzate per diversi campioni in analisi

In dettaglio in Figura 2, le particelle raccolte su filtri in fibra di vetro sono state analizzate al microscopio elettronico a scansione (SEM) per osservarne la morfologia. La quantità rimanente di campione è stata estratta con cicloesano e il solvente è stato analizzato con una gascromatografia liquida (GC). Lo scopo era quello di separare le particelle dal filtro senza contaminare il particolato. Raschiando le particelle direttamente dal filtro, sono emerse visibili contaminazioni da fibre di filtro. Ciò è particolarmente negativo in quanto questi filtri sono rivestiti di Teflon. Il Teflon compromette i risultati dell'analisi termogravimetrica siccome subisce trasformazioni nell'intervallo di temperature di interesse per l'ossidazione della parte carboniosa [A6]. L'estrazione ha mostrato una bassa efficienza, tuttavia, ha permesso di eliminare le contaminazioni da fibre. Le particelle, dopo essere asciugate, sono state caratterizzate con la TGA. Questo strumento consente di riscaldare il campione e di osservare come il campione perde peso in funzione della temperatura. Tale procedura risulta utile sia per studiare la cinetica sia per capire la composizione di un campione, in base alla temperatura a cui evapora. Alla fine della TGA tutta la frazione carboniosa è stata ossidata, quindi il residuo risultava composto solo dalla frazione incombustibile, la cenere. Le ceneri sono state poi analizzate con una spettroscopia a raggi-X a dispersione di energia (EDS) per definirne la composizione.

Una serie di campioni sono invece stati collezionati su filtri di quarzo. Essi, essendo più fragili, risultano inadatti all'osservazione del rapporto tra la quantità di ceneri e di fuliggine. Tuttavia, in quanto resistenti ad alte temperature, tali filtri non impattano i risultati delle analisi termogravimetriche posizionandosi quindi come adatti agli studi cinetici. In questo caso, i campioni sono stati ottenuti creando piccoli dischi di filtro con il particolato sopra ed inserendo due dischi di campione sovrapposti dentro all'apparato sperimentale della TGA, come illustrato in Figura 3.

Un campione è stato raccolto su un filtro di Teflon. Questi filtri sono meno fragili e quindi potrebbero risultare migliori per raschiare il PM da essi. Tuttavia, i risultati hanno mostrato che la contaminazione da parte delle fibre del filtro era presente.

Ulteriori analisi come la diffrazione di raggi-X (XRD) e il plasma accoppiato induttivamente (ICP) sono state impiegate per limitati campioni.

Figura 3: Preparazione dei campioni raccolti su filtri di quarzo per gli studi cinetici tramite TGA

Risultati e discussione

Lo scopo della ricerca risulta in un esame critico del particolato diesel da veicoli pesanti da vari punti di vista. In dettaglio, le emissioni sono state valutate tramite un contatore di particelle aerodinamiche (APC) ed un micro sensore di fuliggine (MSS), fornendo preziose indicazioni sulla correlazione tra le condizioni operative del motore e le emissioni. L'ispezione visiva del particolato è stata condotta con il microscopio elettronico a scansione (SEM) durante tutta la durata del progetto, offrendo l'opportunità di osservare le particelle e formulare varie ipotesi. Inoltre, la reattività della fuliggine è stata studiata calcolando le temperature caratteristiche per il processo di ossidazione e i parametri cinetici. Questi ultimi sono stati ottenuti attraverso un metodo isoconversionale. La composizione delle ceneri, residue dopo la TGA, è stata analizzata integrando ICP, XRD e EDS. La frazione di cenere è stata studiata per un numero limitato di campioni e discussa in relazione alla letteratura esistente. Una tecnica di estrazione è stata sviluppata al fine di separare il particolato dal filtro. L'estrazione ha favorito l'absorbimento di alcuni idrocarburi adsorbiti sulla superficie del particolato verso il solvente di estrazione, il cicloesano. L'analisi gascromatografica del solvente ha mostrato che gli stessi composti idrocarburici, principalmente benzene e alcani (C_{11}-C_{34}), sono stati rilevati dall'estratto di diversi campioni, non evidenziando differenze tra carburante fossile e quello contenente una frazione di Biodiesel (7% RME). Infine, è stata condotta una critica analisi dell'influenza della manipolazione dei campioni sui risultati.

I. Emissioni

I dati relativi ad APC e MSS sono stati raccolti dal sistema "AVL PUMA 2" e analizzati con il software "Concerto". I risultati hanno mostrato che quando il motore funziona in condizioni statiche, le emissioni, in termini sia di concentrazione di fuliggine che di numero di particelle,

risultano approssimativamente costanti. I valori specifici delle emissioni cambiano tra le due condizioni operative a causa del diverso consumo di carburante, della temperatura dei gas di scarico e del carico. I carichi medi e bassi sono correlati a maggiori emissioni di ceneri e fuliggine, mentre le operazioni ad alto carico producono meno emissioni. Inoltre, è possibile osservare che un minore consumo di combustibile è correlato a maggiori emissioni di fuliggine.

Da Tabella 2, si può notare che il motore produce una minore concentrazione di fuliggine durante la rigenerazione del DPF (descritta dal campione "Soot regeneration"), tuttavia, il numero totale di particelle, è più elevato rispetto alle altre due condizioni testate. Probabilmente, a indicazione della presenza di particelle più piccole generate durante tale processo. Questo è dovuto alla generazione di una maggiore quantità di particelle di nucleazione durante le condizioni di rigenerazione, che possono aumentare le particelle emesse di diversi ordini di grandezza [A7] [A8].

Per il campione "pressure sweep" è stato osservato che al variare delle condizioni operative all'interno di un ciclo, le emissioni di particolato variano. Ogni variazione delle condizioni operative, come una diminuzione della velocità, è stata associata a un picco nelle emissioni di fuliggine. La correlazione inversa tra il consumo di carburante e le emissioni di fuliggine non è stata osservata per questo ciclo, probabilmente a causa della graduale diminuzione del carico, generalmente associata a un aumento delle emissioni.

Tabella 2: Emissioni medie di fuliggine e di particelle misurate con l'MSS e l'APC durante la raccolta dei campioni "soot regeneration", "soot loading" e "pressure sweep", correlate alle condizioni operative del motore a 8 cilindri

PARAMETRO	Nome identificativo del campione in analisi		
	"Soot regeneration"	**"Soot loading"**	**"Pressure sweep"**
Coppia [Nm]	2500	600	0 - 3400
Portata di gas di scarico [kg/h]	2500	1500	800-2900
Velocità del motore [rpm]	1800	1800	860 - 1800
Temperatura in uscita dal motore [°C]	490	220	250-460
Consumo di carburante [g/min]	elevata	ridotta	Variabile tra elevata e ridotta
Emissione media di fuliggine [g/h]	2	14.5	1.2
Emissione media di particelle [#/h]	$1.3 \cdot 10^9$	$2.1 \cdot 10^7$	$1.49 \cdot 10^7$

II. Morfologia

Durante l'analisi al microscopio elettronico a scansione (SEM) della fuliggine, è stato arduo identificare le particelle di cenere a causa delle loro ridotte dimensioni e quantità.

Per quanto concerne l'analisi morfologica delle ceneri, si evince che la procedura di estrazione utilizzata su alcuni campioni potrebbe aver influenzato la morfologia delle particelle incombuste. I campioni sottoposti a questa procedura presentavano dimensioni leggermente maggiori, sia in termini di diametro delle singole particelle che di agglomerati. Tra i campioni del motore a 6 cilindri, "STD5" e "oil consumption" hanno presentato particelle con diametri compresi tra 0.5 e 1 µm, mentre i campioni "900rpm", "1700rpm" e "2300rpm" erano rappresentati da particelle con diametri di 0,1-0,5 µm. La variazione potrebbe essere dovuta alla

rapida alternazione tra l'avvio e l'arresto del motore, caratteristico di questi ultimi campioni. Ciò può portare a un aumento della produzione di ceneri e influenzarne le dimensioni.

I campioni del motore a 8 cilindri, raccolti sui filtri al quarzo, hanno mostrato un'ampia variazione nelle dimensioni delle particelle di cenere. Il campione "soot loading" era caratterizzato da una maggiore quantità di ceneri e da particelle più grandi rispetto al campione "soot regeneration". Questo potrebbe essere il risultato della minore pressione di iniezione di combustibile nel motore. Le maggiori emissioni di particolato in generale sono state evidenziate, per questo campione, anche dai risultati dell'APC. Sono state rilevate alcune particelle di composizione metallica, esse sono il risultato della corrosione e dell'abrasione del motore e aumentano la frazione di cenere nei gas di scarico.

III. Cinetica e reattività

Al fine di valutare la reattività della fuliggine, i campioni sono stati caratterizzati con la TGA attraverso il riscaldamento dei campioni secondo il programma presentato in Tabella 3. Tre diverse velocità di riscaldamento sono state utilizzate durante lo step ossidativo, rispettivamente pari a β= 3, 5 e 10 [°C/min]. I risultati sperimentali, coerenti con quelli di altri studi, dimostrano che quando la velocità di riscaldamento aumenta, le curve di perdita di massa si spostano verso temperature più elevate come risultato dell'aumento della velocità di riscaldamento che riduce l'esposizione del campione al ossidante [A9].

Le curve normalizzate di perdita di peso dei campioni in analisi, ottenute con il programma di riscaldamento presentato in Tabella 3 e relativo al solo passaggio di ossidazione con β= 5 [°C/min], sono sintetizzate in Figura 4. I campioni "900rpm", "1700rpm" e "2300rpm" sono stati esclusi da tale analisi per la limitata quantità di campione disponibile. La figura mostra, inoltre, i risultati dell'analisi di un noto carbone sintetico, il Printex-U, utilizzando lo stesso programma di riscaldamento impiegato per gli altri campioni.

Tabella 3: Programma di riscaldamento, composto da 9 fasi, e impiegato durante la TGA per i campioni raccolti sperimentalmente

Passo	Descrizione dell'operazione
1	Atmosfera iniziale: azoto 100 [mL/min]
2	Condizione isoterma per 10 [min] a 50 [°C]
3	Rampa di temperatura con velocità di riscaldamento pari a β=10 [°C/min] partendo da 50 [°C] e arrivando a 400 [°C]
4	Condizioni isoterme per 60 [min] a 400 [°C]
5	Raffreddamento ad una velocità di raffreddamento pari a 10 [°C/min] partendo da 400 [°C] e fino a 50 [°C]
6	Condizioni isoterme per 10 [min] a 50 [°C]
7	Cambio di atmosfera per l'ossidazione: ossigeno 10 [mL/min] e azoto 90 [mL/min]
8	Rampa di temperatura con velocità di riscaldamento pari a β= 3, 5 o 10 [°C/min] partendo da 50 [°C] e arrivando a 800 [°C]
9	Condizioni isoterme per 60 [min] a 800 [°C]

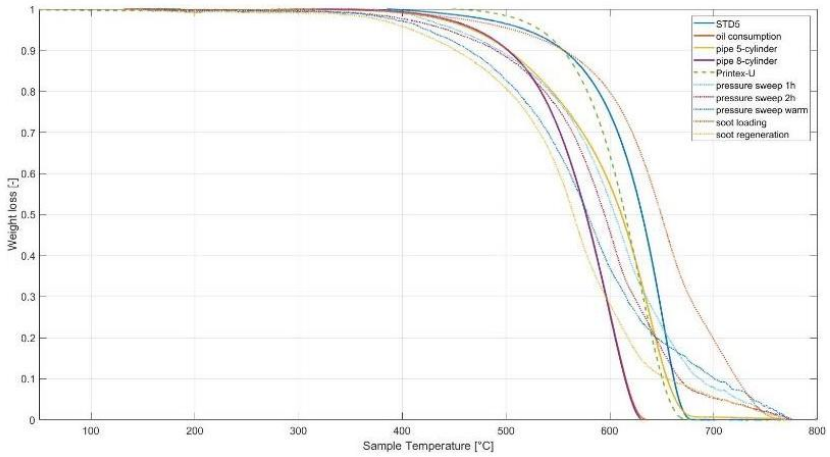

Figura 4: Passo ossidativo normalizzato sul peso in funzione della temperatura [°C] del campione ottenuto durante una rampa di riscaldamento pari a $\beta = 5$ [°C/min], per i campioni in analisi

I risultati in Figura 4 sono difficili da comparare tra di loro, per questa ragione è consueto presentare solo alcune temperature caratteristiche che identificano i principali passi dell'ossidazione. Queste temperature sono la temperatura di ossidazione del 10% di fuliggine (T_{10}), la temperatura alla quale la perdita di massa risulta più rapida ($MLRT_{max}$) e temperatura di ossidazione del 90% di fuliggine (T_{90}). Il paragone tra queste temperature è presentato in Figura 5.

L'impatto che le diverse condizioni operative hanno sulla reattività è osservabile dai valori di $MLRT_{max}$, che varia tra 569 e 652 °C. Questi valori risultano leggermente più alti se confrontati con quelli della letteratura, dove il $MLRT_{max}$ si colloca comunemente tra 440 e 640 °C [A9] [A10] [A11] [A12] [A13]. I valori di T_{10} ricavati sono coerenti con quelli di altri ricercatori, mentre il parametro T_{90} presenta limiti superiori per i campioni raccolti su filtri di quarzo. Ciò potrebbe essere dovuto alla resistenza alla diffusione dell'aria sul campione o alla quantità limitata di PM presente durante le analisi su filtro.

I campioni raccolti dai silenziatori erano attesi a presentare una minore reattività a causa dell'invecchiamento della fuliggine. Tuttavia, le loro temperature caratteristiche mostrano risultati simili rispetto agli altri campioni in analisi. Il campione "Pipe 8-cylinder" ha un $MLRT_{max}$ inferiore rispetto a "Pipe 5-cylinder", il che può essere dovuto al fatto che il motore è stato utilizzato solo per 3 giorni dopo la pulizia dell'ingresso del silenziatore, quindi la fuliggine ha avuto meno tempo per invecchiare. Nonostante questo, una evidente differenza tra campioni collezionati durante il funzionamento del motore e quelli esposti alle condizioni dei gas esausti per un tempo prolungato, non è stata osservata.
Il campione di "soot regeneration" è stato ottenuto in condizioni di pieno carico e il consumo di carburante è stato inferiore rispetto al "soot loading". Il che ha portato a una quantità minore di fuliggine, ma più reattiva.

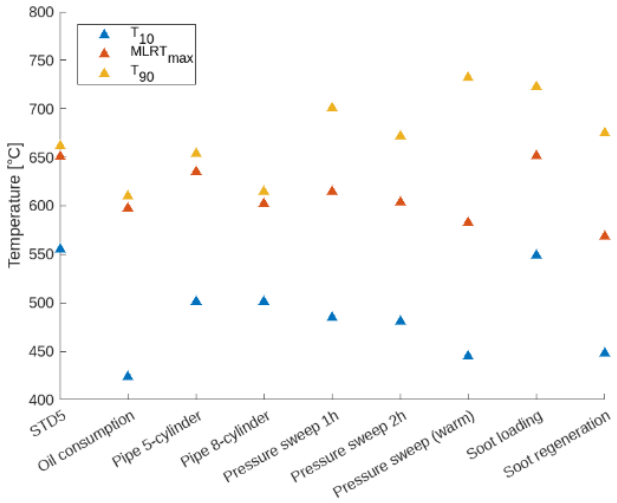

Figura 5: Confronto tra le temperature caratteristiche di ossidazione T_{10}, $MLRT_{max}$ e T_{90} per diversi campioni in analisi, ossidati alla velocità di riscaldamento β=5 [°C/min]

Oltre allo studio delle temperature caratteristiche, la reattività del particolato è stata valutata associando la perdita di peso durante l'analisi termogravimetrica ai parametri caratteristici di una equazione di Arrhenius, cioè l'energia di attivazione (E_a) ed il fattore pre-esponenziale (A). Il metodo di calcolo utilizzato è isoconversionale e non isotermo: il campione è scaldato a tre diverse rampe di riscaldamento (β =3, 5 e 10 [°C/min]) e i dati raccolti sono approssimati nell'equazione di Flynn-Ozawa-Walls (FWO), presentata in *Eq. A1.1.* Durante l'applicazione di tale modello, noto anche come uno dei "model-free", diversi valori di conversione (α) sono valutati ricavando la temperatura (T_α) associata a tale conversione. In questo modo, per ogni valore di α =0.1-0.9 viene calcolata l'energia di attivazione isoconversionale (E_α). I valori medi dei parametri cinetici calcolati sono mostrati in Tabella 4. [14]

$$ln\ ln\ (\beta)\ = const - 1.052 \cdot \left(\frac{E_\alpha}{R \cdot T_\alpha}\right) \qquad \text{(A1.1)}$$

Come mostrato in Tabella 4, le energie di attivazione dei campioni di fuliggine calcolate si trovano in un intervallo piuttosto limitato e la simile reattività è stata confermata anche attraverso l'analisi delle temperature caratteristiche. Se si confronta con la letteratura scientifica relativa a questo campo, solitamente le energie di attivazione si possono trovare in un intervallo più ampio. Vale la pena notare che la maggior parte degli studi tende a concentrarsi su una gamma ristretta di variabili, come il tipo di motore, il carburante e la preparazione del campione. Questa limitata variabilità può dare l'impressione che la reattività della fuliggine vari notevolmente da uno studio all'altro. Al contrario, lo studio attuale ha valutato che, in un gran numero di condizioni variabili, la reattività non è risultata influenzata in modo significativo.

Tabella 4: Parametri cinetici calcolati con il metodo isoconversionale non isotermo (FWO): E_A media nell'intervallo di conversione α=0.1-0.9, errore massimo associato all'interpolazione (R^2), fattore preesponenziale medio A e k per diversi campioni raccolti su filtri di quarzo durante le condizioni operative del motore e raschiati dai silenziatori

Nome identificativo del campione	**E_a (medio)** [kJ/mol]	**R^2 (minimo)**	**A** [$Pa^{-1}\ s^{-1}$]	**$k_{300°C}$** [$Pa^{-1}\ s^{-1}$]	**$k_{500°C}$** [$Pa^{-1}\ s^{-1}$]
Pipe 5-cylinder	164	0.997	27.5	$3.3\cdot10^{-14}$	$2.4\cdot10^{-10}$
Pipe 8-cylinder	151	0.999	8.7	$1.5\cdot10^{-13}$	$5.4\cdot10^{-10}$
Pressure sweep 1h	160	0.951	222.3	$4.9\cdot10^{-13}$	$3.0\cdot10^{-9}$
Pressure sweep 2h	141	0.995	1.9	$2.6\cdot10^{-13}$	$5.6\cdot10^{-10}$
Pressure sweep warm	138	0.914	10.9	$2.4\cdot10^{-12}$	$4.5\cdot10^{-09}$
Soot loading	162	0.971	23.4	$3.7\cdot10^{-14}$	$2.5\cdot10^{-10}$
Soot regeneration	143	0.723	3.6	$3.2\cdot10^{-13}$	$7.5\cdot10^{-10}$

Il risultato presentato in Figura 4, rivela una limitazione nell'uso dei filtri di quarzo durante la TGA. I campioni analizzati sui filtro mostrano un cambiamento nella pendenza della curva quando il 60-70% della fuliggine è ossidato. Questo è differente dai campioni estratti, raschiati dai silenzi o nel caso della fuliggine di riferimento, Printex-U, che mostrano una semplice diminuzione graduale del peso. Una possibile causa può essere una leggera limitazione di diffusione causata dalla presenza del filtro. Questo effetto diventa più visibile quando la disponibilità di particelle da bruciare è bassa, cioè verso la fine del processo di ossidazione.

Nonostante questo, i calcoli dell'energia di attivazione per i campioni ossidati sui filtri sono risultati nello stesso intervallo di quelli per i campioni ossidati senza filtri, indicando che questa limitazione non influisce sui calcoli dell'energia di attivazione del metodo proposto.

IV. Composizione chimica delle ceneri

Per quanto concerne la composizione delle ceneri, va notato che la presenza di una quantità relativamente piccola di frazione incombustibile all'interno dei campioni collezionati pone un limite all'accuratezza della valutazione. L'EDS è stata effettuata su un'ampia gamma di campioni, mentre l'utilizzo di ICP e XRD è stato solo limitato. Tuttavia, il paragone tra i risultati delle tre tecniche ha permesso di analizzare più criticamente i risultati delle singole analisi.

L'EDS, effettuata sulla frazione di cenere dopo la TGA, è stata eseguita su diversi punti di ogni campione per avere un risultato più generale e meno condizionato dall'eterogeneità locale della composizione di cenere. Ogni risultato è stato poi mediato aritmeticamente. Figura 6 mostra un confronto in termini di peso atomico tra i campioni. In questa figura, i componenti presenti in tracce, oppure, non rilevanti al fine della ricerca, sono stati esclusi. Tra questi figurano i seguenti elementi: alluminio (Al), carbonio (C), cromo (Cr), ferro (Fe), potassio (K), molibdeno (Mo), ossigeno (O), silicio (Si), titanio (Ti), vanadio (V) e tungsteno (W).

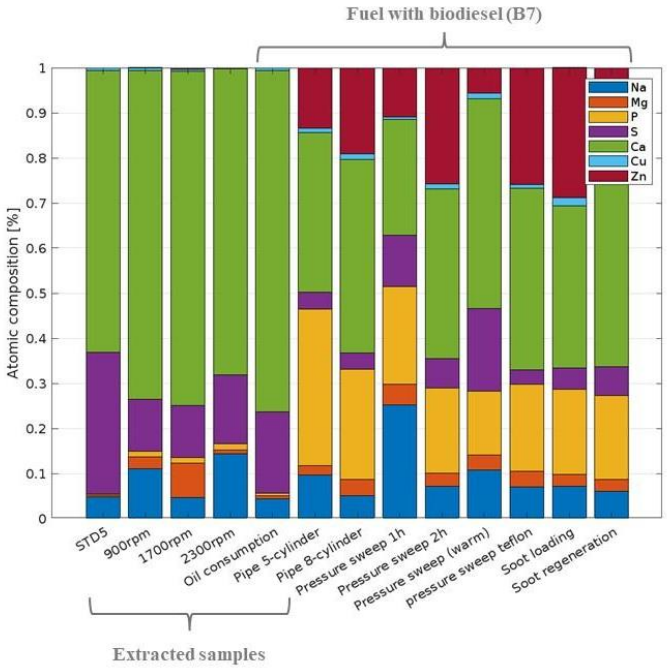

Figura 6: EDS: Confronto della composizione atomica delle ceneri [mol%] in termini di Sodio (Na), Magnesio (Mg), Fosforo (P), Zolfo (S), Calcio (Ca), Rame (Cu) e Zinco (Zn) per i campioni in analisi, in relazione al combustibile ed evidenziando i campioni estratti con cicloesano

I risultati mostrano che, nel complesso, gli elementi derivati dall'olio lubrificante come calcio (Ca), zinco (Zn), fosforo (P) e magnesio (Mg) formano la parte predominante della composizione mentre gli elementi derivati dalla corrosione e dall'usura del motore sono presenti in minore quantità. Contrariamente a quanto previsto, il Ca non è sempre stato il composto più abbondante e sono stati rilevati bassi livelli di zolfo (S). Il composto più comune trovato nelle ceneri dei motori diesel è il $CaSO_4$ [A15] [A16] [A17]. La quantità limitata di zolfo può essere attribuita alla TGA eseguita prima dell'EDS delle ceneri. La TGA non è del tutto rappresentativa dell'ambiente del DPF durante la rigenerazione. Il raggiungimento di temperature elevate (800°C in questo studio) può provocare un certo grado di desolforazione durante l'analisi termica [A18].

La ricerca ha evidenziato che le indagini sulla composizione delle particelle di cenere producono risultati diversi a causa di contaminazioni, dei diversi approcci per escludere elementi non rilevanti e della variabilità dei risultati dovuta all'utilizzo di diverse tecniche analitiche. Inoltre, è emerso che l'EDS può fornire risultati differenti in termini di composizione a seconda delle diverse parti del campione analizzate, a causa dell'eterogeneità del campione stesso. Al fine di superare queste criticità, viene proposto un approccio semplificato per valutare le somiglianze nella composizione tra diversi campioni e diversi studi. Questo approccio mira a ridurre la variabilità intrinseca confrontando valori adimensionali. La Tabella 5 mostra il rapporto, in termini di massa atomica e peso, tra gli elementi chiave dei campioni analizzati, al fine di esplorare potenziali correlazioni.

Dai risultati riportati nella Tabella 5 si può dedurre che la procedura di estrazione potrebbe aver avuto un impatto sulla concentrazione di Mg, P e Zn, poiché i campioni estratti presentavano bassi o assenti quantità di questi elementi, come si può vedere anche nella Figura 6. Le frazioni del motore a 8 cilindri riportate nella Tabella 5 mostrano che le quantità molari

di Zn e P erano comparabili per tutti i campioni, indicando che probabilmente nei campioni erano presenti diversi fosfati, ma le quantità di questi non sono variate tra i diversi campioni. Per questa serie di test, anche il rapporto Ca/Mg mostra una correlazione. L'abbondanza di Ca rispetto a S indica che probabilmente erano presenti diversi composti e che gli atomi di calcio erano condivisi tra i diversi composti.

Tabella 5: Frazione tra gli elementi rilevanti delle ceneri per i campioni corrispondenti presentati come frazione molare (frazione di peso): mol/mol (wt/wt)

	Campione	**Zn/P** mol/mol(wt/wt)	**Ca/S** mol/mol(wt/wt)	**Ca/Mg** mol/mol(wt/wt)	**Ca/Zn** mol/mol(wt/wt)
Estratti	STD5	-	2 (2.5)	159 (262.2)	-
	900 rpm	-	6 (8.0)	29 (47.1)	-
	1700 rpm	0.4 (0.7)	6 (8.0)	10 (15.8)	183 (112.3)
	2300 rpm	-	4 (5.6)	74 (121.3)	-
	Oil consumption	0.1 (0.3)	4 (5.2)	108 (117.3)	997 (661.0)
Motore 8-cilindri	Pipe 5-cylinder	0.4 (0.8)	9 (11.8)	17 (27.9)	3 (1.6)
	Pipe 8-cylinder	1 (1.6)	11 (14.4)	12 (19.7)	2 (1.4)
	Pressure sweep 1h	1 (1.1)	2 (2.8)	6 (9.5)	2 (1.5)
	Pressure sweep 2h	1 (2.9)	6 (7.3)	13 (21.3)	1 (0.9)
	Pressure sweep warm	0.4 (0.8)	3 (3.2)	14 (22.7)	8 (5.1)
	Pressure sweep Teflon	1 (2.8)	12 (15.6)	12 (19.7)	2 (1.0)
	Soot loading	2 (3.2)	8 (9.6)	14 (22.3)	1 (0.8)
	Soot regeneration	1 (2.0)	8 (9.5)	18 (29.5)	3 (1.7)

Un'analisi ICP è stata condotta su un campione corrispondente a "pressure sweep 1h" per avvalorare i risultati ottenuti dall'analisi EDS e per stimare la frazione di ceneri conoscendo la quantità degli elementi costituenti le ceneri. Il filtro di quarzo è stato caricato con 1,014 mg di PM e digerito in una miscela di acidi. I risultati dell'analisi ICP hanno mostrato che la maggior parte degli elementi erano al di sotto della soglia di analisi. Tuttavia la conoscenza della quantità di Zn, Ca e Cu ha permesso di stimare la quantità dei composti caratteristici delle ceneri $Zn_3(PO_4)$, $CaSO_4$ e $CuSO_4$ attraverso un confronto molare e di stimare la quantità di ceneri approssimando la frazione incombustibile alla quantità di questi tre composti. Il risultato, pari a 0.109 mg, corrisponde a circa 11% della massa iniziale del campione di particolato.

Sebbene nel presente studio sia stata eseguita una sola analisi ICP, sono stati ottenuti risultati parziali che indicano un rapporto molare Ca/Zn di 1.3. Questo campione era analogo al "pressure sweep 1h", presentato nella Tabella 5, dove il rapporto molare Ca/Zn era pari a 2.

L'analisi di diffrazione dei raggi X è stata eseguita sulla frazione incombustibile residua dalla TGA del campione“pipe 8-cylinder”, in quanto unico con una frazione di ceneri sufficiente a condurre l’analisi (approssimativamente 1 [mg] di cenere). La XRD ha permesso di identificare con successo diversi picchi: i picchi (2θ: 21,5°; 26,6°) indicano la presenza di $Zn_3(PO_4)_2$ [19], mentre i picchi (2θ: 21,8; 25,9; 27,9; 43,1) suggeriscono la presenza di $Zn_3Mg(PO_4)_2$, in linea con i risultati di A. Sappok [A20]. Uno dei picchi attesi a indicazione della presenza di $CaSO_4$ si posiziona a 2θ=25.2 [A19], tuttavia, esso non è stato rilevato.
La presenza di $CaSO_4$ in questo campione è stata suggerita dall'abbondanza di Ca e S nell'analisi EDS e la mancanza di picchi di $CaSO_4$ può essere dovuta alla quantità limitata di ceneri per

un'analisi accurata. Un'altra possibile spiegazione riguarda un cambiamento di fase che il $CaSO_4$ potrebbe aver subito a causa delle alte temperature durante la TGA. La letteratura mostra che i diffrattogrammi dei campioni di cenere a temperature superiori a 800 [°C] presentano diversi cambiamenti [A19]. La spiegazione più probabile però è correlata a una minore quantità di strutture cristalline all'interno delle ceneri. Ciò è in accordo con il lavoro di S. Bagi [A15] che ha dimostrato che il residuo incombustibile del particolato dei gas di scarico diesel post TGA può presentare la mancanza di picchi XRD caratteristici a causa della presenza dominante di strutture amorfe. Non è possibile valutare se la struttura sia prevalentemente cristallina o amorfa dalle immagini SEM presentate poiché i cristalli possono essere di ordini di grandezza inferiori alla risoluzione del microscopio. Tuttavia, sono state osservate alcune strutture cristalline, come ad esempio nella Figura 3.6 (3) presente nella versione estesa dell'elaborato. D'altro canto, A. McGeehan [A21] ha identificato con successo l'anidride $CaSO_4$ mediante XRD da un campione di ceneri provenienti dal DPF. La struttura e la fase delle ceneri possono subire diverse modifiche in seguito a diversi cicli di rigenerazione del DPF [A19], pertanto il confronto tra le ceneri del DPF e quelle raccolte durante il funzionamento in corso può presentare differenze strutturali.

Tutti i risultati presentati sono stati correlati con i risultati presenti in letteratura a descrizione della composizione delle ceneri come mostrato in Tabella 6. Il confronto nella Tabella 6 rivela che a differenza dei risultati presenti in letteratura, l'intervallo dei valori ottenuti durante questo progetto è molto variabile, Tuttavia, i risultati della letteratura rientrano spesso nell'intervallo dei valori trovati. Ciò dimostra l'elevata eterogeneità delle ceneri raccolte, che probabilmente si riduce al minimo quando le ceneri si accumulano nel DPF. Ciò è in linea con A.G. Sappok [A18], il quale deduce, dopo aver analizzato il PM raccolto durante un'operazione in corso su un filtro di carta tramite microscopia elettronica a trasmissione di scansione (STEM), che la distribuzione del fosforo e degli elementi metallici nelle ceneri era altamente eterogenea.

Tabella 6: Confronto dei rapporti di massa [wt/wt] degli elementi costituenti le ceneri relativi all'attuale ricerca e quelli presenti in letteratura

			EDS			ICP	
Rapporto [wt/wt]	**Estratti**	**Motore 8-cilindri**	**J. A. Mcgeehan** [22]	**J. A. Mcgeehan** [21]	**A. Liati** [17]	**S. Bagi** [19]	**S. Bagi** [19]
Zn/P	-	0.84-3.23	1.10, 1.09	1.44	1.04	1.14	1.13
Ca/S	2.49-7.98	2.82-15.57	0.83, 1.36	1.42	0.85	0.68	1.09
Ca/Zn	-	0.77-5.06	2.34, 2.94	2.21	1.03	1.86	2.11
P/S	0.01-0.11	0.75-6.34	0.32, 0.42	0.45	0.80	0.32	0.46

Uno sguardo più attento alla Tabella 6 permette di osservare che il rapporto Ca/S è risultato significativamente più basso se confrontato con tutti i risultati della letteratura. Ciò potrebbe essere dovuto all'effetto di desolforazione durante la TGA e i miglioramenti in termini di riduzione dello zolfo negli oli combustibili. Il rapporto Ca/Zn in termini di massa è risultato pari a 3.85 durante l'analisi ICP, quindi superiore a quello riportato nella Tabella 6 ma comunque all'interno dell'intervallo presentato per l'analisi EDS.

Nonostante il tentativo di stabilire una correlazione tra la presente ricerca e altri studi attraverso la Tabella 6, fare confronti quantitativi e definitivi è considerato poco realistico. La composizione delle particelle di cenere è spesso influenzata in modo significativo dagli additivi presenti nell'olio lubrificante utilizzato durante il funzionamento, piuttosto che dalle condizioni operative [A18] [A23]. Di conseguenza, composizioni diverse dell'olio possono dare origine a prodotti post-combustione diversi. Tuttavia, la valutazione della composizione delle particelle di cenere rimane una prospettiva interessante, in quanto offre l'opportunità di stimare la frazione di cenere e quantificare la quantità attraverso l'integrazione di ICP, XRD e altre tecniche analitiche.

I risultati combinati di XRD, EDS e ICP suggeriscono che la maggior parte delle ceneri del PM dei gas di scarico diesel è probabilmente in fase amorfa. Tuttavia, sono necessarie ulteriori misurazioni XRD per verificare questa ipotesi, poiché la piccola quantità di campione e l'importante effetto del rumore di fondo potrebbero aver giocato un ruolo.

V. Frazione di cenere rispetto alla fuliggine nella composizione del particolato

Il rapporto tra ceneri e fuliggine nella composizione del particolato è stato valutato solo per pochi campioni a causa di diverse limitazioni legate alle indagini e alle apparecchiature. Inoltre, ogni campione analizzato possiede peculiarità intrinseche. Di conseguenza, la frazione di cenere deve essere presa in considerazione solo come valore indicativo.
La curva di perdita di peso per ogni campione è stata suddivisa in tre regioni per ottenere i risultati:

- frazione organica volatile (VOF), la frazione persa durante il condizionamento, cioè il riscaldamento fino a 400 [°C] in atmosfera inerte.
- Fuliggine, la frazione bruciata durante l'ossidazione.
- Cenere, frazione rimanente dopo l'ossidazione.

La Figura 7 confronta la così ricavata composizione del particolato per i campioni “STD5”, “oil consumption”, “pipe 5-cylinder”, “pipe 8-cylinder” e “pressure sweep Teflon”. Da questi risultati, la frazione di ceneri è stata stimata essere contenuta tra il 3 ed il 23% in peso, con valori più elevati nei campioni raschiati dai silenziatori.

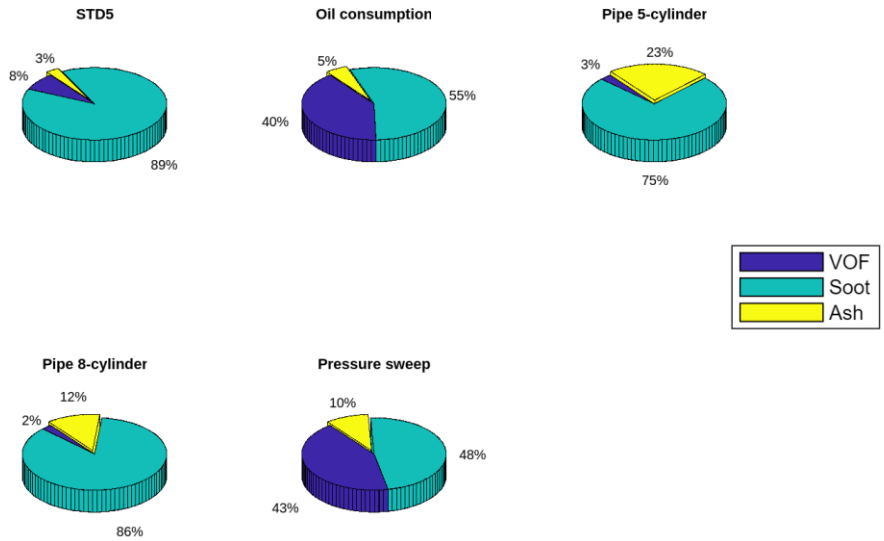

Figura 7: Composizione in peso del particolato per i campioni “STD5”, “oil consumption”, “pipe 5-cylinder”, “pipe 8-cylinder” e “pressure sweep Teflon” ottenuta dall'analisi delle curve di perdita di peso (TGA)

In dettaglio in Figura 7, il confronto tra i campioni “STD5” e “oil consumption” rivela che la frazione di biodiesel nel combustibile di quest’ultimo potrebbe aver avuto impatto sulla frazione di VOF. I VOF sono stati riportati anche in letteratura in frazioni più elevate quando un combustibile non fossile è utilizzato [A4]. Il paragone tra i due campioni collezionati dai silenziatori ha mostrato che maggiore frazione di cenere nel “pipe 5-cylinder”, probabilmente come effetto del maggior tempo trascorso all'interno del sistema di post-trattamento delle emissioni. Il campione "pressure sweep" presentato nella Figura 7 è stato raschiato da un filtro in Teflon. Pertanto, la frazione di ceneri rappresentata era superiore alla quantità effettiva a causa della contaminazione da fibre di teflon. I risultati devono essere interpretati solo come un'indicazione del limite superiore della frazione di ceneri per quanto concerne questo campione.

Confrontando i risultati presentati in Figura 7 con le ricerche condotte in questo campo, è emerso che la frazione di ceneri determinata durante questa ricerca è risultata generalmente superiore ai risultati proposti dalla letteratura, riassunti nella Tabella 7. Anche se l'analisi EDS condotta sui campioni estratti non ha indicato alcuna contaminazione da fibra di vetro, rimane plausibile la presenza di un certo grado di contaminazione. Tuttavia, i risultati di S. Bagi [A15] rivelano che una frazione di cenere superiore all'1% può essere osservata in determinate condizioni operative, allineandosi con i risultati ottenuti nel presente studio.

Tabella 7: Confronto della composizione del particolato, con particolare attenzione alla frazione di cenere, tra le diverse ricerche presenti in letteratura

	A. Sappok [A18]	**S. Bagi** [A15]	**M. Zhang** [A24]	
Modalità operativa del motore	(1682 rpm, 25% di carico) e (1682 rpm, 75% di carico)	Somma di servizio a lungo raggio, consegna regionale e servizio urbano	Bassa velocità Alto carico	Alta velocità Alto carico
Frazione di ceneri [%wt]	0.5	3.12	>0.5	1
Frazione di fuliggine [%wt]	87.5	-	91	92
VOF [%wt]	12.4	-	9	7

Conclusioni

Il presente lavoro si propone di aumentare la conoscenza in campo del particolato diesel cercando di stimare la frazione di cenere prodotta durante il funzionamento dei motori. Inoltre, evidenzia con uno sguardo critico, i limiti e i potenziali problemi che potrebbero sorgere durante lo studio della cinetica di ossidazione della fuliggine e della frazione di cenere. Una parte dello studio si è concentrata sulla ricerca dei filtri più adatti e sull'analisi della loro influenza sui risultati. Le seguenti principali conclusioni possono essere indirizzare in risposta alle domande chiave che hanno caratterizzato l'investigazione.

1. Il rapporto ceneri/fuliggine per i motori diesel pesanti è risultato ostico da stimare con precisione a causa delle limitazioni intrinseche dei diversi metodi di raccolta. È probabile che si verifichino contaminazioni da parte delle fibre dei filtri sui quali il particolato viene raccolto. Infatti, esse sono state osservate durante la ricerca. La frazione di cenere e fuliggine è stata stimata tra il 3 e il 31% in peso ed è risultata più elevata nei campioni prelevati dai silenziatori. Probabilmente, come effetto della prolungata deposizione di particolato, nel tempo, una parte della fuliggine reagisce all'interno del sistema mentre la cenere si accumula portando a diventare una frazione più influente all'interno della composizione del particolato. L'influenza delle diverse condizioni operative sulla produzione di ceneri è risultata difficile da valutare a causa dell'elevato numero di variabili tra i campioni raccolti. Il confronto tra due campioni suggerisce che l'effetto del biodiesel nel carburante può portare ad una frazione di VOF più ampia nella composizione del PM. Inoltre, l'effetto dell'invecchiamento è stato correlato a un aumento della frazione di ceneri. La definizione di un intervallo per il rapporto fuliggine-cenere fornisce preziose indicazioni sulla frazione di cenere presente nei motori, soprattutto in quanto ottenuta con analisi che dovrebbero ridurre al minimo la contaminazione dei filtri. Questa scoperta rappresenta un risultato positivo con

importanti implicazioni per il futuro della modellazione dei DPF: analizzando una serie di cicli di guida reali, oltre a quelli tipicamente impiegati per il controllo delle emissioni, questo studio amplia la nostra comprensione delle emissioni di PM in varie condizioni.

2. La fuliggine ha mostrato caratteristiche morfologiche simili e, cosa più interessante, energie di attivazione molto simili (138-164 kJ/mol), confrontando campioni completamente diversi, provenienti da motori diversi, con carburanti diversi e raccolti con differenti metodi. La similitudine in quanto a reattività può essere dedotta anche dai valori di MLRTmax, che sono stati riportati come comparabili per tutti i campioni in analisi. Questo risultato apre nuove possibilità per l'impiego di diversi tipi di fuliggine nella fase di ricerca e della modellazione dei filtri antiparticolato diesel, con il potenziale di riflettere più accuratamente il particolato generato durante le reali condizioni stradali. Inoltre, questa scoperta è importante per migliorare la comprensione delle proprietà della fuliggine che si accumula nel DPF e per ottimizzare le strategie di rigenerazione.

3. La caratterizzazione della composizione delle ceneri si è rivelata ardua a causa della quantità limitata di ceneri disponibili sui filtri utilizzati per la raccolta dei campioni, nonché del potenziale di contaminazione da parte di agenti esterni e dei filtra di collezionamento stessi. Pertanto, per valutare la composizione delle ceneri e per valutare l'affidabilità dei risultati, sono state utilizzate diverse tecniche, tra cui una revisione della letteratura scientifica pertinente e un confronto tra diversi metodi sperimentali.

   3.1 L'EDS è spesso utilizzato in letteratura per l'analisi della composizione delle ceneri. Tuttavia, in questa come in altre ricerche, la composizione sembra essere estremamente variabile da campione a campione. Mentre il Ca è stato indicato come il costituente principale, in tutti i campioni è stata rilevata una concentrazione inaspettatamente elevata di Na.

   3.2 Diversi campioni sono stati estratti utilizzando cicloesano per ridurre le contaminazioni da parte del filtro adoperato per il collezionamento, probabilmente inevitabili se quando il particolato è raschiato dalla superficie del filtro. Purtroppo, esaminando criticamente i risultati dell'EDS, si può dedurre che la procedura di estrazione potrebbe aver influenzato la composizione delle ceneri. I campioni estratti hanno presentato una frazione ridotta o non rilevabile di Mg, P e Zn.

   3.3 L'ICP ha permesso una valutazione solo parziale del campione, poiché diversi elementi attesi nella composizione chimica delle ceneri, sono risultati al di sotto della soglia di rilevazione. Nonostante questo, le quantità di Ca, Zn e Cu sono state rilevate con successo. Ciò ha permesso di valutare un confronto parziale tra il campione denominato "pressure sweep 1h" analizzato con ICP e con EDS, mostrando analogie nei risultati.

   3.4 L'analisi XRD potrebbe essere uno strumento efficace per individuare la composizione dei campioni di ceneri, anche se la quantità limitata di campioni ha influenzato il risultato: sono stati rilevati soltanto $Zn_3(PO_4)_2$ e $Zn_3Mg(PO_4)_2$. L'assenza di picchi caratteristici per $CaSO_4$ suggerisce la presenza di una frazione significativa di composti delle ceneri in fase amorfa, coerentemente con i risultati precedenti in letteratura.

Nel complesso, l'EDS è risultato il metodo più adatto, in quanto ha permesso di analizzare il maggior numero di campioni. L'uso di altre analisi è stato limitato dalla scarsa quantità di ceneri disponibili. La XRD può essere interessante perché permette di esaminare i composti piuttosto che gli elementi, ma i limiti delle dimensioni dei campioni ne rendono difficile l'impiego per le ceneri raccolte durante il funzionamento del motore. L'impiego di più tecniche di analisi in parallelo può migliorare la comprensione della composizione delle ceneri e contribuire a raggiungere maggiori livelli di validazione.

4. Qualsiasi metodo di raccolta del particolato che prevede l'uso di filtri apporta inevitabilmente una sorta di contaminazione al campione e può rendere alcune analisi inadatte o prive di significato.

   4.1 I filtri al quarzo sono i più adatti per gli studi cinetici, poiché sono inerti nell'intervallo di temperature di ossidazione della fuliggine. Tuttavia, risultano fragili e quindi rovinano i risultati quando l'obiettivo è la stima della frazione di cenere.

   4.2 Quando il Teflon è contenuto nei filtri (fibre di teflon puro o fibra di vetro rivestita di Teflon), esso altera i risultati della TGA, rendendo la curva di perdita di peso non significativa. Inoltre, l'analisi termogravimetrica eseguita solo sul filtro ha mostrato che per entrambi i tipi di filtri, alla fine del programma di riscaldamento della TGA saranno presenti dei residui. Pertanto, se sono presenti contaminazioni del filtro, la stima della frazione di ceneri, ottenuta pesando il campione dopo l'analisi termogravimetrica, sarà aumentata dalle contaminazioni. Per questa ragione l'analisi della composizione delle ceneri, ad esempio eseguita con EDS, sarà alterata.

   4.3 Il vantaggio dei filtri in fibra di vetro rispetto ai filtri al quarzo è che sono meno fragili, quindi se l'obiettivo è la frazione di ceneri, l'uso di questo filtro può essere abbinato a una procedura di estrazione per separare il particolato dal filtro senza creare contaminazioni. La procedura di estrazione può avere successo nel ridurre al minimo le contaminazioni del filtro prima della TGA: l'EDS dei campioni estratti ha mostrato che i componenti identificativi dei filtri in fibra di vetro non erano presenti, al contrario di quando il PM veniva raschiato dal filtro. Tuttavia, le basse rese di estrazione sono un fattore limitante per la procedura. L'uso di una procedura di estrazione deve essere ulteriormente studiato poiché potrebbe avere effetti sulla composizione delle ceneri, come presentato nei risultati dell'EDS.

Bibliografia (relativa alla sintesi)

[A1] B. Giechaskiel *et al.*, “Assessment of a Euro VI Step E Heavy-Duty Vehicle’s Aftertreatment System,” *Catalysts*, vol. 12, no. 10, Art. no. 10, Oct. 2022, doi: 10.3390/catal12101230.

[A2] R. Andersson and B. Andersson, “The effect of exhaust gas composition on the kinetics of soot oxidation and diesel particulate filter regeneration,” *Fuel*, vol. 220, pp. 453–463, May 2018, doi: 10.1016/j.fuel.2018.02.037.

[A3] *Commission Regulation (EU) No 582/2011 of 25 May 2011 implementing and amending Regulation (EC) No 595/2009 of the European Parliament and of the Council with respect to emissions from heavy duty vehicles (Euro VI) and amending Annexes I and III to Directive 2007/46/EC of the European Parliament and of the Council (Text with EEA relevance)Text with EEA relevance*. 2011. Accessed: Jan. 16, 2023. [Online]. Available: https://eur-lex.europa.eu/legal-content/EN/TXT/?uri=CELEX%3A02011R0582-20221210

[A4] M. Lapuerta, R. Ballesteros, and J. Rodríguez-Fernández, “Thermogravimetric analysis of diesel particulate matter,” *Meas. Sci. Technol.*, vol. 18, no. 3, pp. 650–658, Mar. 2007, doi: 10.1088/0957-0233/18/3/015.

[A5] Z. Zhang, R. Dong, G. Lan, T. Yuan, and D. Tan, “Diesel particulate filter regeneration mechanism of modern automobile engines and methods of reducing PM emissions: a review,” *Environ. Sci. Pollut. Res.*, vol. 30, no. 14, pp. 39338–39376, Mar. 2023, doi: 10.1007/s11356-023-25579-4.

[A6] J.-Y. Park, J.-H. Lee, C.-H. Kim, and Y.-J. Kim, “Fabrication of polytetrafluoroethylene nanofibrous membranes for guided bone regeneration,” *RSC Adv.*, vol. 8, pp. 34359–34369, Oct. 2018, doi: 10.1039/C8RA05637D.

[A7] B. Giechaskiel, “Solid Particle Number Emission Factors of Euro VI Heavy-Duty Vehicles on the Road and in the Laboratory,” *Int. J. Environ. Res. Public. Health*, vol. 15, no. 2, Art. no. 2, Feb. 2018, doi: 10.3390/ijerph15020304.

[A8] S. Yoon *et al.*, “Characteristics of particle number and mass emissions during heavy-duty diesel truck parked active DPF regeneration in an ambient air dilution tunnel,” *Atmos. Environ.*, vol. 122, pp. 58–64, Dec. 2015, doi: 10.1016/j.atmosenv.2015.09.032.

[A9] J. Rodríguez-Fernández, F. Oliva, and R. A. Vázquez, “Characterization of the Diesel Soot Oxidation Process through an Optimized Thermogravimetric Method,” *Energy Fuels*, vol. 25, no. 5, pp. 2039–2048, May 2011, doi: 10.1021/ef200194m.

[A10] H. N. Sharma, L. Pahalagedara, A. Joshi, S. L. Suib, and A. B. Mhadeshwar, “Experimental Study of Carbon Black and Diesel Engine Soot Oxidation Kinetics Using Thermogravimetric Analysis,” *Energy Fuels*, vol. 26, no. 9, pp. 5613–5625, Sep. 2012, doi: 10.1021/ef3009025.

[A11] J. Gao, C. Ma, S. Xing, L. Sun, and H. Liyong, “A review of fundamental factors affecting diesel PM oxidation behaviors,” *Sci. China Technol. Sci.*, vol. 61, Sep. 2017, doi: 10.1007/s11431-016-9117-x.

[A12] X. Liang *et al.*, “Experimental investigation of diesel soot oxidation reactivity along the exhaust after-treatment system components,” *Fuel*, vol. 302, p. 121047, Oct. 2021, doi: 10.1016/j.fuel.2021.121047.

[A13] D. Zhang, Y. Ma, and M. Zhu, “Nanostructure and oxidative properties of soot from a compression ignition engine: The effect of a homogeneous combustion catalyst,” *Proc. Combust. Inst.*, vol. 34, no. 1, pp. 1869–1876, Jan. 2013, doi: 10.1016/j.proci.2012.05.096.

[A14] S. Vyazovkin *et al.*, “ICTAC Kinetics Committee recommendations for collecting experimental thermal analysis data for kinetic computations,” *Thermochim. Acta*, vol. 590, pp. 1–23, Aug. 2014, doi: 10.1016/j.tca.2014.05.036.

[A15] S. Bagi, C. J. Kamp, V. Sharma, and P. B. Aswath, “Multiscale characterization of exhaust and crankcase soot extracted from heavy-duty diesel engine and implications for DPF ash,” *Fuel*, vol. 282, p. 118878, Dec. 2020, doi: 10.1016/j.fuel.2020.118878.

[A16] A. Liati and P. Dimopoulos Eggenschwiler, “Characterization of particulate matter deposited in diesel particulate filters: Visual and analytical approach in macro-, micro- and nano-scales,” *Combust. Flame*, vol. 157, no. 9, pp. 1658–1670, Sep. 2010, doi: 10.1016/j.combustflame.2010.02.015.

[A17] A. Liati, P. Dimopoulos Eggenschwiler, E. Müller Gubler, D. Schreiber, and M. Aguirre, “Investigation of diesel ash particulate matter: A scanning electron microscope and transmission electron microscope study,” *Atmos. Environ.*, vol. 49, pp. 391–402, Mar. 2012, doi: 10.1016/j.atmosenv.2011.10.035.

[A18] A. G. Sappok and V. W. Wong, “Detailed Chemical and Physical Characterization of Ash Species in Diesel Exhaust Entering Aftertreatment Systems,” presented at the SAE World Congress & Exhibition, Apr. 2007, pp. 2007-01–0318. doi: 10.4271/2007-01-0318.

[A19] S. Bagi, R. Bowker, and R. Andrew, “Understanding Chemical Composition and Phase Transitions of Ash from Field Returned DPF Units and Their Correlation with Filter Operating Conditions,” *SAE Int. J. Fuels Lubr.*, vol. 9, no. 1, pp. 239–259, Apr. 2016, doi: 10.4271/2016-01-0898.

[A20] A. Sappok and V. W. Wong, “Lubricant-Derived Ash Properties and Their Effects on Diesel Particulate Filter Pressure-Drop Performance,” *J. Eng. Gas Turbines Power*, vol. 133, no. 3, Nov. 2010, doi: 10.1115/1.4001944.

[A21] J. A. Mcgeehan *et al.*, “On The Road to 2010 Emissions: Field Test Results and Analysis with DPF-SCR System and Ultra Low Sulfur Diesel Fuel,” presented at the Powertrain & Fluid Systems Conference & Exhibition, Oct. 2005, pp. 2005-01–3716. doi: 10.4271/2005-01-3716.

[A22] J. McGeehan *et al.*, “Analysis of DPF Incombustible Materials from Volvo Trucks Using DPF-SCR-Urea With API CJ-4 and API CI-4 PLUS Oils,” *SAE Int. J. Fuels Lubr.*, vol. 2, no. 1, pp. 762–780, Jun. 2009, doi: 10.4271/2009-01-1781.

[A23] M. Morcos, P. Ayyappan, and T. Harris, “Characterization of DPF Ash for Development of DPF Regeneration Control and Ash Cleaning Requirements,” presented at the SAE 2011 World Congress & Exhibition, Apr. 2011, pp. 2011-01–1248. doi: 10.4271/2011-01-1248.

[A24] M. Zhang *et al.*, “An investigation into the impact of burning diesel/lubricant oil mixtures on the nature of particulate emissions: Implications for DPF ash-loading acceleration method,” *J. Energy Inst.*, vol. 93, no. 3, pp. 1207–1215, Jun. 2020, doi: 10.1016/j.joei.2019.11.004.

Table of contents

List of Figures

List of Tables

List of acronyms and abbreviations

APC	Aerodynamic Particle Counter
CI	Compression Ignition
DOC	Diesel Oxydation Catalyst
DPF	Diesel Particulate Filter
EDS	Energy Dispersive Spectroscopy
EGR	Exhaust Gas Recirculation
EPA	Environmental Protection Agency
FWO	Flynn-Ozawa-Wall
GC	Gas Chromatography
GHG	Greenhouse Gas
HC	Hydrocarbon
ICP	Inductively Coupled Plasma
FOT	Final Oxidation Temperature
FT-IR	Fourier-transform infrared spectroscopy
KAS	Kissinger-Akiha-Sunose
MSS	Micro Soot Sensor
$MLRT_{max}$	Maximum Mass Loss Rate Temperature
OBD	On Board Diagnostics
PAH	Polycyclic Aromatic Hydrocarbons
PFDS	Partial Flow Dilution System
PM	Particulate Matter
PN	Particulate Number
PTFE	Polytetrafluoroethylene
SCR	Selective Catalytic Reduction
SEM	Scanning Electron Microscope
SOF	Soluble Organic Fraction
SOT	Starting oxidation temperature
STEM	Scanning Transmission Electron Microscopy

TGA	Thermogravimetric Analysis
ULSD	Ultra-Low Sulphur Diesel
VOF	Volatile Organic Fraction
WHSC	World Harmonized Steady-state Cycle
WHTC	World Harmonized Transient Cycle
XRD	X-Ray Diffraction

List of employed symbols

A pre-exponential factor [Pa^{-1} sec^{-1}]

α conversion fraction

β linear ramp rate: $\beta = \frac{dT}{dt}$ [°C/min]

E_a activation energy [kJ/mol]

E_α isoconversional activation energy [kJ/mol]

θ diffraction angle

k reaction rate constant

p_{O_2} oxygen partial pressure

R gas constant [J/mol K]

t time [min]

T temperature [°C]

Chapter 1

Introduction

The major environmental health risk in Europe is air pollution, and road transport represents one of the main culprits [1] [2] . In the context of diesel on-road vehicles, heavy-duty engines contribute significantly to emissions and, hence, to the impact on health. Nowadays, the diesel engine states as first choice in several industrial application and for heavy-duty vehicles in spite of an on-going development in electrification of the transport sector. Euro VI is the current legal requirement for emissions from diesel vehicles [3]. Euro VI is expected to be replaced shortly by legislation that sets stricter limits. The necessity to be prepared for new standards as well as the desire to improve the quality of the air in the cities are the driving forces in the improvement of the exhaust aftertreatment system within a vehicle.

Diesel engines are preferred over gasoline engines for heavy-duty applications because of their superior fuel efficiency and ability for high torque output. The cost of these benefits results in higher emissions. The emissions are mitigated by the aftertreatment system, which is composed by several modules. One of those is the diesel particulate filter (DPF), which aims to lower the particulate matter (PM) emissions. A step behind the improvement of its technology is the understanding of the pollutants the exhaust after-treatment system may face.

Within this framework, it is crucial to understand the composition, the properties and the amount of particulate matter exiting the combustion engine. The active research on oxidation behavior and structures is the foundation of decreasing PM emission and optimization of the particulate after-treatment devices. The focus of the work is on heavy-duty vehicles.

1.1 Framework of the investigation and literature review

This section describes the emission legislation, the structure of the diesel engine and the aftertreatment system for heavy-duty trucks as a framework for a more detailed description of the particulate formed within those vehicles. Furthermore, the formation, the composition, the reactivity, the emissions and factors affecting those characteristics of the particulate matter are discussed.

1.1.1 History of emission legislations and current regulations

From the earliest days of industrialization, emissions from factories and vehicles have posed a growing threat to the health of our planet and its inhabitants. The United States were the first to introduce a car pollution regulation, known as the Clean Air Act, in 1963, predominantly in reaction to the smog issues in Los Angeles. [4] Meanwhile in European Union, from the 1970s different EU countries began to implement their emission standards to mitigate the effects of environmental pollution. A decade later, the European Commission proposed the creation of a unified standard across the European Union and 1992 the first European Emission Standard. It is known as Euro I and it was implemented and applied to new passenger cars, then extended to cover other types of vehicles, including trucks and buses [5]. The implementation of further Euro standards as pollution emission limits is a complex process that spans several decades. Briefly, Euro II was introduced in 1995 [6], followed by Euro III in 2000 [7]. The Euro IV and Euro V standards were introduced in 2005 and 2008, respectively. [8] These standards were much more stringent than previous versions and required significant changes to engine design and emissions control systems. The current standard, Euro VI, was implemented in 2014,

further tightening emissions limits for nitrogen oxides (NO_x) and PM. It is evident that the standards for combustion gases and particulates have increased significantly between Euro I and Euro VI. For instance, between Euro I and Euro VI, for compression ignition (CI) heavy-duty vehicles, heavy-duty compression-ignition (CI) engines were restricted by 95 percent from emitting nitrogen oxides and by 97 percent for particulates. A simplified comparison of the evolution of the European standards for limiting NO_x and PM emissions from heavy-duty vehicles is summarized in *Figure 1.1*.

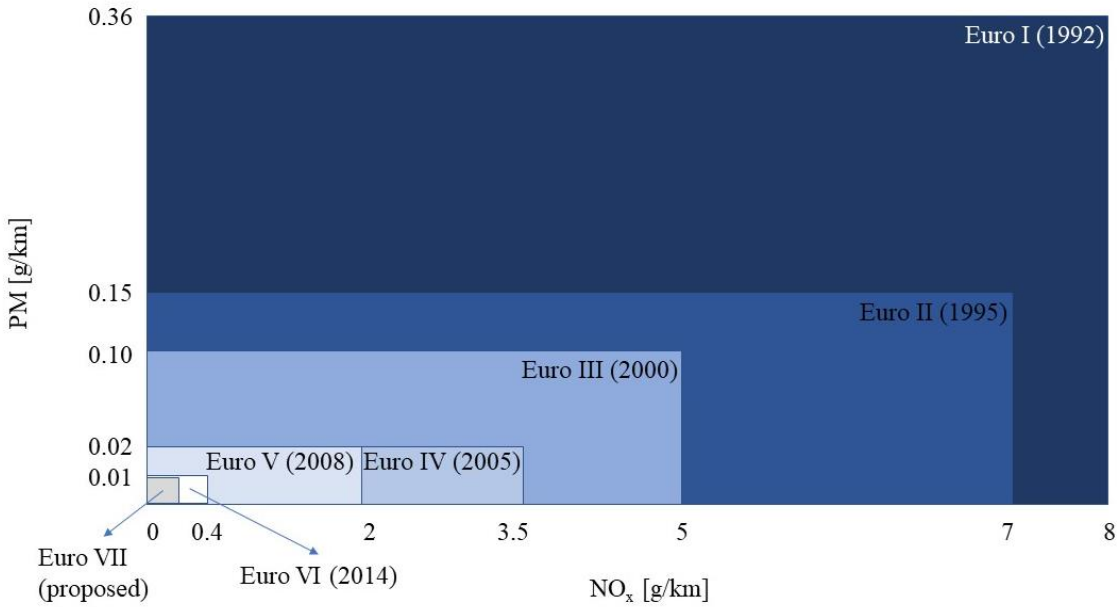

Figure 1.1: Simplified summary of the progression of the European standards for CI heavy-duty vehicles

Euro VI was implemented by Regulation (EU) No 582/2011 but it revised several times to introduce additional elements. Compared to the previous standard, Euro VI updated the duty cycles to World Harmonized Transient Cycle (WHTC) and World Harmonized Steady-state Cycle (WHSC); introduces off-cycle testing, limitations on the Particulate Number (PN), stricter On-Board Diagnostic (OBD) requirements and ammonia concentration limits. A more stringent standard, Euro VII is expected to be the implemented in the near future. *Table 1.1* outlines the prescribed thresholds for regulated pollutants, including carbon monoxide (CO), total hydrocarbons (THC), nitrogen oxides (NO_x), ammonia (NH_3), and particulate matter, for both the current European emission standard and its proposed successor.

Table 1.1 European emission standards Euro VI [9] and Euro VII [10] for heavy-duty diesel engines

		Regulated pollutants					
Tier	**Test cycle**	**CO** [g/kWh]	**THC** [g/kWh]	**NO_x** [g/kWh]	**NH_3**	**PM** [g/kWh]	**PN** [1/kWh]
Euro VI	WHSC	1.5	0.13	0.4	10 [ppm]	0.01	$8 \cdot 10^{11}$
	WHTC	4.0	0.16	0.46	10 [ppm]	0.01	$6 \cdot 10^{11}$
Euro VII (proposed)	$WHTC_{cold}$	3.5	0.2	0.35	0.065 [g]	0.012	$5 \cdot 10^{11}$
	$WHTC_{hot}$	0.2	0.05	0.09	0.065 [g]	0.008	$2 \cdot 10^{11}$

Within the United States, the current Environmental Protection Agency (EPA) emissions standards for heavy-duty vehicles are the Phase 2 Greenhouse Gas (GHG) Emission Standards. Direct comparisons between European and American standards are challenging due to differences in testing procedures and requirements. The US standards for heavy-duty truck PM emissions can be considered more stringent than the present European standards, with a limit of 0.01 g/bhp-hr (equivalent to 0.0075 g/kWh) for heavy-duty CI engines, expected to be lowered to 0.005 g/bhp-h. [11]

1.1.2 Diesel engine and exhaust aftertreatment system

The fundamental part of the diesel engine is the combustion chamber, located inside the engine cylinders. There the diesel fuel is sprayed in the form of small droplets through an injector. The fuel is converted into mechanical energy during the combustion process, which releases exhaust gases. Part of the exhaust gases can be recirculated to be mixed with fresh intake air that is about to enter the combustion chamber through an exhaust gas recirculation unit (EGR), if present. The exhaust gases will successively pass through the aftertreatment system to be then released into the atmosphere.

The aftertreatment system includes the diesel oxidation catalyst (DOC), the diesel particulate filter (DPF) and a selective catalytic reduction unit (SCR). DOC is utilized to reduce the unburned hydrocarbons (HC) and CO through oxidation. DPF reduces PM emissions while SCR mitigates NOx emissions [1]. *Figure 1.2* shows a representation of a Scania engine with an XPI, rail fuel injection system, and Euro VI emissions control system.

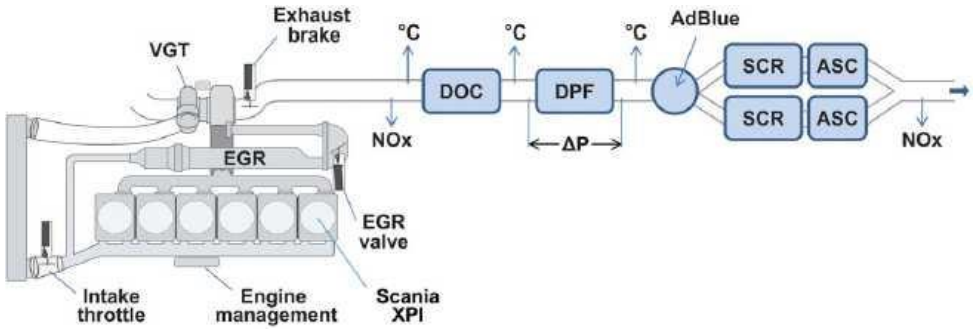

Figure 1.2 Example of an aftertreatment system: Scania Euro VI emission control system [12]

1.1.3 Particulate matter composition

The combustion within the engine produces exhaust emissions containing different products, among those, the solid particles are the most complex to describe. Exhaust particulate matter is defined as a filtrable material that can be obtained by dilution and cooling down of the exhaust gas. That includes solids and liquids that condense on the particle´s surface during the cooling. The basic composition includes a carbonaceous fraction that is commonly known as soot, ash, soluble organic fractions and eventual other impurities. The fraction of sulphates is correlated to the amount of sulfur in the lubricating oil and in the fuel. During the combustion, the sulfur is oxidized into sulphates. The various components can be found in different percentages depending on the engine type and engine load [13]. A general representation of the main constituents of the PM is shown in *Figure 1.3*.

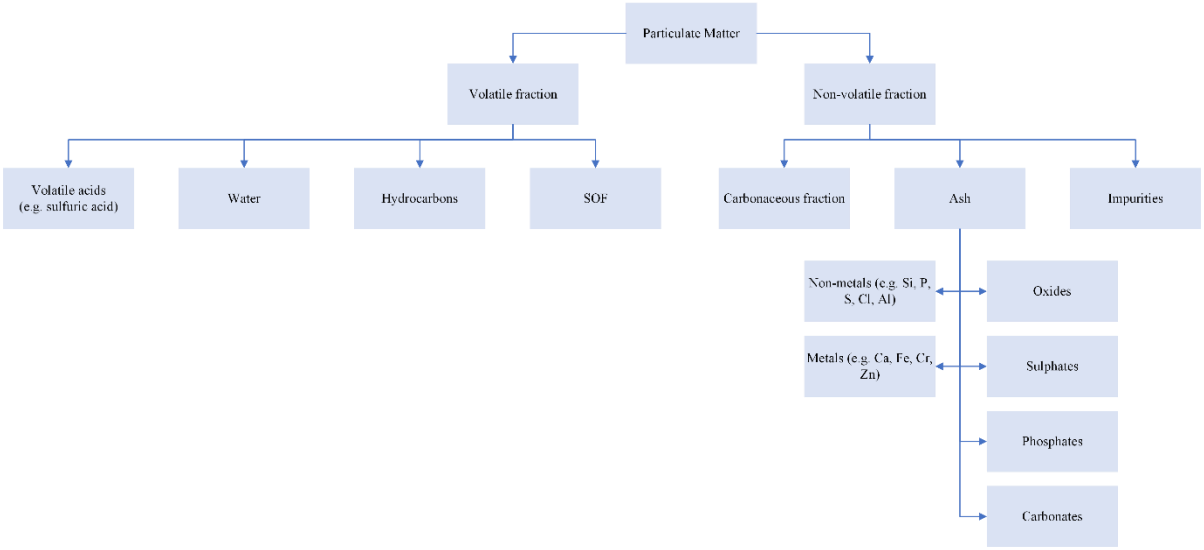

Figure 1.3 Schematic representation of the main constituents of the particulate matter ("adapted from [14], [15]")

Ash can be identified as incombustible material that remain in the DPF after regeneration. The elemental composition is highly variable, mostly due to fuel and lubricant formulations, duty cycles, operating environment, and possible fluid leakage. Analysis of the compounds reveals that the main constituents are metal oxides, sulphates and phosphates. The ash elements can be divided into four categories depending on their generation source, as briefly reported below. [16]

1. Lubricant oil-related: calcium (Ca) and magnesium (Mg) are oil detergents while zinc (Zn) and phosphorous (P) are the anti-wear additives, within the lubricant.
2. Engine corrosion and abrasion-related: the main component of this category is Fe, but also copper (Cu), aluminum (Al) and chromium (Cr) can be originated by this source.
3. Fuel and biofuel-related: biodiesel contains significant amount of sodium (Na) and potassium (K). Both significantly increase ash accumulation in the particulate filter, therefore there is currently a limitation of 5 ppm of Na and K combined in the fuel.
4. Other sources: ash can originate from coolant leaks, while trucks and engines working in mining environment are expected to contain a high amount of dust-related ash.

Each source comprise a different fraction of the final ash. The main contribution comes from metallic additives in the lubricating oil, and the most present elements are sulphates and phosphates of Zn, Mg and Ca. Generally, Ca, Zn and Mg make up between 30 and 40 per cent

in weight. Fe, resulting from engine wear and corrosion, accounts for 0.5-2%, while the sum of sulfur and elementary phosphates is around 20%. The weight percentage of atomic oxygen in ash is consistent in various instances and is approximately 40%. Na and K are negligible, except for biodiesel fuels. [16]

1.1.4 Particulate matter formation

The formation of solid particles, as well as their final composition, shape and size depend mostly on the temperature and the location within the system. The collected PM is affected by all the stages it goes through: the cylinder inside the compression engine, the injector, the exhaust system and the external environment.

In compression engines the creation of soot is a complex process that occurs in a matter of microseconds within the flame. Liquid fuel is sprayed through the nozzles of the injector and atomized due to high injection pressure. The small droplets will ignite producing particulate matter precursors. The air-fuel ratio distribution is heterogeneous within the engine. In the fuel-rich areas, in proximity of the flame center, pyrolytic reactions are favored. One of the main products of these reactions is acetylene [17]. Traditionally, those processes are favored when the temperature is between 1400 and 2800 K. [13]

Many details of soot formation are still unclear. However, it is widely accepted that under the operating conditions of the combustion chamber, aromatization from acetylene as the main precursor is thermodynamically promoted and allows the formation of polycyclic aromatic compounds (PAH). The polyaromatic rings are dangerous pollutants that can also be found as adsorbate on the formed soot particles and are harmful for human health. Subsequently to when PAH are formed, nucleation occurs. All the processes described take place within a short period of time (10^{-7}–10^{-5} seconds). Therefore, nucleation is likely to occur when the exhausts are still in the combustion chamber.

As the nuclei grow and agglomerate on the surface, they will create larger particles, identified as “spherules”. Spherules are building blocks for the future aggregated particles, resulting from the collision between particles. These particles, defined as primary particles, are typically close to a spherical shape and range in size from 20 to 50 nm, while the agglomerated particles can reach 0.1-10 μm in diameter [18]. The formation process is illustrated in *Figure 1.4*. In exhaust steam, the surface of the agglomerates may be coated with the volatile substances, resulting the formation of wet particles [14]. The last stage is the oxidation of particulate matter. This is a particularly important step, as it leads to a reduction in soot content. Soot oxidation takes place in the cylinder and can occur during any of the previous described stages of particulate evolution, from pyrolysis to agglomeration. Different species such as O, O_2, H_2O ,CO_2 and OH are able to oxidize the soot due to their proximity to the diesel flame. However, the principal oxidant in the stoichiometric flame zone is the OH radical, while in the lean zone this role is covered by oxygen radicals. [19]

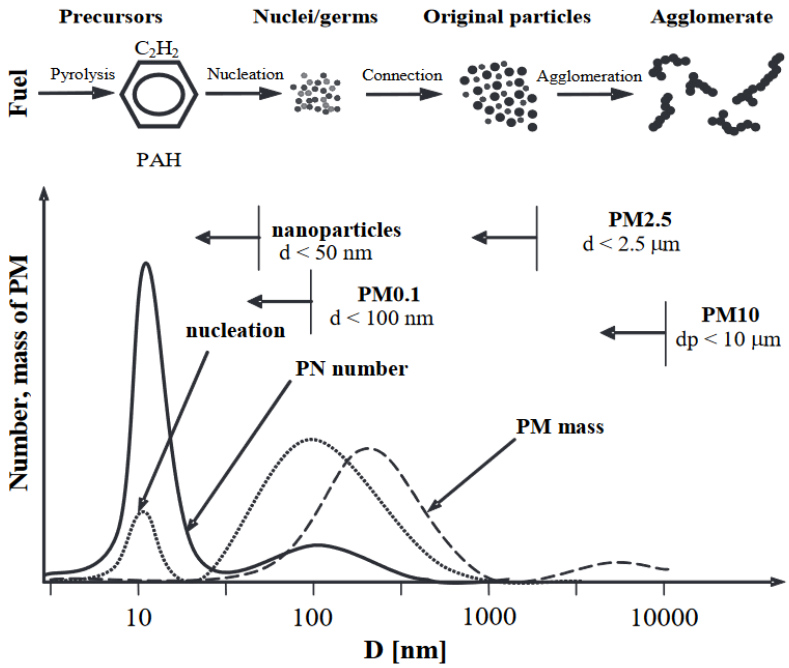

Figure 1.4 Commonly accepted pattern of particle formation and their size distribution [20]

Soot is not the only constituent of the particulate matter but it constitutes the backbone of the particles that are formed. Low-volatile hydrocarbons are adsorbed and condensed on this structure. These processes take place when the exhaust gases are cooled down and diluted in air. Low-volatility hydrocarbons are derived from unburnt fuel and lubricating oil. The contribution of lubricating oil has a significant impact on particulate mass. The contribution is larger at high vehicle speeds. [19]

Ash particles, which are small in size at the engine outlet, can be found within soot agglomerates. These particles are transported along with the soot particles throughout the aftertreatment system. The presence of ash in soot agglomerates has been confirmed by numerous studies. An example of the structure a solid particle may have at engine outlet is illustrated in *Figure 1.5*. Ash and soot can combine in different ways, according to mechanisms that have not yet been clarified. For example, the small ash particles may be embedded within or attached to the surface of soot agglomerates. [16]

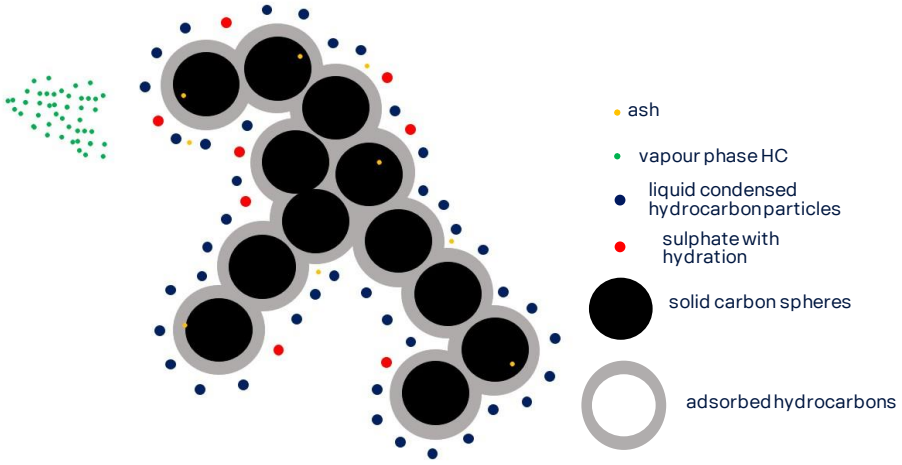

Figure 1.5 Schematic representation of the agglomerated solid particle (“adapted from [21])

Over long periods of time, the ash accumulates in the DPF and grow. The ash particles can reach up to 10 µm in diameter [22], exceeding the size of the soot agglomerates on which the individual ash nanoparticles were previously carried. The ash accumulation rate is between 0.4 and 1.1 mg/km for heavy-duty diesel engine truck on highway operation [16]. They can be removed from the DPF throughout filter cleaning.

1.1.5 Factors influencing particulate matter

The composition of solid particles varies depending on the fuel, additives and operating conditions. In addition, collection methods can also influence the observed results. [23] [24] [25]

Use of Biodiesel

The thrive for a more sustainable transport sector and the depletion of oil-derived fuel reserves in recent decades have fostered interest in the development of alternative fuels and the use of blends between fossil and bio-based fuels. Saturated and unsaturated methyl esters or ethyl esters containing between 12 and 20 carbon atoms in the carbon chain are the common biodiesel components [26]. Soot originated from biodiesel is characterized by a higher reactivity which is then reflected in a lower amount of PM emitted from the vehicle. The higher reactivity is a result both of smaller average particle size, that lead to a bigger surface available for reactions, and higher oxygen content [27]. From a morphological point of view, biodiesel soot is characterized as less ordered nanostructures and wider distance between graphene layers [28]. Furthermore, the number of agglomerated particles (50 - 1000 nm) decreases with the increase of biodiesel in fuel blends while the number of nucleation particles (<50 nm) increases [26]. A drawback of biofuel application results in a higher emission of NO_x. in most of the operative conditions, due to the higher oxygen content in these fuels [27] [29].

Fuel additives

Fuel additives such as cetane improvers, detergents, dispersants, lubricity improvers, and metal deactivators can reduce particulate matter emissions in diesel engines by improving combustion and reducing wear on engine components. Cetane improvers increase the cetane number of diesel fuel, leading to more complete combustion [30]. Detergents keep fuel injectors clean, improving combustion. Dispersants break up and disperse particles in the fuel, reducing particulate matter formation during combustion. Lubricity improvers improve the lubrication of diesel fuel, reducing wear on fuel injectors and other engine components. Metal deactivators prevent the formation of harmful metallic compounds in the fuel, reducing particulate matter formation during combustion. Metal fuel additives may be used to lower the concentration of the emitted particulate matter. Nevertheless, iron-based fuel additives might increase the number of the emitted nanoparticles [31]. Complex interactions between numerous factors, such as the engine type/model year, number of engine cylinders, and operating cycles, can make it difficult to determine how different fuel properties affect PM emissions [32].

Lubricant oil

Several studies have revealed a strong correlation between lubricant consumption and engine particulate emissions. With the lowering of PM emissions from fuels, lubricant-related emissions have grown in importance. Lubricants have high viscosities and complicated compositions that make evaporation, combustion and atomization difficult [33]. Lubricating oil mist can enter cylinders due to high pressure in piston rings and metal additives might convert to gas during combustion of oil droplets. These gases may condense onto carbon particles as exhaust gases cool, or form ash nanoparticles directly if the ash-to-carbon ratio is high [16]. Therefore, lubricants states as the primary source of ash that will accumulate within DPF and their amount and chemistry will affect the ash composition and properties.

Metal additives showed no major effects on the morphology of the exhaust PM. Nevertheless, different additives can improve the oxidation reactivity of soot by changing the nanostructure and graphitization degree of the emitted particles, potentially acting as a catalyst to promote the oxidation process. Zn-based additives slightly increase the mean soot diameter and increase the soot reactivity while Ca and Mo-based additives reduce the mean diameter of soot particles and decrease the particulate reactivity. Even if Ca and Mo should be able to promote oxidation reactions, they alter the physicochemical properties of the PM. In particular, that leads to more ordered structure and higher graphitization degree, hence lower reactivity. [33]

While some older commercial oils have about 2% inorganic content, newer oils contain about 1% ash. Therefore, for the same oil consumption, oils with different ash content will have an impact on the amount of PM emitted and the rate of ash accumulation in the DPF [34].

Operative conditions

It is crucial to note that the specific influence of operating conditions on PM emissions will be determined by the characteristics and operating conditions of the specific engine in question, and may thus differ from one engine to another.

When it comes to operating conditions, the impacts on emissions can be very different and it is difficult to make generalizations. The following are some known correlations, although

they do not have absolute validity. PM emissions tend to increase at high temperature cycles [1]. The proportion of ash production has been reported to be relatively low during high engine load situations, but much higher under low load modes such as idling and engine braking [16]. It has been demonstrated that increased injection pressure results in more complete combustion, leading in lower PM output. Increased injection pressure, though, causes an increase in NO_x production as effect of a higher temperature within the combustion chamber [35].

PM collection and analysis methods

The exhaust gas sampling system's design is crucial for delivering repeatable and reliable results. It is in charge of pre-conditioning the sample and minimizing physical and chemical changes to the species being examined. Exhaust gas can be sampled either diluted or undiluted and may require further conditioning prior to analysis. Diluted sampling involves diluting the exhaust gas with air to lower its temperature and concentration, while undiluted sampling involves collecting a sample of raw exhaust gas without dilution. The two most common types of dilution systems are full flow (constant volume sampling, CVS) and partial flow. The whole exhaust gas stream produced by the engine is mixed with air in the full flow system. In the latter case a sample of gas is collected from the raw exhaust and diluted with air in partial flow systems. [25]

The USEPA, *United States Environmental Protection Agency*, defines the particulate matter as the mass collected on a filter from a diluted and cooled down to 52 °C exhaust flow. Therefore, the position within the aftertreatment system, the time after the formation in which the particles are collected and the collection method are of a great impact on the resulting final composition. Several processes such as nucleation, condensation and adsorption occur transforming the volatiles previously in gaseous form in solids and liquids when the system is cooled. The extent of those phenomena is defined by how cooling and dilution are performed and thus alter the final composition. [36]

There is a potential for sampling-related concerns that could impact the accurate measurement of particulate matter. These issues may include coagulation, sample loss, deposition, and condensation of particles within the dilution tunnel and sampling system. For instance, prolonged sampling may lead to changes in the size and shape of particles due to the accumulation of fresh particles on top of older particles. Additionally, the design of the system may result in the deposition of some particles within the sampling system itself. It is important to consider these potential problems in order to ensure accurate and reliable measurements. [25]

1.1.6 Soot oxidation reactivity in literature

Within the system, the soot is reactive and changes through oxidative reactions over time. Soot reactivity is influenced by the composition and the physicochemical properties of the PM. The factors that might have an impact on the soot oxidation are divided into engine-related and uncorrelated. The engine-correlated factors include the fuel properties, engine operating conditions and the engine design. Referring to the operative conditions, when the engine run at a different speed and load the combustion conditions change enormously, therefore, it will produce a diesel PM with different microstructures. The uncorrelated factors are caused by aging, the atmosphere conditions the sample will face and even how an eventual thermogravimetric analysis (TGA) is conducted. Multiple studies have found that the oxidation reactivity of diesel soot is a complex result of several factors that cannot be attributed to a single variable such as nanostructure, particle size, or ash content. The outcome of oxidative reactivity is determined by the interaction of several parameters. Soot from biodiesel, for example, has a

higher degree of graphitization, which may lessen reactivity; yet, biodiesel soot is frequently more reactive due to smaller particle size [37].

Soot aging can be explained as a decrease of active sites on the soot surface due to local temperatures and residence time within the aftertreatment system. The mechanism of soot aging has not been completely understood, however, the studies conducted suggest that it can be related to the decrease of active C-H sites available for reactions. The effect is a decrease in reactivity for particle´s growth. [38]

The oxidative reactivity of soot can be assessed by the determination of kinetic parameters, such as activation energy (E_a), pre-exponential factor (A), and reaction rate constant (k), derived from experimental data collected by different thermal analysis methods. Thermogravimetric analysis (TGA) is extensively utilized for this purpose. The mass loss rate obtained from this analysis usually is represented as normalized values of the derivative of the degree of conversion (α) relative to the temperature (T). The degree of conversion is given in *Eq. 1.1*, where m_0 is the initial weight, m_t is the weight at time t, and m_∞ is the final weight. [39]

$$\alpha = \frac{m_0 - m_t}{m_0 - m_\infty} \tag{1.1}$$

The parametrized degree of conversion dα/dT can be expressed according to *Eq. 1.2* as a function of the reaction model $f(\alpha)$ and temperature through the reaction rate constant $k(T)$. The majority of kinetic models neglect the dependence on the pressure $h(P)$. The temperature dependence shown in *Eq.1.2* can be expressed through an Arrhenius-type equation, as presented in *Eq. 1.3*. The choice of the reaction model depends on the specific reaction studied and several reaction models can be found in the literature. [39]

$$\frac{d\alpha}{dT} = k(T) \cdot f(\alpha) \cdot h(P) \tag{1.2}$$

$$k(T) = A \cdot e^{-\left(\frac{E_a}{R \cdot T}\right)} \tag{1.3}$$

The model formulation depends on whether the experiment is performed in isothermal conditions, as shown in *Eq. 1.4*, or in non-isothermal conditions, *Eq. 1.5*. [40]

$$\frac{d\alpha}{dT} = A \cdot e^{-\left(\frac{E_a}{R \cdot T}\right)} \cdot f(\alpha) \tag{1.4}$$

$$\frac{d\alpha}{dT} = \frac{A \cdot p_{O_2}}{\beta} \cdot e^{-\left(\frac{E_a}{R \cdot T}\right)} \cdot f(\alpha) \tag{1.5}$$

In non-isothermal methods, rearrangement and integration of *Eq.1.4* yields *Eq.1.6*, where $g(\alpha)$ represents the integral form of the reaction model. This integral has no analytic solution and several numerical approximations have been proposed. In the case of isoconversional methods, which are also known as “model-free”, the integral can be expressed in a general form shown in *Eq. 1.7,* where $\beta = dT/dt$ is the chosen heating rate. In the latter equation, B and C are constants that depend on the approximation. In an isoconversional method, the conversion is

assumed to be a function of temperature only. The integral is solved for different values of α (usually $\alpha = 0.05\text{-}0.95$) and by obtaining the relative temperature for this conversion (T_α) from the weight loss curves. In this manner, the corresponding isoconversional activation energy (E_α) can be evaluated. [39]

Examples of isoconversional methods are the Kissinger-Akiha-Sunose (KAS) and the Flynn-Ozawa-Wall (FWO). The Murray-White approximation, with B=2 and C=1, leads to the KAS, while the Doyle approximation [41], with B=0 and C=1.052, leads to the FWO method. [39]

$$g(\alpha) \equiv \int_0^\alpha \frac{d\alpha}{f(\alpha)} = A \cdot \int_0^t e^{-\left(\frac{E_a}{R \cdot T}\right)} dt \tag{1.6}$$

$$\ln\left(\frac{\beta}{T_\alpha^B}\right) = const - C \cdot \left(\frac{E_\alpha}{R \cdot T_\alpha}\right) \tag{1.7}$$

1.1.7 Factors affecting the thermogravimetric analysis (TGA) results

Several factors may affect the thermogravimetric analysis and be a cause for not alike results. The two general shortcomings associated with the use of TGA for characterizing the soot oxidation reaction are the dependence of kinetic parameters on experimental conditions and the possibility that under certain operating conditions the reaction is diffusion-controlled. The final results might be influenced by the amount of adsorbed volatiles, the initial sample´s mass, the air flow rate, the heating ramp and the type of crucible. The volatiles affects the final oxidation temperature. When the hydrocarbons condense on the soot surface, this decreases the amount of available surface for the oxidation and hence the oxidation temperatures are shifted towards higher temperatures for wet soot, if compared with dry soot. Performing a devolatilization, allows to obtain more accurate kinetic results since the effect of the hydrocarbon´s condensation will not be present. Working with a small amount of sample, generally below 1 mg can negatively affect the repeatability of the experiment. Contrarily, sample with high initial mass, is characterized by a thicker layer on the crucible and its oxidation may be dominated by diffusive effects. The results might also be affected by the air flow rate. Below a certain threshold the amount of oxygen can be not sufficient to perform the oxidation at the defined temperature. What mostly affects the results is the selection of the heating ramp. Using low ramps, allows to improve the resolution and thus more accurate results. [42] [43]

1.2 Work motivation, research questions, methodology and thesis delimitations

Optimization of the DPF is a crucial aspect in the development of more effective emissions control strategies for heavy-duty vehicles in order to meet the incoming more stringent emission regulation, that further limit the number of emitted particles. In this framework, the understanding of soot oxidation kinetics and ash content are relevant for several reasons: The DPF has to be optimized, extensive research has been conducted in this field, which has highlighted the necessity of employing multiple models to achieve an improved DPF performance. It is important to understand what kind of particulates can be suitable to mimic real road condition emissions to optimize the tests as a first step to develop valid models. Additionally, it is important to comprehend the nature of particulate matter (PM) that the DPF

is likely to encounter across various points of the engine map. A comprehensive understanding of the quantity and build-up of ash and soot that accumulates within the DPF can provide critical insights into optimizing regeneration strategies, which aims to burn the soot fraction. To address these needs, the following research questions can be formulated.

1. What is the ash to soot ratio in heavy-duty diesel engines during different operative conditions?
2. Is soot oxidation reactivity similar or different for various engines and operative conditions?
3. Which experimental techniques are more suitable to characterize the ash samples?
4. How the collection methods and sample's handling affect the final results and which is the most suitable way to obtain reliable data in terms of oxidation reactivity, ash to soot ratio and ash composition?

The study involved multiple stages, starting with a comprehensive review of existing literature in the field. Different experimental techniques were analyzed to understand which can better suit the samples. In particular, a broad study on thermogravimetric analysis (TGA) was conducted to define the most suitable heating program and pre-run preparations, such as sample holder cleaning. Small samples, below 1 mg, were tested to study the repeatability of the results while working on the lower side of the equipment sensitivity. Another part of the research focused on the reduction of the contamination of the samples by filters used for PM collection and the development of an extraction technique to lower those contaminations. To estimate the kinetic parameters of the soot oxidation reactivity, MATLAB was employed. The project changed dynamically throughout time, adapting to new discoveries and by facing different challenges.

The aim of the thesis was to investigate a suitable approach to obtain the target goals. Due to the project being broad and the limited amount of samples, the repeatability have to be investigated throughout future works. While the characterization work performed in the laboratory environment was controlled, the samples itself were collected from the engine test beds where other experimental works were carried out in parallel. For this reason, the samples were affected by multiple uncontrollable factors such as residues from past tests. Besides, several variables as for example fuel, lubricant oil and operating cycles were defined by the needs of other experimental set-ups carried out while the samples of this research were collected. The absence of adequate flexibility in defining and controlling all operational conditions, combined with a limited samples availability, has posed significant challenges in formulating a conclusive statement with a high degree of confidence. Each of the investigated areas requires deeper focus and further tests to validate the obtained results.

1.3 State of art of the research in the field

To address the research questions, a comprehensive review of the current state of research in this field was undertaken.

1.3.1 Ash fraction evaluation

The literature about engine exhaust particles composition puts a focus on the results from WHTC test. During a WTHC the engines are subjected to acceleration, deceleration and idle conditions. This operation causes continuous changes of diameter, surface area and composition of the particles as the particles are not collected during the different phases. What happens

instead is that the diesel exhaust accumulates of a filter during the whole cycle and is analysed only at the end. This makes it challenging to understand which conditions have a greater impact on the particulate formation and which is the soot/ash ratio in transient conditions. The average emission of PM after a WHTC cycle for a heavy-duty diesel engine have a composition similar to the one shown in *Figure 1.6*.

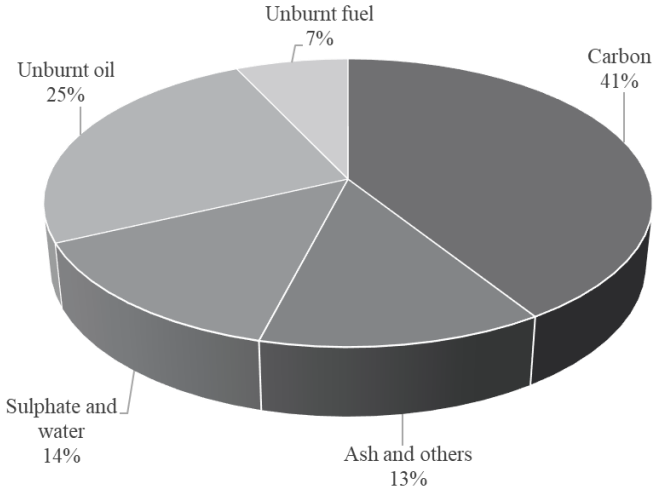

Figure 1.6 An example of composition of the particulate matter in a diesel engine ("adapted from [36]")

The estimation of the ash fraction is commonly derived from the prescribed operational conditions defined by certification cycles, but its applicability to other points on the engine map may not have been thoroughly evaluated. Even though the estimation of the amount of ash might be critical for a better regulation of the DPF regeneration, that currently is mainly assessed by measuring the pressure drop downstream the filter. The pressure drop however, does not allow to distinguish between solid deposits of ash and of soot. Some examples from the literature regarding the evaluation of ash fraction in different operative conditions are presented below.

The measure of a pre-DPF PM composition determined by thermogravimetric analysis (TGA) was performed by A. Sappok [44] showing an ash fraction of 0.5% and a combustible fraction of 87.2% in weight, which result significantly lower if compared with the ash fraction from certification cycles, as for example presented in *Figure 1.6*.

Another result of the ash fraction can be found in the work of S. Bagi [45], who collected diesel soot on filters before the aftertreatment systems of a 6-cylinder engine under the same driving conditions and performed TGA to evaluate the fraction of incombustibles, which was determined to be 3.12% by weight.

M. Zhang [46] had analyzed the PM composition obtained under three different operating conditions. The first condition (low speed, high load) and the second condition (high speed, low load) resulted in an ash fraction below 0.5% and a carbon fraction of 91 and 85%, respectively. The third condition (high speed, high load) produced an ash fraction of 1% and a combustible fraction of 92%. PM was collected on quartz filters, extracted and analyzed by TGA.

1.3.2 Soot oxidation kinetics: kinetic parameters evaluation

Various kinetic parameter results can be found in the literature, obtained with different engines, operating conditions and modelling methods. Typically, activation energy for engine diesel soot ranges between 80 and 200 kJ/mol [40] [42] [47]. An overview of some of them is shown in *Table 1.2*. The study presented in the first row of the table, analyses soot collected between the DOC and the DPF. Naturally, the reactivity of the soot collected after the DOC will be lower if compared to the pre-DOC soot due to aging and a higher degree of graphitization. The study described in the third row of *Table 1.2* is carried out by collecting soot on a filter and then extracting it with a solvent.

Table 1.2 Review of kinetic parameters (E_A, A and k_c) obtained in literature with thermogravimetric analysis, characterizing exhaust diesel soot

Engine	Engine conditions	Fuel	Kinetic parameters			Methods/ models	Oxidation atmosphere [vol%]	Reference
			A $[\frac{1}{Pa \cdot s}]$	E_A $[\frac{kJ}{mol}]$	k_C $[\frac{1}{Pa \cdot s}]$			
4- cylinder 2.0 L	1667 rpm 78 Nm	Diesel	1.16	113	$8{,}3 \cdot 10^{-9}$ at 450°C	Arrhenius	Air	J. Rodríguez-Fernández [43]
6-cylinder 6.9 L	2400 rpm 156 Nm	ULSD 20% Biodiesel	-	120 119	$2.6 \cdot 10^{-8}$ $3.2 \cdot 10^{-8}$ at 500°C	Arrhenius	Air	J. Song [48]
4-cylinder 2 L	1400 rpm	Diesel	-	145	-	Arrhenius	10% O_2 90% He	J. Wei [49]
6-cylinder 6.9 L	-	Diesel	-	160	-	Free-model	5% O_2 95% N_2	J.O. Müller [50]
Cummins ISX 15L	-	Diesel	-	139	-	Free-model (KAS)	10% O_2	C. Su [51]
-	-	Diesel	$2.8 \cdot 10^{7}$	161	-	Arrhenius	4.5-22% O_2	M. Kalogirou [52]
4-cylinder 2L	-	ULSD	$3.9 \cdot 10^{6}$	141 ±7	-	Arrhenius	2.7-24.4% O_2	C. J. Tighe [53]

In the literature, experiments are often carried out using a synthetic soot referred to as Printex-U. This soot is composed of carbon black and exhibits a higher degree of graphitization [54], which can result in higher activation energy estimates compared to diesel exhaust soot. *Table 1.3* displays some kinetic studies performed on Printex-U.

Table 1.3 Review of activation energy evaluations obtained in literature with thermogravimetric analysis, characterizing carbon black (Printex-U)

Ea $[\frac{kJ}{mol}]$	**Model**	**Oxidation atmosphere [vol%]**	**Reference**
175	Friedman	10% O_2 90% N_2	S. Jian [55]
145	KAS	10% O_2 90% N_2	C. Su [51]
136-221	Arrhenius	Air	Z. Meng [56]

The oxidation behaviors of diesel soot can be described through characteristic temperatures that synthetically report the main features of an non-isothermal thermogravimetric curve and might allow an easier comparison between different samples. Those temperatures are starting oxidation temperature (SOT), final oxidation temperature (FOT), maximum mass loss rate temperature ($MLRT_{max}$), T_{10} and T_{90}, respectively corresponding to the temperatures equivalent to the sample mass loss of 10 and 90 percent during the oxidation step. In *Table 1.4* several examples of the characteristic exhaust soot temperatures are listed. It is noteworthy to mention that variations in heating rates and oxidation conditions can cause the oxidation temperatures to change slightly, resulting in different values reported in the literature depending on how the experiments were conducted.

Table 1.4 Literature review of characteristic oxidation temperatures T_{10} (sample mass loss of 10%), MLRTmax (maximum mass loss rate temperature), T_{90} (sample mass loss of 90%) describing exhaust soot weight loss results

Reference	**Details**	**T_{10} [°C]**	**T_{MLRT} [°C]**	**T_{90} [°C]**
H. N. Sharma [42]	Diesel fuel	499-541	607-640	647-685
X. Liang [57]	Diesel fuel	-	573-608	-
D. Zhang [58]	Diesel fuel	-	590-615	-
J. Rodríguez-Fernández [43]	Diesel fuel	277-306	441-474	539-577
J. Rodríguez-Fernández [43]	Biodiesel fuel	226-266	330-448	448-545
J. Gao [47]	Review of multiple studies	150-595	-	500-685
Z. Meng [56]	Printex-U, heating rate 10 [°C/min]	521	587	588

1.3.3 Ash composition

Extensive literature discusses the common compounds generated by CI engines and several estimations of their quantitative abundance in the ash can be found, as presented with some examples in *Table 1.5,* where the elements are considered in compounds and *Table 1.6,* where the abundance of the single elements is showed. The main compound is typically $CaSO_4$ while relevant components can be $MgSO_4$, Zn_2P_2O, $Mg_2P_2O_7$, $MgZn_2(PO_4)_2$, $CaZn_2(PO_4)_2$ [16]. Those compounds can be identified by X-ray fluorescence (XRF) and X-ray diffraction (XRD). Nevertheless, the composition is commonly estimated from ash collected from DPF. This ash is easier to collect because of the high amount deposited on the filter, but is the result of the entire history of lubricant oils and operative conditions the filter witnessed.

Contrarily, the analysis of the composition of ash collected from ongoing operations over a short period of time is challenging since it involves working with extremely small amounts that are difficult to isolate, highly likely to be contaminated and heterogeneous.

Table 1.5 Ash composition in literature: weight percentage of metallic oxides in ash collected from DPF

Compound [wt%]	**Ash A** G. A. Merkel [15]	**Ash B** J. A. Mcgeehan [59]	**Ash C** A. Sappok [60]	**Ash D** A. Liati [61]	**Ash E** A. Liati [61]	**Ash F** D. M. Young [62]
CaO	29.6	23.2	10.7	9.2	10.2	27.6
ZnO	9.9	12.7	28.4	7.9	9.0	8.2
MgO	5.5	2.3	8.8	9.4	9.6	1.7
SO_3	38.8	34.1	16.7	19.2	27.5	-
P_2O_3	15.8	15.2	22.3	14.1	12.3	10.4
Fe_2O_3	0.41	3.1	-	17.2	7.9	1.6

Table 1.6 Ash composition in literature: elemental composition of field ash collected from DPF

Element [wt%]	**Ash 1** J. A. Mcgeehan [59]	**Ash 2** J. A. Mcgeehan [59]	**Ash 3** J. A. Mcgeehan [63]	**Ash 4** A. Liati [64]	**Ash 5** S. Bagi [45]
Ca	20.4	22.0	16.8	3.3	9.8
Zn	10.0	10.0	10.7	2.8	6.4
Mg	0.35	0.2	5.3	10.9	0.4
S	14.6	15.6	11.4	10.9	2.6
P	6.9	6.9	9.8	2.1	2.0
Fe	1.3	1.9	1.5	0.9	5.3
K	0.1	0.1	-	-	1.9
Na	0.9	0.9	0.2	1.1	

1.3.4 Samples handling

Diesel particulates are emitted in a gaseous stream from the engine. Therefore, a step behind its analysis is to develop efficient methods to collect the particulate matter. A common approach [65] is to dilute a portion of the exhaust stream with air and pass it through filters. The PM accumulates on the filters and can then be analyzed. Several filters are available for such purposes and have been used in research in this area. Examples of available filters include: Teflon-coated fiberglass [45], pure fiberglass [58], pure Teflon [49], and quartz filters [57].

The choice of filter depends on the research endeavor. Polytetrafluoroethylene (PTFE) is not recommended for use above 250 °C, so it is advisable to avoid Teflon and PTFE-coated filters when thermogravimetric analysis (TGA) or other thermal methods using higher temperatures are involved. [66] Quartz filters, meanwhile, can be used for kinetic studies, as has been done by X. Liang [57], since the fibers do not lose weight below 1000 °C [67].

Removing the PM from the filters can be challenging because of the small amount of fine particles deposited on the filter fibers and the possibility of contamination by the filter fibers. For this reason, several extraction methods have been developed to separate the PM from the paper filters or to characterize the polycyclic aromatic hydrocarbons (PAH) adsorbed on the surface of the PM, such as Soxhlet extraction with toluene [68]. Alternatively, the PM can be scraped from the filter surface, as was done by S. Bagi [45], who also aided the separation by gently tapping the filter.

Some authors mention that the non-combustible residue after TGA analysis may contain contamination [43] [69], nevertheless the critical discussion of the contaminations affecting PM characterization has not been fully assessed.

1.4 Thesis structure

The thesis is structured in four chapters. Chapter 1 introduces the problem and describes the background of the investigation. It presents the research questions and correlates them with a comprehensive review of the relevant literature, showing the state of the art of research in this field and the method of investigation used in subsequent sections. Chapter 2 presents all the experimental set-ups and describes the methodology for each analysis. The results are presented and discussed in Chapter 3, which is divided into sections that aim to critically discuss the results in relation to the research questions. Lastly, Chapter 4 exposes the final conclusions that can be drawn from the study and recommendations for future researchers in this field.

Chapter 2

Experimental

The experimental procedures that are described in this chapter cover the collection and the analysis performed on the exhaust diesel particulate matter. Particulate samples were collected from engine test cells by means of a partial flow dilution system (PFDS). Samples were collected on glass fiber (Pallflex TX40HI20), quartz (Pallflex Tissuquartz) and Teflon (Teflo2µm) filters. Characteristics such as soot concentration in the exhaust flow and particulate number concentration were assessed with a micro soot sensor (MSS) and an aerodynamic particle counter (APC), respectively. The samples collected on fiberglass filters were extracted with cyclohexane and the solvent was analyzed with a liquid gas chromatography (GC). Additionally, two soot samples were scraped off from the silencer's inlet to the aftertreatment system. Then, all the samples were characterized with TGA, and scanning electron microscopy (SEM) coupled with an energy dispersive x-ray spectroscopy (EDS). Additional analysis such as X-ray diffraction (XRD) and inductively coupled plasma (ICP) were employed for limited samples.

2.1 Engine details

Several engines were utilized in the research, they were an Euro V 6-cylinder (550 HP) and an Euro VI 8-cylinder (650 HP) engines with an XPI fuel injection system. A sample from a 5-cylider (360 HP) engine was analyzed as well. The details relative to the fuel and lubricant oil are synthetized in *Table 2.1* and *Table 2.2*. The employed fuels were ultra-low sulfur diesel. In all the engines the EGR system was not active.

Table 2.1 Diesel fuel specifications for heavy-duty vehicles employed during the collection of the PM

Name	**B07**	**B0**
Description	Used for certification of Euro VI engines. It contains 7% of RME and does not have detergent within.	Used for certification of Euro IV and Euro V engines. It does not contain RME or detergents.
Fuel specification	1546061-35	1546061-3
Density at 15 °C [Kg/m^3]	833-837	833
Cetane number	52-56	52-54
Distillation T50 [°C]	245	245
Distillation T95 [°C]	345-360	345-350
FBP [°C]	370	370
CFPP [°C]	-5	-5
Kinematic viscosity at 40 °C [mm^2/s]	2.3-3.3	2-3-3.3
Sulphur content [mg/kg]	10	10
Water content [%(w/w)]	0.02	0.02
Ash content [%(w/w)]	0.01	0.01

Table 2.2 Lubricant oil specifications

Name	LDF-5 5W-20	LDF-3 10W-40
Description	Scania´s newest heavy-duty diesel oil, characterized by a lower ash content.	Scania´s heavy-duty diesel oil, valid for Euro V and Euro VI engines with an after-treatment system.
Ash content [%]	≥1	≥1.9

2.2 Experimental engine test cell and sampling details

The exhaust from the engine is diluted with controlled, cooled, dry, hydrocarbon-free dilution air. This flow rate must be proportionate to the engine exhaust gas flow rate. To manage the response time and temperature, the dilution chamber is situated close to the exhaust source. A dilution of 5:1 was employed. The entire flow through the filter is measured by a second mass flow device within the PFDS. [25]
The experimental set up, as shown in *Figure 2.1,* includes an AVL 472 SPC, a partial flow dilution system approved for the collection of exhaust particles from internal combustion engines, a MSS and an APN, for an on-line analysis of the soot concentration and particle number detection during the test.

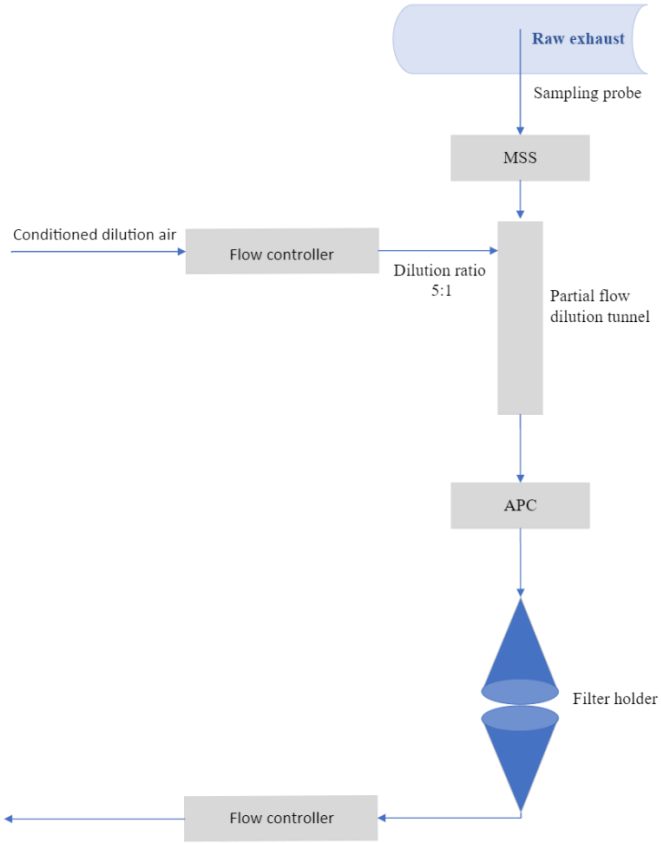

Figure 2.1 Experimental set up PFDS [25] coupled with a micro soot sensor (MSS), an aerodynamic particle counter (APC) and a filter holder containing the filter for each sampling

The samples of PM were collected from different operative conditions, *Table 2.3* summarize the conditions under which the different samples were collected, while *Table 2.4* presents the details on the sample "pressure sweep", which was collected on multiple filters. Ulterior details relative to the samples and the cycles are reported in the Appendix A and B.

Table 2.3 Detailed description of the samples collected with information about the vehicle engine, ash concentration in weight in the lubricating oil, and combustible used

Sample name	Engine	Lubricant oil	Fuel	Description
STD5	6-cylinder	1% ash	B0	Engine´s durability cycle. The sample was collected on 2 filters, each collection time was of 3h. On fibre glass filter.
900 rpm	6-cylinder	1% ash	B0	Alternation of engine working at 900 rpm with full load and shout downs, every few seconds. On fibre glass filter.
1700 rpm	6-cylinder	1% ash	B0	Alternation of engine working at 1700 rpm with full load and shout downs, every few seconds. On fibre glass filter.
2300 rpm	6-cylinder	1% ash	B0	Alternation of engine working at 2300 rpm with full load and shout downs, every few seconds. On fibre glass filter.
Oil consumption	6-cylinder	1% ash	B7	Engine´s oil consumption test. The sampling lasted 4h. On fibre glass filter.
Pipe 5-cylinder	5-cylinder	-	-	Scraped deposit from the silencer´s inlet.
Pipe 8-cylinder	8-cylinder	1.9% ash	B07	Scraped deposit from the silencer´s inlet. The sampling was performed 3 days after cleaning the section.
Pressure sweep	8-cylinder	1.9% ash	B07	Gradual decrease in speed from 1800 to 860 [rpm] in 1h.
Soot loading	8-cylinder	1.9% ash	B07	Test at 1600 [rpm] and 600 [Nm] for 1h. On quartz filter.
Soot regeneration	8-cylinder	1.9% ash	B07	Test at 1800 [rpm] and full load, similar to conditions observed during DPF regeneration. On quartz filter.

Table 2.4 Pressure sweep samples details

Pressure sweep 1h	Gradual decrease in speed from 1800 to 860 [rpm] in 1h. On quartz filter.
Pressure sweep 2h	Gradual decrease in speed from 1800 to 860 [rpm] for 2 times, 2h of sampling. On quartz filter.
Pressure sweep (warm)	Gradual decrease in speed from 1800 to 860 [rpm], the engine was already warm when the sample was collected, approximately 1h of sampling. On quartz filter.
Pressure sweep (Teflon)	Same conditions of "Pressure sweep 1h" but on a Teflon filter.

2.3 Micro soot sensor (MSS)

Exhaust flow soot concentration was detected by the AVL 483 MSS and it can be reported as shown in *Eq. 2.1*, where $Q24$ is the exhaust flow rate in [kg/h], MSS the instantaneous measured soot concentration in [g/m^3] and ρ_{air} is the density of air at 0°C.

$$soot\ concentration\ \left[\frac{g}{h}\right] = \frac{Q24 \cdot MSS}{\rho_{air}(0°C)} \tag{2.1}$$

2.4 Aerodynamic particle counter (APC)

Particulate number is evaluated by the particle counter AVL 489 APC advanced. *Eq. 2.2* allows to visualize the concentration of the particles. The multiplicative factor 5 eliminates the effect of the dilution within the set-up where particles are sampled while APC is the particle´s concentration expressed as [#/m^3].

$$particles\ concentration\ \left[\frac{\#}{h}\right] = \frac{Q24 \cdot APC}{\rho_{air}(°C)} * 5 \tag{2.2}$$

2.5 Thermogravimetric analysis (TGA)

To study the ash to soot ratio and the reactivity of the soot a thermogravimetric analysis was performed with the Perkin-Elmer TGA 8000, the details are described in *Table 2.5*.

Table 2.5 Detailed specifications of the Perkin-Elmer TGA 800

Ambient temperature [°C]	35
Resolution [mg]	0.01
Sensitivity [°C]	± 0.1 °C
Crucible´s inner diameter [mm]	7
Crucible´s height [mm]	2
Max temperature [°C]	1200
Temperature control range [°C]	20-1200

The heating program, described in *Table 2.6* and graphically presented in *Figure 2.2*, is composed by multiple phases. An initial heating up to 400 °C aims to evaporate the volatile organic fraction (VOF). This conditioning step is fundamental to perform for a more accurate soot reactivity analysis. Eventual condensed elements inside the porous structure of the PM might reduce the available area and hence lower the reactivity. The temperature was held for 60 minutes. Subsequently, soot oxidation was performed through a temperature ramp and with an oxidizing atmosphere composed of 10% of oxygen in nitrogen. Even though it is common in literature to find oxidation with air, the experiment aims to mimic the oxidation conditions in the exhaust of diesel engines, where the oxygen content ranges between 5 and 15 per cent [70].

Table 2.6 Heating program, composed by 9 steps, and employed during the TGA analysis for the experimentally collected samples

Step	Description of the action occurring
1	Initial atmosphere Nitrogen 100 [mL/min]
2	Isothermal for 10 [min] at 50 [°C]
3	Ramp with ramp rate β=10 [°C/min] from 50 [°C] to 400 [°C]
4	Isothermal for 60 [min] at 400 [°C]
5	Cool 10 [°C/min] from 400 [°C] to 50 [°C]
6	Isothermal for 10 [min] at 50 [°C]
7	Changing atmosphere to Oxygen 10 [mL/min] and Nitrogen 90 [mL/min]
8	Ramp with ramp rate β= 3, 5 or 10 [°C/min] from 50 [°C] to 800 [°C]
9	Isothermal for 60 [min] at 800 [°C]

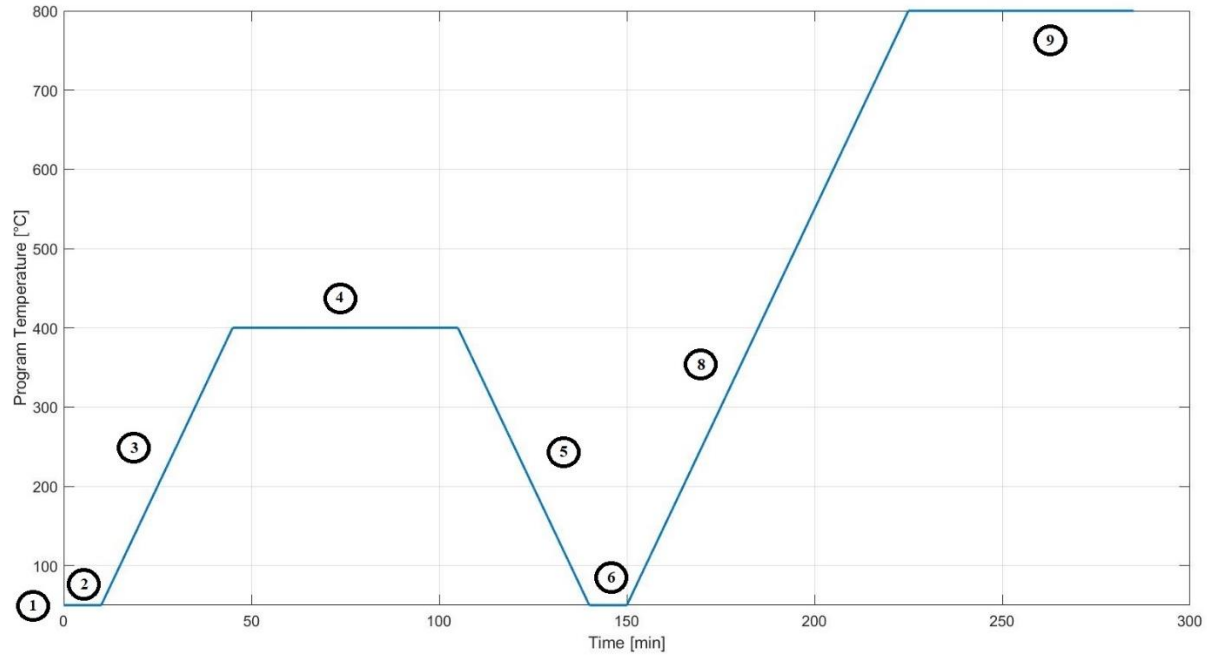

Figure 2.2 Heating program employed during the TGA of the research samples

Samples with limited availability (STD5, 900 rpm, 1700 rpm, 2300 rpm and oil consumption) were oxidized with a ramp rate β= 5 °C/min after being extracted with cyclohexane from the filters and dried. The extraction procedure is reported in the Appendix C. The remaining samples were oxidized by using 3 different heating ramp rates, equal to 3, 5 and 10 °C/min in order to study the kinetics of the oxidation. The samples deposited on the inlet of the silencers were removed from the metal surface and placed in the TGA pan with no extraction process involved. Samples actively collected during operation of the 8-cylinder engine were collected on quartz filters and analyzed on the filter. Each sample consisted of two 5.5 mm diameter filter discs with the PM deposited on it. The dimension was tailored to be placed in the pan of the TGA. The employed procedure is visually presented in *Figure 2.3*.

Figure 2.3 Preparation of the samples collected on quartz filters for kinetic studies and procedure employed for TGA

Non-isothermal tests were preferred for the extraction of kinetic data. The main advantage of ramping results is the possibility to cover the entire temperature window where the reaction occur with one test. In that way, the parameters can be estimated without the necessity to perform the same experiment multiple time at different temperatures as it is on contrary required

for the estimation from isothermal tests. [43] Alumina crucibles was preferred to the platinum ones since platinum might have a catalytic effect on the soot oxidation reaction and therefore spoil the results.

Preliminary to each test, a blank sample TGA was performed. It consists in carrying out a TGA with the same heating program to an empty crucible. This aims to eliminate the systematic error due to upward buoyant force. When the temperature increases, the density of the air surrounding the sample decreases, reducing the buoyancy force and therefore the sample will appear heavier. [39] Additionally, prior to use, each crucible was cleaned with a gas burner to reduce the influence of cleanliness and handling on the analysis outcome.

The evaluation of non-isothermal runs with different heating rates (β) allowed to perform the calculation of the kinetic parameters by applying the FWO isoconversional method. For such purpose, the expression in *Eq. 1.7* can be re-written as *Eq.2.3*. [42]

$$log\beta = log\left(\frac{Ap_{O2}E_a/R}{-\ln(1-\alpha)}\right) - 2.315 - 0.457 \cdot \frac{E_a}{RT} \quad (2.3)$$

2.6 Gas chromatography (GC)

The Agilent 8890 GC was employed to perform a liquid gas chromatography on the solvent from PM extraction. The target was to investigate any hydrocarbons adsorbed during the process. To account for possible contamination of the sample due to the filter itself, a solvent placed in contact with a clean filter was also analyzed.

2.7 Scanning electron microscopy and energy dispersive spectroscopy (SEM-EDS)

Zeiss Sigma VP electron microscope was used to reveal morphological features of the collected particles with high magnification and resolution. The particulate, prior to any kind of manipulation, was glued to the stub by using a double-sided adhesive carbon tape. Tactlessly, the analysis may lead to emphasize the presence only of bigger particles: the smaller particles penetrate deeper in the particulate cake formed on the filter while big particles set on its top. [71]

Each sample was analyzed with SEM-EDS also after the thermogravimetric analysis. The objective was to investigate in detail the morphology of the ash particles through microscopy and to characterize the elemental composition through energy-dispersive X-ray spectroscopy. To perform the EDS, the electrons were accelerated to a potential of 20 kV and the working distance between the sample and the EDS detector was set at 12 mm. Whereas different working distances and potentials were applied during microscopic analysis to enhance the visual effect.

2.8 X-Ray diffraction (XRD)

X-ray powder diffraction was performed with Bruker XRD D2 Phaser on the ash of sample "Pipe V8", as it was the only sample after TGA with sufficient weight to perform the analysis. The sample was placed on a pure silicon sample holder that allow analysis of small weights, even below one milligram. Isopropanol was employed as solvent to disperse the particles on the surface of the sample holder. The total measuring time was nine hours: a long scan time was selected to improve peak resolution.

2.9 Inductively coupled plasma (ICP)

ICP, as well as EDS, are commonly utilized to analyses the ash elemental composition, in order to identify ash sources and their relative contributions [16]. Therefore, a sample equivalent to "pressure sweep 1h" was collected and sent for an external ICP analysis at ALS Scandinavia AB. The PM-loaded quartz filter, due to the limited amount of particulate present, was not subjected to any kind of pre-treatment, such as removal of adsorbed HC through conditioning, in order to reduce any handling losses. Therefore, the soluble organic fraction was not estimated for this sample. The filter was dissolved in a mixture of in HNO_3, HF and H_2O_2 in a closed Teflon vessel in a microwave oven and the concentration of metals was examined. The purpose of the analysis was to indirectly estimate the ash content from the amount of relevant elements detected.

Chapter 3

Results and discussion

This section provides a comprehensive summary of the major findings of the current investigation, which aimed to undertake a critical examination of diesel particulate matter from various perspectives. Specifically, the emission rate and weight of particles were evaluated during their collection via APC and MSS, yielding valuable insights into the correlation between engine operational conditions and emissions. Visual inspection of the PM was conducted with SEM throughout the project, providing an opportunity to observe the particles and formulate various hypotheses. In addition, the reactivity of the soot was investigated by studying the characteristic temperatures and calculating the kinetic parameters through an isoconversional method. The composition of the ash, residual after TGA was analyzed by integrating ICP, XRD, and EDS. The ash fraction was studied for a limited number of samples and discussed in relation to existing literature. Finally, a thorough critical analysis of the influence of sample handling on the obtained results is presented.

3.1 PM emissions during ongoing operations: Aerodynamic particle counter (APC) and soot concentration (MSS) measurements

The emission of particles poses significant challenges to public health and environmental protection. It is therefore essential to identify the conditions that lead to high emissions of particles to facilitate the development of effective mitigation strategies. In this regard, this section of the study examined the factors that contribute to high particle emissions and their implications for engine design and operation.

The data collected by the AVL PUMA 2 testbed automation system were analyzed in the software Concerto. The results for the samples soot regeneration, soot loading, and pressure sweep are presented respectively in *Figure 3.1*, *Figure 3.2* and *Figure 3.3* and summarized in *Table 3.1*. During the pressure sweep sample testing the APC worked only for a short part of the test, therefore, the results are just partial. The specific values of fuel consumption are omitted for confidentiality reasons. Even if those results are important to expand the knowledge of the emissions in different operating points, the particulate number emissions do not consider the particles below 23 nm because of the equipment limitation. Solid particles below 23 nm, such as particles down to 10 nm (PN10) are currently part of the unregulated emissions, however, represent a not negligible part of the emissions for heavy-duty vehicles, according to the literature. [72]

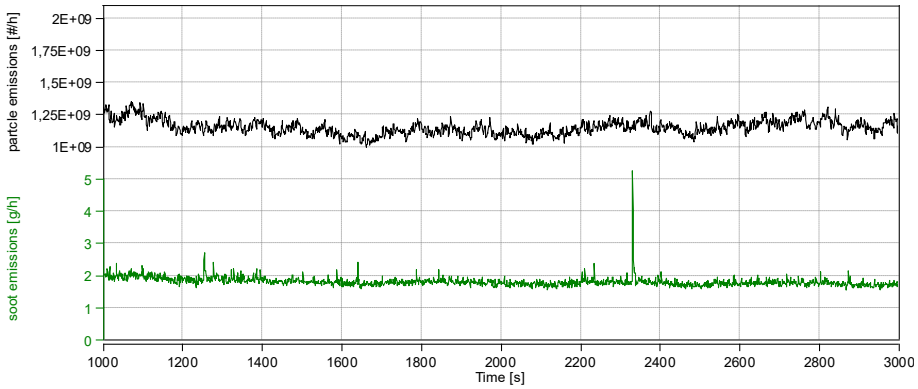

Figure 3.1 Soot and particulate emissions during the collection of the sample "soot regeneration" versus cycle time [s]

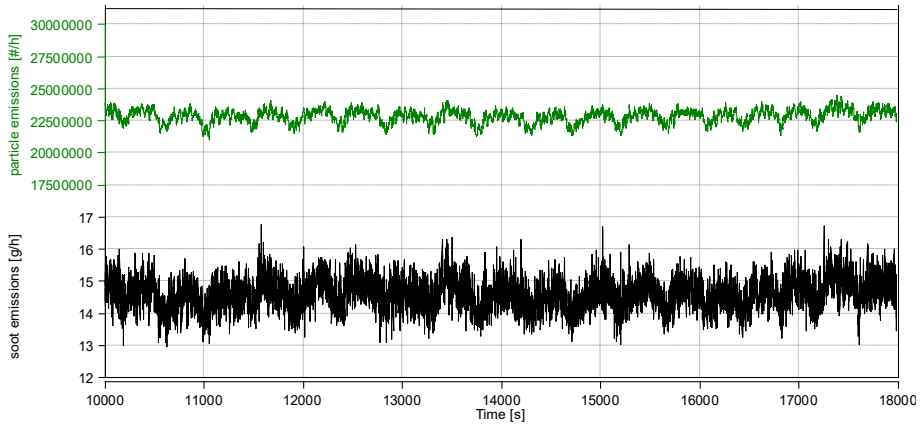

Figure 3.2 Soot and particulate emissions during the collection of the sample "soot loading" versus cycle time [s]

From in *Figure 3.1* and *Figure 3.2* is evident that when the engine runs in static conditions, the emissions, in terms both of soot concentration and particle number, result approximately constant. The specific values of the emissions change between the two operative conditions because of different fuel consumption, exhaust temperature and loading for the two distinct samples. Medium and low loads are correlated to higher ash and soot emissions while high load operations produce lower emissions. Furthermore, it is possible to observe that lower fuel consumption is correlated to higher soot emissions.

The "soot regeneration" sample was collected during active regeneration of the DPF, which is accomplished by raising the exhaust temperature. Particulate matter emissions may increase during this procedure. From *Table 3.1*, it can be seen that the engine produces a lower concentration of soot during DPF regeneration, but the total number of particles is higher compared to the other two conditions tested, probably indicating smaller particles generated during the process. This is due to the generation of a higher amount of nucleation particles during the regeneration conditions, which can increase the emitted particles by several orders of magnitude [72] [73]. The concentration of particles, however, resulted lower compared to the other conditions in analysis probably as a correlation to the high load. In conclusion, even though the total quantity of particles released was low, a large number of small particles were produced.

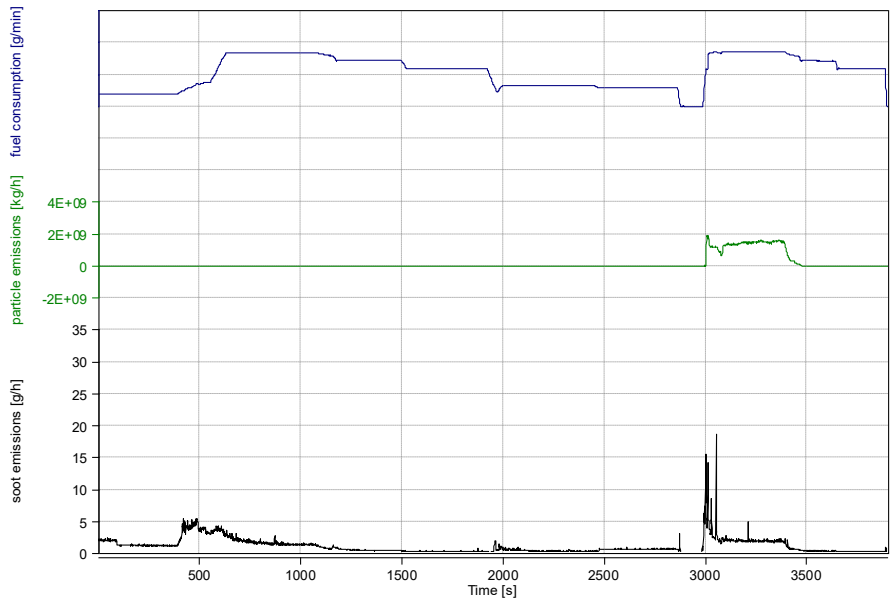

Figure 3.3 Soot emissions, particulate emissions and qualitative fuel consumption during the collection of the sample "pressure sweep 1h" versus cycle time [s]

As the operating conditions change within a cycle, particulate emissions vary, as shown in *Figure 3.3* for the “pressure sweep” sample. During the collection of this sample, the engine speed and load were reduced in steps, with each step corresponding to approximately 10 minutes. The steps can be seen in the change in fuel consumption. The beginning of this test is characterized by higher PM emissions, which is characteristic of a cold start [74]. Every change of the operative conditions as a decrease in speed, was associated with a peak in soot concentration emissions. The inverse correlation between the fuel consumption and the soot emissions was not observed for this cycle, probably because of the gradual decrease in load which is generally associated with an increase in emission rate.

In general, the measurements highlight the conditions that lead to high particulate emissions, such as cold start, changes in driving pattern as speed and load variations, and changes in engine maneuvering to ensure DPF regeneration. The least can lead to a high number of small particles that can be of concern to health and the environment. Among the operating modes in which the engine operates, it has been observed that idling and motoring increase soot production, while high loads present lower emissions.

Table 3.1 Average soot and particle emissions measured with the MSS and the APC during the collection of the samples "soot regeneration", "soot loading" and "pressure sweep", correlated with the operative conditions of the 8-cylinder engine

Parameter	Sample		
	Soot regeneration	**Soot loading**	**Pressure sweep**
Torque [Nm]	2500	600	0 - 3400
Gas flow exhaust [kg/h]	2500	1500	800-2900
Engine speed [rpm]	1800	1800	860 - 1800
Temperature engine outlet [°C]	490	220	250-460
Fuel consumption [g/min]	high	low	variable between high and low
Average soot emission [g/h]	2	14.5	1.2
Average particle emission [#/h]	$1.3 \cdot 10^{9}$	$2.1 \cdot 10^{7}$	$1.49 \cdot 10^{7}$

It is important to keep in mind that the specifics of diesel engine particle emissions can change based on the type of engine, fuel quality, and driving conditions. Therefore, it is crucial to consider these factors when conducting research and developing mitigation strategies.

3.2 PM morphology analysis with scanning electron microscopy

This section analyzes the results of SEM imaging in order to evaluate possible morphological differences between the samples collected under different conditions. The imaging was performed on the PM rich in the combustible soot fraction and on the non-combustible fraction remaining after the TGA, which is the ash. Morphological studies are relevant to critically analyze the results of the other characterization techniques. The surface of the aggregates shows the area available for reaction affecting the reactivity and therefore related to the oxidation kinetics. Observation of ash particles can improve the understanding of soot reactivity: several studies have reported that when PM aggregates are in an environment that favors oxidation of the carbonaceous fraction, the aggregates shrink and the fine ash particles transported on the aggregates agglomerate together [45]. The final size of these ash particles can even reach the millimeter scale [45]. The study of ash aggregates can provide insight into the reactivity of the combustible fraction [45]. Furthermore, the observation of ash can be aimed at investigating possible crystalline structures. The structure in which the ash is present will affect the ash packing density within the DPF [75].

3.2.1 Scanning electron microscopy of PM

A qualitative SEM analysis of soot particles from the different operative conditions allows to infer that there were no significative differences in terms of primary particles dimensions or aggregate structure. Primary particles with diameters in the range of 20-200 nm were detected for all the samples. In *Figure 3.4* are presented few examples. "Oil consumption" sample showed slightly bigger particles if compared to others. The observed result runs counter to the anticipated outcome when employing a biodiesel blend, as expounded upon earlier. Notwithstanding, additional variables, such as engine operative conditions, may have exerted influence. *Figure 3.5* shows PM aggregates collected on a quartz filter in the conditions of the soot regeneration sample but with a shorter collection time, equal to 5 minutes. The objective of the study was to enhance the preservation of the aggregate structure. However, the positional

instability of the aggregates on the filter fibers impeded the observation of primary particles at higher resolutions. From *Figure 3.5* is possible to observe that the PM aggregates present variable dimensions in the exhaust flow: the majority are in the nanometric scale, with some exceptions that can reach up to 20 µm. A similar analysis was performed during the soot loading test, with the same outcome. This result is in line with the findings of other researchers.

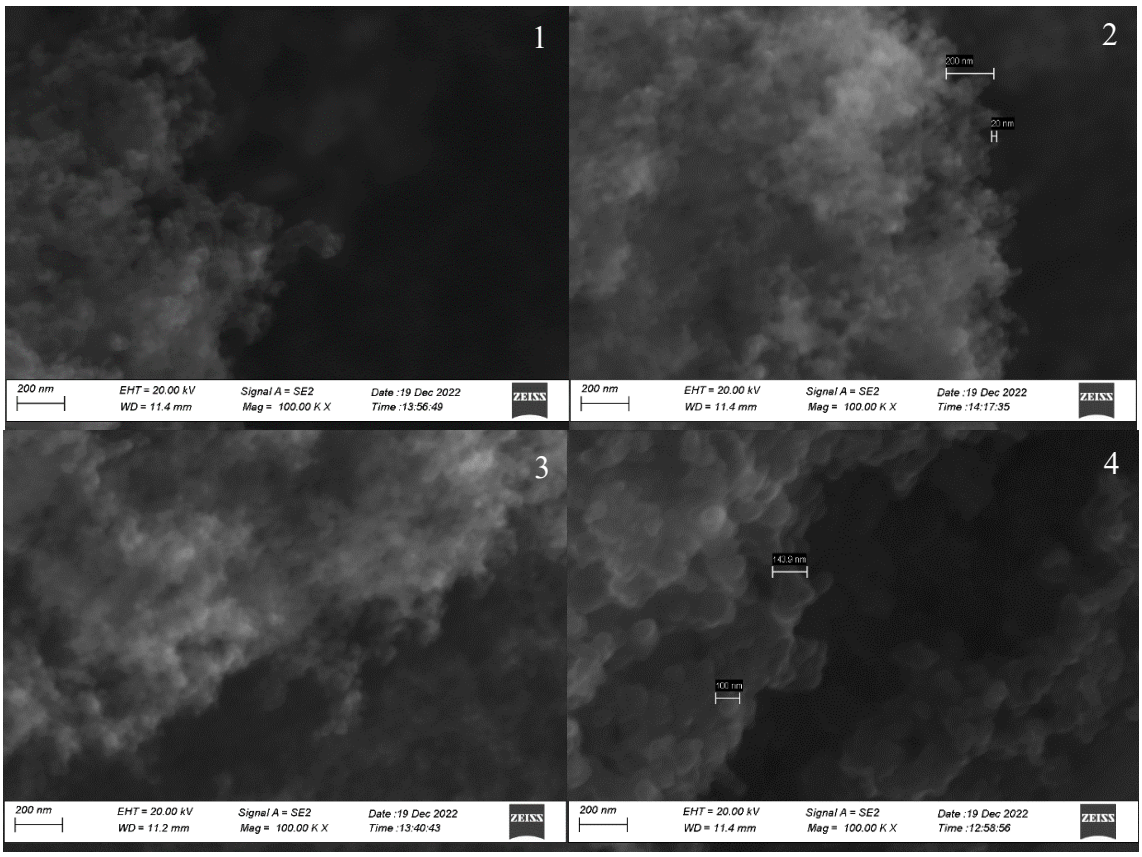

Figure 3.4 SEM images of samples 900 rpm (1), 1700 rpm (2), 2300 rpm (3) and oil consumption (4), magnification 100.000 kX

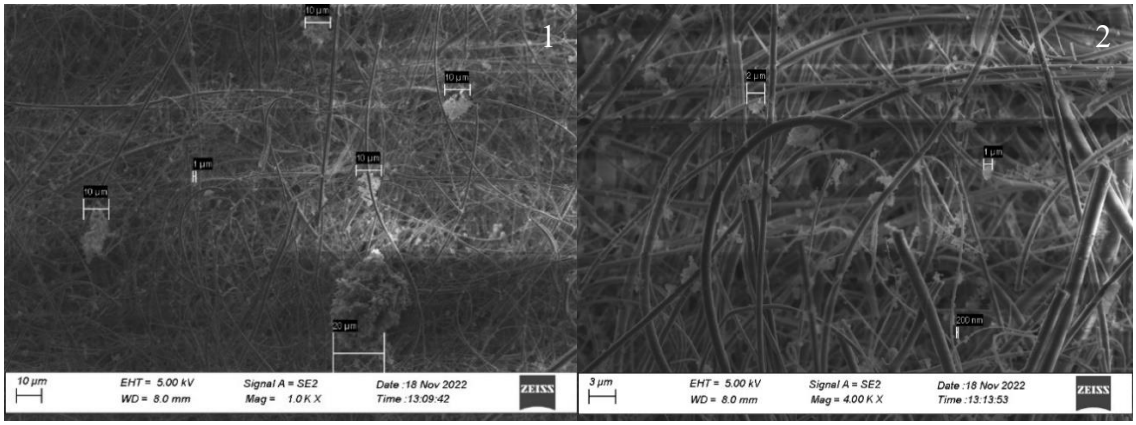

Figure 3.5 SEM images of the sample " soot regeneration", magnification 1.0k X (1) and magnification 4.0k X (2)

3.2.2 Scanning electron microscopy of ash

During the microscopy of soot, it was difficult to identify the ash particles due to their small size and reduced quantity. An ulterior SEM-EDS analysis was conducted on the ash after the TGA. The results of the EDS analysis are presented in Section 4.3. From the results shown in *Figure 3.6, Figure 3.7,* and *Figure 3.8,* it was possible to infer that the extraction procedure might have affected the ash morphology. The samples underwent this procedure displayed a slightly larger size, both in terms of single particle diameter and agglomerates. Additional images can be found in the Appendix D.

Among the samples from the 6-cylinder engine, "STD5" and "oil consumption" exhibited particles with diameters ranging from 0.5-1 μm, while "900rpm," "1700rpm," and "2300rpm" were represented by particles with diameters of 0.1-0.5 μm. The variation might be due to the rapid cyclic operation of starting and stopping the engine, characteristic of the latter samples. That can lead to an increase in ash production and influence its dimension.

In the two samples collected from the inlet of the silencers, there were found no relevant examples of particles below 100 nm. In addition, the sample " pipe 8-cylinder" presented qualitatively smaller particles than "pipe 5-cylinder". This can be due to a lower aging and less agglomeration because of a shorter deposition time in the pipe.

The samples from the 8-cylinder engine, collected on the quartz filters, displayed a wide variation in ash particle sizes, as shown in *Figure 3.8.* Overall, particles with diameter around 40-50 nm were common while the ones over 100 nm were seldom observed. Of the samples presented in *Figure 3.8*, the "soot loading" sample was characterized by a larger amount of ash and bigger particles than the "soot regeneration" sample. This may be a result of lower injection pressure, which was previously mentioned as leading to higher PM emissions. The higher PM emissions for this sample were also showed through the results of the APC.

Some metallic composition particles were detected during the analysis, an example is presented in *Figure 3.9*. These are the result of engine corrosion and abrasion and increase the ash fraction in the exhaust.

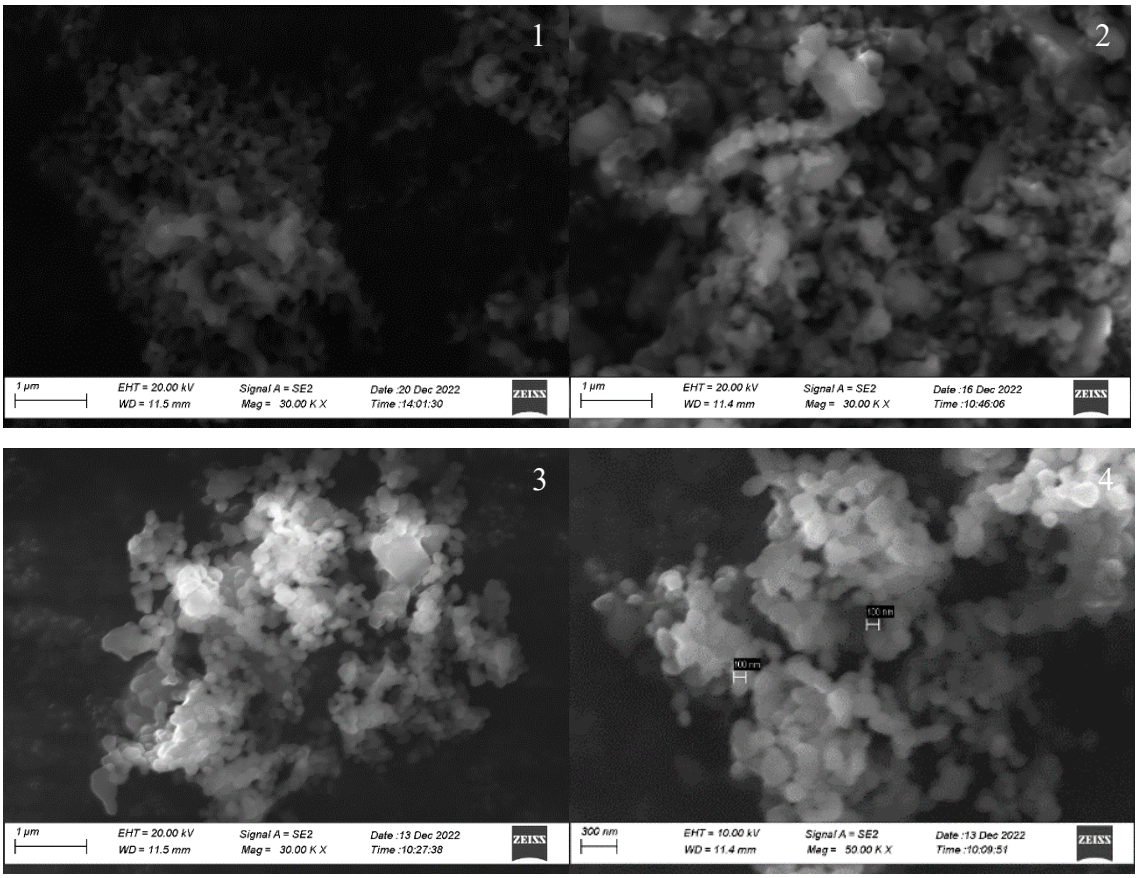

Figure 3.6 Microscopy: ash comparison of samples 900rpm (1), 1700rpm (2), 2300 (3), zoom on 2300rpm (4) at magnification of 30.0k X

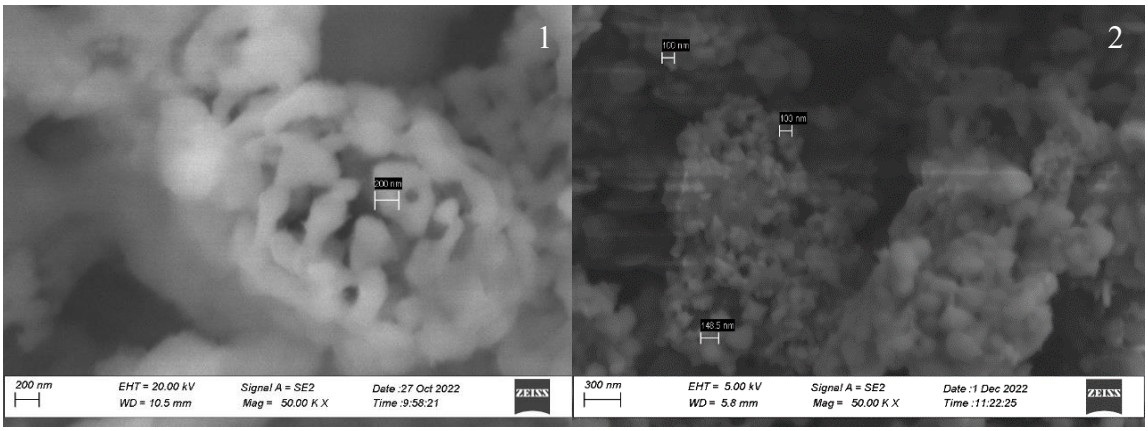

Figure 3.7 Microscopy: ash comparison of samples Pipe 5-cylinder (1) and Pipe 8-cylinder (2), magnification 50.0k X

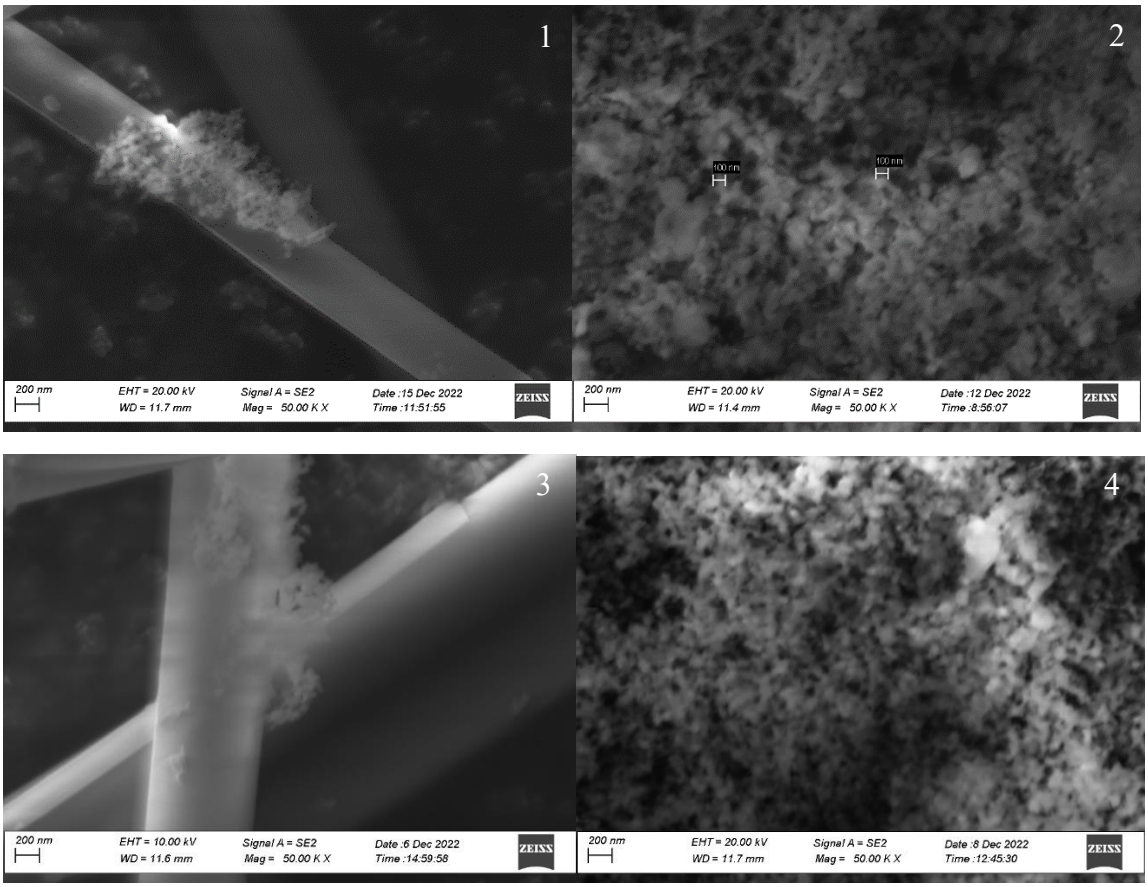

Figure 3.8 Microscopy: ash comparison of samples pressure sweep (1,2), soot regeneration (3) and soot loading (4), magnification 50.0k X

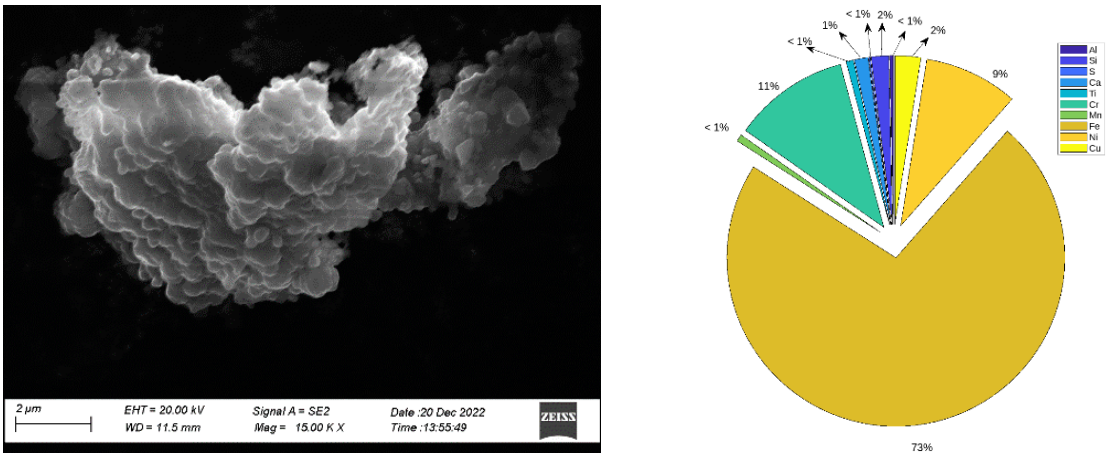

Figure 3.9 Metal ash particle from sample 900 rpm, magnification 15.0k X (right) and its compositional analysis with EDS at EHT=20kV and WD=11.5 mm (left)

3.3 Soot oxidation reactivity studies via thermogravimetric analysis

The following section focuses on the results obtained from the weight loss curves. Samples "900 rpm", "1700 rpm" and "2300 rpm" were excluded from the thermogravimetric analysis as the amount after the extraction was not sufficient to perform an accurate analysis. The normalized weight loss curves of the sample in analysis, obtained with the heating program presented in in *Table 2.6* are summarized in *Figure 3.10*. The figure displays, in addition, the analysis results of a well-known reference carbon, namely Printex-U, using the identical heating program as employed for the other samples.

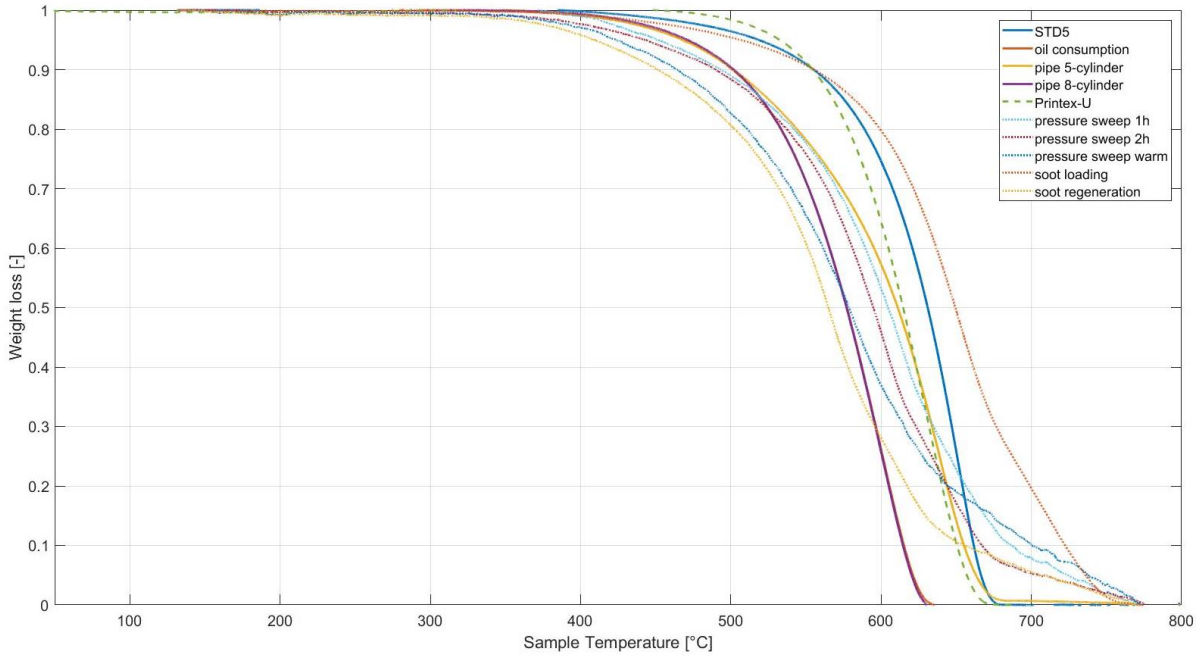

Figure 3.10 Normalized oxidation step of the weight loss curve in function of the sample temperature, obtained at β= 5 [°C/min], for the samples in analysis

Several preliminary analyses were performed on the most abundant sample, Pipe 5-cylinder. *Figure 3.11* shows the oxidation step of the weight loss curve of the latter, performed with different initial weights to show that also samples below 1 mg can bring to sufficiently accurate results, especially for what concerns kinetic studies. The observed slight variation in the residual incombustible fraction is expected and attributed to the composition's heterogeneity, particularly in small samples.

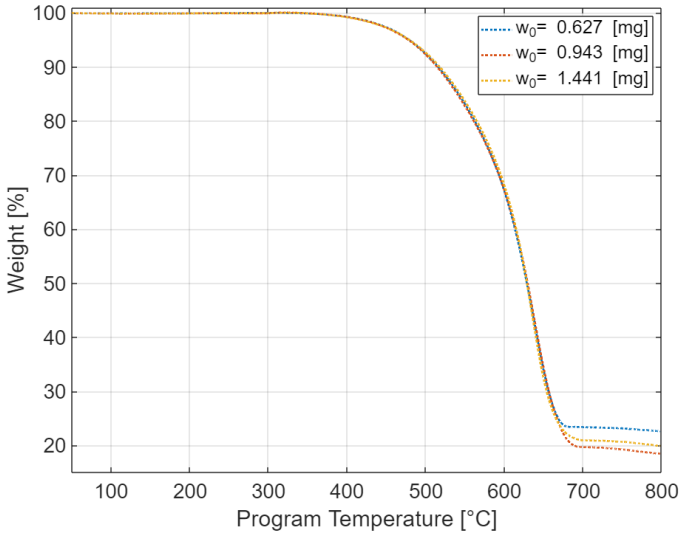

Figure 3.11 Comparison between the oxidation steps at β= 5 [°C/min] with different weights for the sample "Pipe 5-cylinder"

3.3.1 Characteristic temperatures evaluation

The characteristic temperatures: starting oxidation temperature (SOT), final oxidation temperature (FOT), maximum mass loss rate temperature (MLRTmax), T_{10} and T_{90}, presented in the *Section 1.3.2* were estimated for the samples in analysis. MLRTmax was estimated from the derivative of the mass loss curve. Those values and t_{ox}, the oxidization time defined by *Eq.3.1* are reported *Table 3.2*.

$$t_{ox} = \frac{FOT - SOT}{\beta} \tag{3.1}$$

Table 3.2 Characteristic oxidation temperatures SOT (starting oxidation temperature), FOT (final oxidation temperature), $MLRT_{max}$ (maximum mass loss rate temperature), T_{10} (sample mass loss of 10%), T_{90} (sample mass loss of 90%), and the oxidation time (t_{ox}) for the samples in analysis at different heating rates [°C/min]

Sample	**Heating rate** [°C/min]	**SOT** [°C]	**$MLRT_{MAX}$** [°C]	**FOT** [°C]	**T_{10}** [°C]	**T_{90}** [°C]	**t_{ox}** [min]
STD5	5	450	651	673	555	662	45
Oil consumption	5	302	598	638	424	610	67
Pipe 5-cylinder	3	340	618	653	484	632	104
	5	361	635	680	501	654	64
	10	370	661	715	522	678	35
Pipe 8-cylinder	3	330	582	620	485	595	97
	5	350	602	636	501	615	57
	10	359	627	665	527	643	31
Pressure sweep 1h	3	360	587	798	466	681	146
	5	365	615	798	485	701	87
	10	366	635	798	495	710	43
Pressure sweep 2h	3	355	587	798	471	661	148
	5	360	604	798	481	672	88
	10	370	628	798	500	709	43
Pressure sweep warm	3	340	563	798	435	718	153
	5	360	583	798	445	732	88
	10	365	603	798	462	747	43
Soot loading	3	340	643	745	528	697	135
	5	360	652	760	549	723	80
	10	370	688	785	584	743	42
Soot regeneration	3	320	555	798	445	682	159
	5	339	569	798	448	675	92
	10	360	603	798	474	691	44

The experimental results, consistent with those of other studies, demonstrate that when heating is increased, characteristic temperatures rise. The loss mass rate curves move toward higher temperatures as a result of increased heating rates that shorten the sample's exposure to the oxidant. [43]

The characteristic temperatures for all the samples, heated at 5 °C/min, were compared in *Figure 3.12*. Here, the impact that different operative conditions have on the reactivity is observable from the values of $MLRT_{max}$, which ranges between 569 and 652 °C. Those values result slightly higher if compared to literature (*Table 1.4*), where $MLRT_{max}$ commonly lies between 440 and 640 °C [42] [43] [47] [57] [58]. Previous researchers have found that for diesel soot, the parameter T_{10} can assume widely different values, ranging between 150 and 595 °C. Whereas the parameter T_{90} may lie in the interval 500 - 685 °C. [47] The values of T_{10} were coherent with previous researchers while T_{90} exhibited higher upper limits for the samples collected on quartz filters. Diffusion resistance of the air on the sample or the limited amount of PM present during the analyses on filter might be cause for that. Proof for this assumption is the fact that the FOT was hardly reached or, resulted higher than expected. Additional studies

where samples are collected in the same conditions and where the influence of the filter during the TGA is investigated, are required.

Nevertheless the samples collected from the silencers are expected to be less reactive due to soot aging, their reactivity results similar to the other samples. “Pipe 8-cylinder” engine has a lower $MLRT_{max}$ compared to “Pipe 5-cylinder”, that can be due to the fact that the engine was used just for 3 days after the cleaning of silencer’s inlet, therefore the soot had less time to age.

Samples “ soot loading” and “soot regeneration” were collected from the same engine and in the same time interval but with different operative conditions. Sample “soot regeneration” was obtained in full load conditions and the fuel consumption was lower than during “soot loading”. Which brought to a smaller amount but of more reactive soot. Since the “soot loading” sample contained a significantly higher amount of PM, the lower reactivity might also be due to morphological reasons as more layers of soot were deposited one on another on the filter.

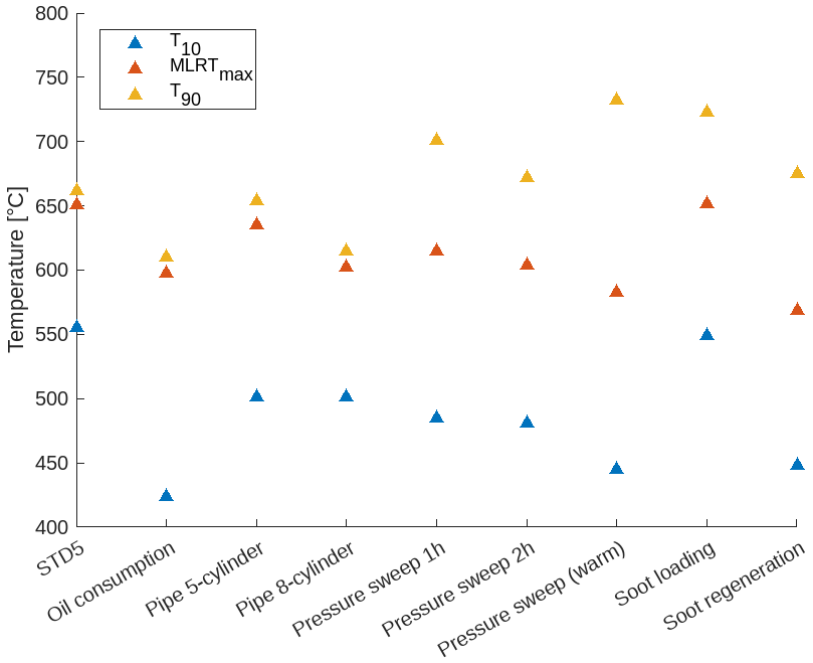

Figure 3.12 Comparison between characteristic oxidation temperatures T_{10}, $MLRT_{max}$ and T_{90} for several samples in analysis, oxidized at heating rate β=5 [°C/min]

Samples relative to the pressure sweep test have shown that when the sample is collected from an already warm engine, the PM results slightly more reactive. Whereas there was no significant difference in reactivity of the PM sampled in 1 or 2 hours of the cycle. The sample collected on a Teflon filter, was scraped off and analyzed with the TGA. The characteristic temperatures of this sample and “pressure sweep 1h” are compared in *Table 3.3*. An optical microscopy analysis performed on the sample “ pressure sweep Teflon” subsequently to the TGA had shown traces of filter material. Teflon spoils TGA results since it vaporizes within the temperature range of soot oxidation [76]. Thus, the substantial difference in results presented in *Table 3.3,* can be due to diffusion limitation on the quartz filter in one sample or to the effect of trace Teflon within the other. Ulterior analyses are required to define the more suitable mode to explore soot oxidation.

Overall, even if each sample derive from different conditions in terms of engine, fuel, operative conditions and collection methods, the results show that the reactivity of soot is quite similar in all the samples. This is coherent with field findings and a broad literature analysis.

Table 3.3 Direct comparison between the characteristic temperatures of the samples "pressure sweep 1h" and "pressure sweep Teflon", from the weight loss curves with β= 5 [°C/min]

Sample	SOT	$MLRT_{MAX}$	FOT	T_{10}	T_{90}
Pressure sweep 1h	365	615	798	485	701
Pressure sweep Teflon	340	552	567	444	556

3.3.2 Soot oxidation kinetic parameters evaluation

The activation energy was calculated for several samples by applying the non-isothermal isoconversional multiple-ramp rates method, FWO, presented in the literature review and in the experimental section. The weight loss curves for the samples oxidized on quartz filters were re-scalded on the carbon fraction, which is expected to be completely oxidized at the end of the TGA. Therefore, the final point of each curve was set as equivalent to a total conversion, as in the curves presented in *Figure 3.13*. In the same figure, the Flynn-Wall-Ozawa plots, obtained by applying the *Eq. 2.3*, are showed for some representative samples. By calculating the slope and the intercept of the line of the Flynn-Wall-Ozawa plots the isoconversional activation energy E_α, the pre-exponential factors and the reaction rate constant were calculated for the conversion α values in the range between 0.1 and 0.9, in steps of 0.1. The variation of E_α with the conversion is reported in *Figure 3.14*.

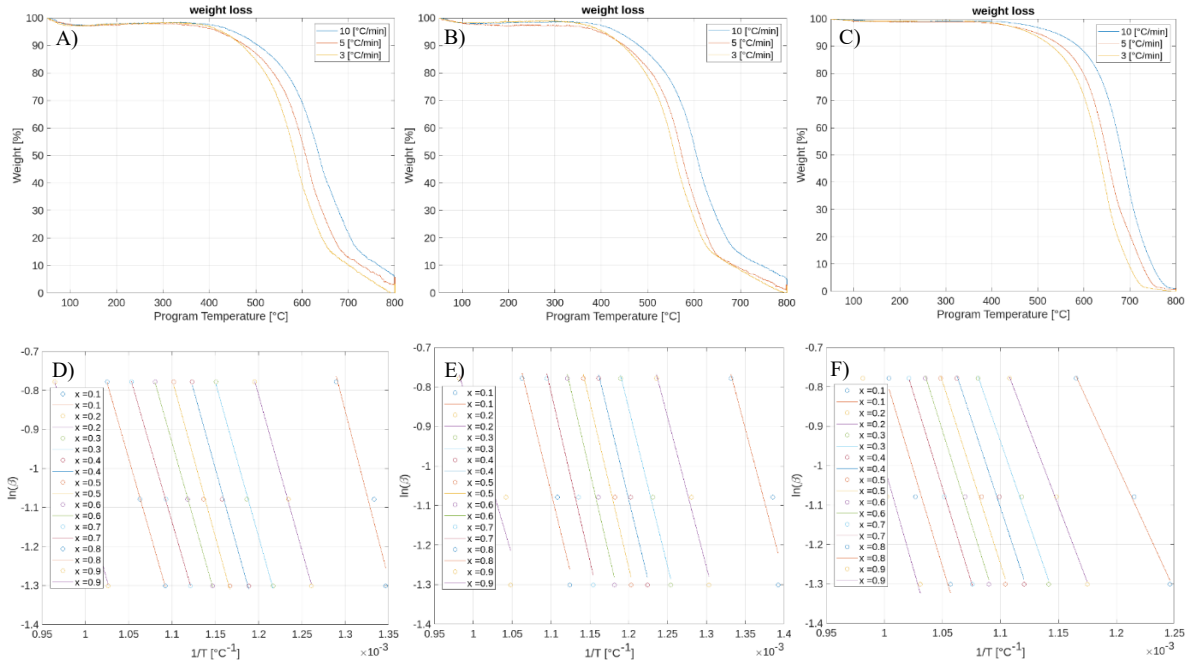

Figure 3.13 Weight loss curves (top) and Flynn-Wall-Ozawa plot (bottom) for the samples pressure sweep (A,D), soot regeneration(B,E) and soot loading (C,F)

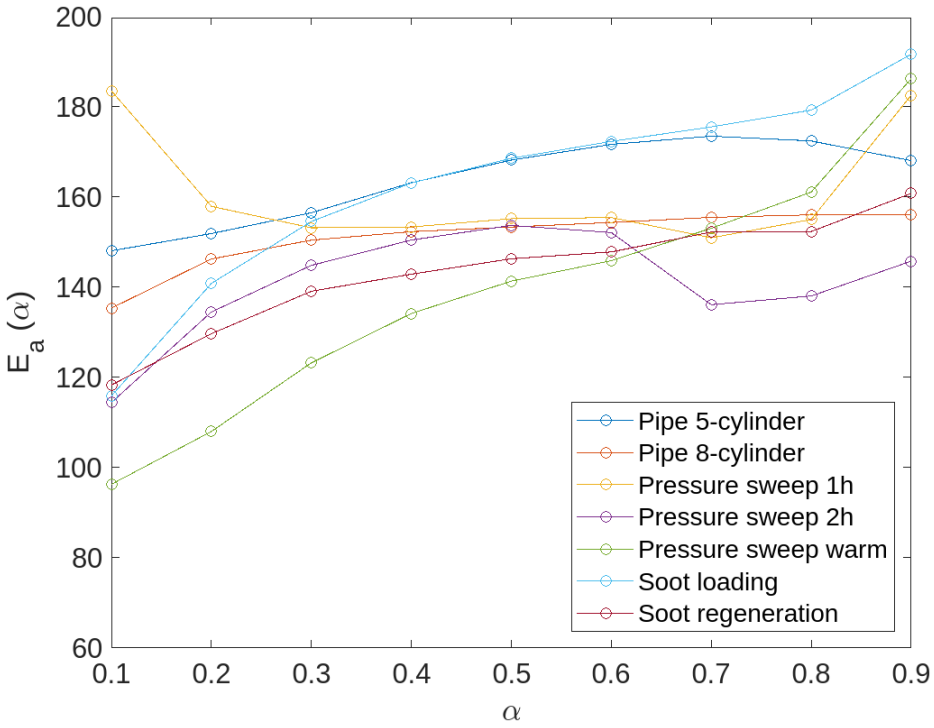

Figure 3.14 Ea calculated by applying the isoconversional method, from the Flynn-Wall-Ozawa equation for conversions α =0.1-0.9

From *Figure 3.14* it is evident that the activation energy presents only small variations in the range α=0.2-0.8 as also consistent with the application of this method in literature. *Table 3.4* summarizes the average values for the activation energy and the other kinetic parameters obtained for those E_A. The activation energies were found to be in the same limited range, between 138 and 164 kJ/mol, to show that even in different conditions, the oxidation of the soot results roughly similar, as concluded also from the analysis of the characteristic temperatures.

The calculation of the activation energy does not require the definition of a reaction model whereas this have to be defined for the calculation of the pre-exponential factor. For such calculation, the first order reaction was assumed, with $f(\alpha) = (1 - \alpha)$.

Table 3.4 Kinetic parameters calculated with the isoconversional non-isothermal multiple-ramp rates method: average E_A in the conversion range α=0.1-0.9, maximum error associated with the interpolation (R^2), average pre-exponential factor A and k for several samples collected on quartz filters during ongoing operations and scraped from the silencers

Sample	E_a (average) [kJ/mol]	R^2 (minimum)	A [$Pa^{-1}\ s^{-1}$]	$k_{300°C}$ [$Pa^{-1}\ s^{-1}$]	$k_{500°C}$ [$Pa^{-1}\ s^{-1}$]
Pipe 5-cylinder	164	0.997	27.5	$3.3\cdot10^{-14}$	$2.4\cdot10^{-10}$
Pipe 8-cylinder	151	0.999	8.7	$1.5\cdot10^{-13}$	$5.4\cdot10^{-10}$
Pressure sweep 1h	160	0.951	222.3	$4.9\cdot10^{-13}$	$3.0\cdot10^{-9}$
Pressure sweep 2h	141	0.995	1.9	$2.6\cdot10^{-13}$	$5.6\cdot10^{-10}$
Pressure sweep warm	138	0.914	10.9	$2.4\cdot10^{-12}$	$4.5\cdot10^{-09}$
Soot loading	162	0.971	23.4	$3.7\cdot10^{-14}$	$2.5\cdot10^{-10}$
Soot regeneration	143	0.723	3.6	$3.2\cdot10^{-13}$	$7.5\cdot10^{-10}$

3.3.3 Soot oxidation reactivity and TGA experimental procedure discussion

The activation energies were found to be in the same limited range and the similar reactivity of the soot samples was assessed also through the analysis of the characteristic temperatures. When compared the literature, the range of values representing the activation energies is quite broad, as reported in *Table 1.2* and *Table 1.3.* It is worth noting that most studies tend to focus on a narrow range of variables, such as engine type, fuel, and sample preparation. This limited variability can create the impression that soot reactivity varies greatly across studies. In contrast, the current study has assessed that under a large numbers of variable condition, the reactivity is not significantly affected.

Figure 3.10 reveals a limitation in using quartz filters in TGA. Samples analyzed on filters display a change in the slope of the curve when 60-70% of the soot is oxidized, unlike samples that were extracted, scraped from the silences or the reference soot Printex-U, which exhibit a simple gradual decrease in weight. This is presumably due to a slight diffusion limitation caused by the presence of the filter, especially when the availability of particles to combust is low, towards the end of the oxidation process. Nevertheless, the activation energy calculations for samples oxidized on filters were found to be in the same range as those for samples oxidized without filters, indicating that this limitation does not affect the proposed method's activation energy calculations.

Scraping the particulate rather than analyzing it on filters can reduce the filter's effect on slowing weight loss. Due to the inherent fragility of quartz fibers, however, there will be significant contamination from fragile quartz fibers. Nevertheless, since the fibers are inert in the proposed heating program, this contamination is expected to have a minor effect on the kinetics. The decision to employ filters was motivated by the aim of achieving more repeatable and controlled use of samples, with similar amounts of soot and filter weight for each sample. However, the diffusion effect towards the end of the oxidation process remains a tradeoff rather than a perfect solution.

As previously stated, the pre-exponential factor was evaluated using the first order model as the specification of the f(α). This choice was justified by the observation of the weight loss curves presented in *Figure 3.10*, which, except for the discussed diffusion effect, showed a smooth decrease in weight with no apparent complex multi-step reactions. Hence, a first order model might be a suitable approximation, as suggested by S. Vyazovkin [77].

The use of models can sometimes lead to errors in the calculation of kinetic parameters. However, they can be calculated in a completely model-independent manner. This could be achieved by taking into account the compensation effect, as discussed in detail by S. Vyazovkin [78]. The compensation effect involves determining the constants a and b specified in *Eq. 3.2* through linear regression using values of pre-exponential factor (A_i) and activation energy (E_i) obtained by fitting the parameters to the experimental data for different reaction models for f(α).

$$lnA_i = a \cdot E_i + b \tag{3.2}$$

This approach allows for a more accurate determination of the kinetic parameters, as it takes into account any potential deviations from the assumed model. Subsequently, a more accurate and model-free value of A can be estimated by using *Eq. 3.2* with the calculated constants a and b. This evaluation is more time consuming, but may improve the approximation of the pre-exponential factor.

According to S. Vyazovkin [77], the isoconversional methods can be considered effective if the difference between the isoconversional activation energies (E_α) obtained with this approach for each sample is less than 30%. The variability of E_α for the analyzed samples was calculated and presented in *Table 3.5*, indicating that for some of the samples, the variability exceeded this threshold. However, it should be noted that part of this effect may be due to the diffusion limitation previously discussed. Nevertheless, it is not uncommon to find greater variations of E_α with α in the literature, and results are often presented in the range α=0.2-0.8. Therefore, reducing the impact of noise in the weight loss curves at the start and conclusion of the oxidation process, some studies, such as H. N. Sharma [42], focus on this specific range.

Table 3.5 Variation of Ea from the mean value calculated ad difference between the highest and the lowest value of Ea divided by the mean value, for each sample

Sample	Variation of Ea from the mean value [%]
Pipe 5-cylinder	15
Pipe 8-cylinder	14
Pressure sweep 1h	20
Pressure sweep 2h	28
Pressure sweep warm	65
Soot loading	67
Soot regeneration	30

3.4 Ash composition evaluation

In this section, an evaluation of the composition of ash particles is conducted through the utilization of various analysis techniques. It should be noted that the presence of a relatively small amount of the incombustible fraction poses a constraint on comprehensive and precise assessments. Although EDS was carried out on a comprehensive range of samples, the utilization of ICP and XRD was restricted to select cases due to limited sample availability. Subsequently, in connection with the literature, the ensuing findings of these analyses are considered and discussed.

3.4.1 Energy Dispersive Spectroscopy (EDS)

Several EDS analyses were performed both on the PM both prior to thermogravimetric analysis and, on the incombustible fraction, lasting afterwards. The compositional analysis of the PM before TGA did not show any relevant result, the carbon fraction was dominant and ash particles were difficult to identify. The most likely reason is the highly localized distribution of trace elements derived from lubricants within the PM agglomerates [16] [44].

The compositional analyses accomplished on the ash fraction post TGA were performed on different points of each sample in order to have a more general outcome. Every result was then arithmetically averaged. *Figure 3.15* shows a comparison in terms of atomic weight among all the samples. To facilitate the reading, elements present in small amounts as well as unusual ones were removed from the composition. The elements detected by the equipment in some of the samples and removed from the analysis are Aluminum (Al), Carbon (C), Chromium (Cr), Iron (Fe), Potassium (K), Molybdenum (Mo), Oxygen (O), Silicon (Si), Titanium (Ti), Vanadium (V), and Tungsten (W). A broader analysis of the composition is presented in the Appendix E. V and W were detected in the 2 samples from the silencer inlet. Those are classical constituents of the DPF, which, however, comes downstream to the silencer.

Overall, the lubricant derived elements such as Calcium (Ca), Zinc (Zn), Phosphorus (P), and Magnesium (Mg) were predominant when compared to the corrosion and wear derived elements. The wear materials, such as the example shown in *Figure 3.9*, were highly localized.

Figure 3.15 shows how variable the composition of an ash sample can be, as confirmed in the literature [16]: the conditions of each experiment will be different. In addition, the ash composition is influenced by engine type, wear, fuel, lubricating oil composition, lubricating oil additives and operating modes [79]. The researchers frequently refer to ash collected from DPF filters since the amounts are larger and thus more suitable for a deeper analysis. Therefore some differences with the results of the project might be present. Possible causes of the compositional variability are the limited amount of sample, the heterogeneity of ash composition within each sample and limitations of the instrument.

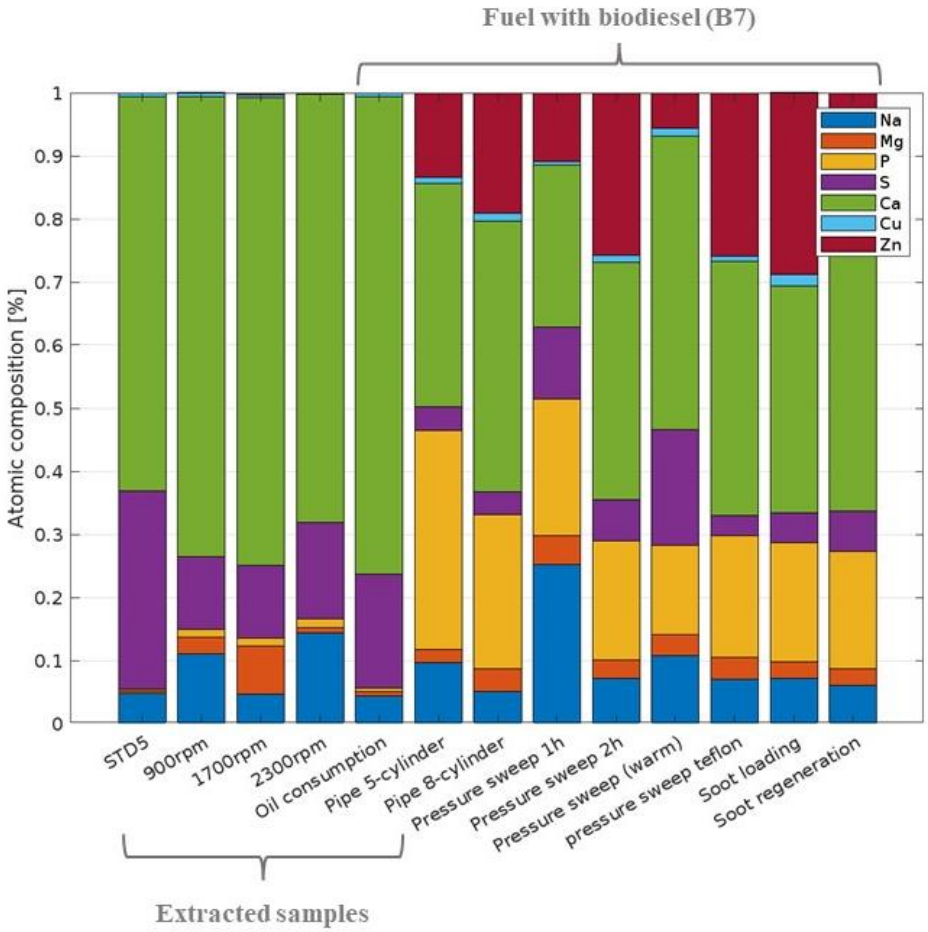

Figure 3.15 EDS: Ash atomic composition [%] comparison for the tested samples with relation to the fuel and highlighting on the samples extracted with cyclohexane

Contrary to the expected, calcium (Ca) was not always the most abundant compound and low levels of sulfur were detected. The most common compound found in diesel engine ash is $CaSO_4$ [80]. For this reason, similar molar concentrations of Ca and sulfur (S) are expected. The limited amount of sulfur can be attributed to the TGA performed prior to the EDS of the ash. TGA is not entirely representative of the DPF environment during regeneration. Reaching high temperatures (800°C in this study) may result in some degree of desulfurization during thermal analysis [44]. This hypothesis can be investigated by coupling the TGA with analyses aimed at evaluating the VOC fraction leaving the sample, for example by means of Fourier transform infrared spectroscopy (FT-IR).

All the extracted samples have shown low or non-detectable levels of magnesium (Mg), zinc (Zn), and phosphorus (P). Whereas similar concentrations of Zn and P were detected for the samples from the 8-cylinder engine, as probable constituents of zinc phosphates.

Nevertheless higher amounts of sodium (Na) and potassium (K) were expected in the samples where a B7 fuel was employed, no evident correlation was detected. A reason might be that the samples were collected not in a laboratory environment and contaminations of the engine by previous fuels are likely to occur. Overall, Na was present in high concentration in all the samples, for unknown reasons.

Any investigation aimed to characterize the composition of ash particles will lead to different results due to contamination, different approaches to exclude non-relevant elements,

and variability in the results due to the use of different available analytical techniques. This research highlighted that EDS can give different results in terms of composition by analyzing different parts of the sample, which can be quite heterogeneous.

Table 3.6 proposes a simplified approach to understand the compositional similarities between samples. This approach aims to minimize the variability inherent to the overall composition and attempts to identify the influence of different engines, fuels, and lubricants by comparing adimentional values. The table shows the ratio, in terms of atomic mass and weight, between the key elements for the samples in the analysis to explore potential correlations.

Table 3.6 Fraction between relevant ash elements for corresponding samples presented as molar fraction (weight fraction): mol/mol (wt/wt)

	Sample	**Zn/P** mol/mol(wt/wt)	**Ca/S** mol/mol(wt/wt)	**Ca/Mg** mol/mol(wt/wt)	**Ca/Zn** mol/mol(wt/wt)
Extracted	STD5	-	2 (2.5)	159 (262.2)	-
	900 rpm	-	6 (8.0)	29 (47.1)	-
	1700 rpm	0.4 (0.7)	6 (8.0)	10 (15.8)	183 (112.3)
	2300 rpm	-	4 (5.6)	74 (121.3)	-
	Oil consumption	0.1 (0.3)	4 (5.2)	108 (117.3)	997 (661.0)
8-cylinder engine	Pipe 5-cylinder	0.4 (0.8)	9 (11.8)	17 (27.9)	3 (1.6)
	Pipe 8-cylinder	1 (1.6)	11 (14.4)	12 (19.7)	2 (1.4)
	Pressure sweep 1h	1 (1.1)	2 (2.8)	6 (9.5)	2 (1.5)
	Pressure sweep 2h	1 (2.9)	6 (7.3)	13 (21.3)	1 (0.9)
	Pressure sweep warm	0.4 (0.8)	3 (3.2)	14 (22.7)	8 (5.1)
	Pressure sweep Teflon	1 (2.8)	12 (15.6)	12 (19.7)	2 (1.0)
	Soot loading	2 (3.2)	8 (9.6)	14 (22.3)	1 (0.8)
	Soot regeneration	1 (2.0)	8 (9.5)	18 (29.5)	3 (1.7)

From the results in *Table 3.6* it can be assessed that the extraction procedure could have had an impact on the concentration of Mg, P and Zn as extracted samples presented low or absent levels of these elements, as seen also in *Figure 3.15.* The fractions from the 8-cylinder engine in *Table 3.6* show that the moles of Zn and P were comparable for all the samples, indicating that different phosphates were likely to be present but did not vary between different samples. In the same samples, the Ca/Mg ratio also exhibits a correlation. The abundance of Ca with respect to S shows that different compounds were likely to be present, and sharing the calcium atoms.

The proposed methodology provides a valuable tool for understanding compositional differences between samples from different sampling procedures, or for comparing results from different characterization techniques, and may be of interest for future analyses and comparisons.

3.4.2 Inductively coupled plasma (ICP)

To corroborate the outcomes obtained from EDS analysis and approximate the ash fraction by determining the composition of metallic constituents within the ash particles, an ICP analysis was conducted on a sample that corresponded to "pressure sweep 1h".

The quartz filter was loaded with 1.014 mg of PM and digested in a mixture of acids. The results of the ICP analysis are summarized in *Table 3.7*. Most of the elements were below the analysis threshold, however, the knowledge of the amount of Zn, Ca and Cu allowed to estimate

the amount of the characteristic ash compounds $Zn_3(PO_4)$, $CaSO_4$ and $CuSO_4$ through a molar comparison, as presented in *Table 3.8*. The estimated amount of ash was 0.109 mg, equal to 11% of the PM mass.

Table 3.7 ICP analysis results: mass content of metals present in the sample analogue to "pressure sweep 1h", with total PM mass on filter equal to 1.01 [mg]

Metal	Amount [µg/tot]	Metal	Amount [µg/tot]
As	<0.1	Ti	<0.02
Cd	<0.02	V	<0.04
Co	0.127	Ca	27.8
Cr	0.447	Fe	4.88
Cu	0.945	Mg	<5
Hg	<0.1	Na	<10
Mn	<0.5	P	<10
Ni	<1	S	<50
Pb	0.0568	Zn	7.22
Sb	<0.02		

Table 3.8 Details of ash compound mass estimation for the sample "pressure sweep 1h"

	Ca	**Cu**	**Zn**
Grams [g]	$2.75 \cdot 10^{5}$	$9.45 \cdot 10^{7}$	$7.22 \cdot 10^{6}$
Moles [mol/sample]	$6.83 \cdot 10^{-7}$	$1.48 \cdot 10^{-8}$	$1.10 \cdot 10^{-8}$

	$CaSO_4$	**$CuSO_4$**	**$Zn_3(PO_4)$**
Moles	$6.83 \cdot 10^{-7}$	$1.48 \cdot 10^{-8}$	$3.68 \cdot 10^{-8}$
Estimated amount [mg/mol]	$9.31 \cdot 10^{-2}$	$2.37 \cdot 10^{-3}$	$1.42 \cdot 10^{-2}$

Reasonably, different kinds of sulphates and phosphates as well as other kinds of contaminants might be present. Nevertheless, the calculation presented in *Table 3.8* allows to roughly estimate the ash content in a procedure significantly different from the one discussed above demonstrating that the ash is a significant portion of the PM composition.

In more comprehensive research, the use of ICP analysis can enhance the confidence level in results obtained from other characterization methods, such as EDS, in terms of ash composition definition. *Table 3.6*, presented atomic ratios between various ash elements were presented, and similar calculations can be applied to the ICP results in molar form to validate consistency between the techniques. Although only one ICP analysis was performed in the present study, partial results were obtained indicating a Ca/Zn molar ratio of 1.3. This sample was analogous to the "pressure sweep 1h", presented in *Table 3.6*, where the molar ratio Ca/Zn= 2. This comparison shows indicates a degree of similarity between the results of these different analyses, but further research is required to draw definitive conclusions.

3.4.3 X-Ray diffraction (XRD)

X-Ray diffraction analysis was performed on the incombustible fraction residue from the TGA of the sample "pipe 8-cylinder". *Figure 3.16* illustrates the resulting diffractogram, while *Table 3.9* lists the peaks detected. The width of the peaks in a diffractogram is inversely proportional to the size of the crystals. A broader peak may indicate smaller crystals, presence of defects in the crystalline structure, or the presence of an amorphous component [81]. Due to the instrumental settings of the XRD, a high baseline noise was observed in *Figure 3.16*. Nevertheless, several broad peaks were detected, suggesting a significant presence of amorphous compounds in the ash sample.

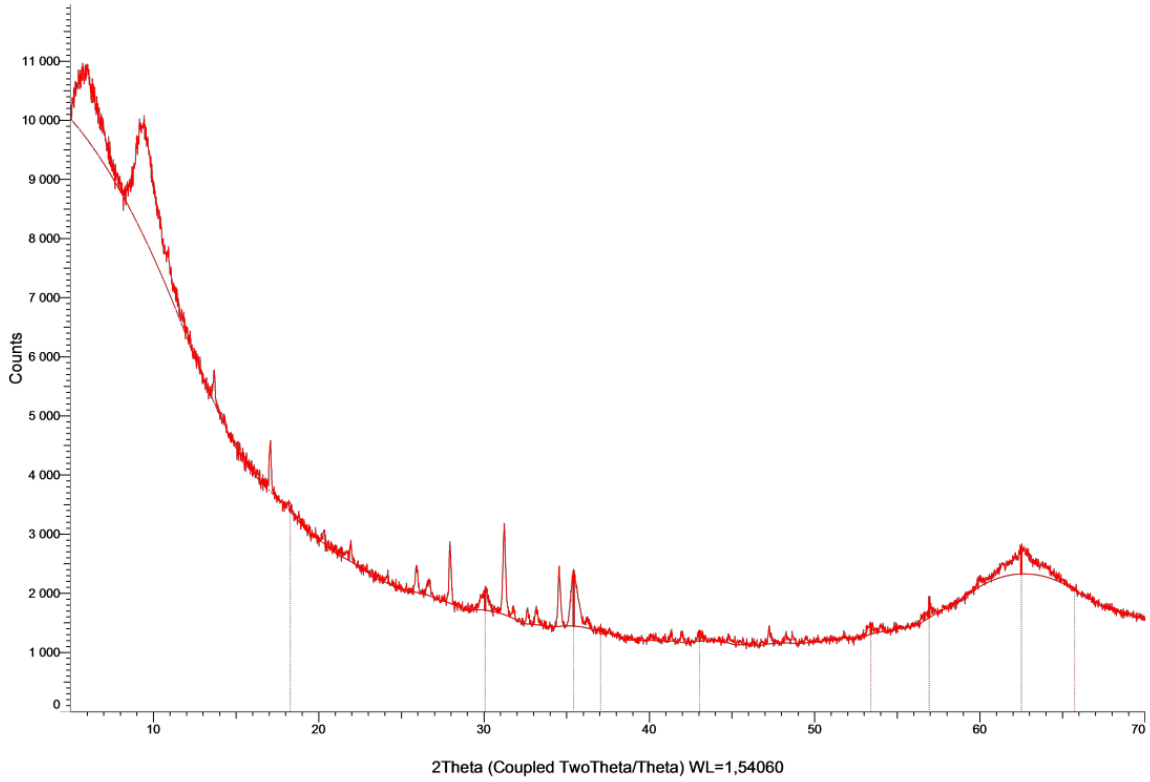

Figure 3.16 XRD diffractogram of sample "pipe 8-cylinder"

According to the results in *Table 3.9,* several peaks have been successfully identified. The peeks (2θ: 21.5°; 26.6°) indicate the presence of $Zn_3(PO_4)_2$ [82]. While the peaks (2θ: 21.8; 25.9; 27.9; 43.1) suggest the presence of $Zn_3Mg(PO_4)_2$, in line with the findings of A. Sappok [83]. A peak at 2θ=25.2 [82], as well as other relevant peaks were expected as an indication of $CaSO_4$.

The presence of $CaSO_4$ in this sample was suggested by the abundancy of Ca and S in the EDS analysis presented in Section 3.4.1. The lack of $CaSO_4$ peaks can be due to the limited amount of ash for an accurate analysis. Another possible explanation involves a phase change that $CaSO_4$ may have undergone due to the high temperatures during the TGA. Literature shows that the diffractograms of ash samples at temperatures greater than 800 °C present several changes. [82]

The most likely explanation is correlated with a the lower amount of crystalline structures within the ash. This is in accordance with the work of S. Bagi [45] who has shown that the incombustible residue from diesel exhaust PM after TGA oxidation can present lack of characteristic XRD peaks due to the dominant presence of amorphous structures. Whether the structure is mostly crystalline or amorphous cannot be assessed from the SEM images presented

in the Section 3.3.2 since the crystals can be orders of magnitude smaller than the resolved size. However, some crystal structures have been observed as for example in *Figure 3.6 (3)*.

Alternatively, A. McGeehan [63] has successfully identified anhydride $CaSO_4$ by means of XRD from a DPF ash sample. The structure and phase of the ash can withstand several changes by being subjected to several DPF regeneration cycles [82], thus the comparison of DPF ash and ash collected from ongoing operation may exhibit structural differences.

Further investigations are required to evaluate the fraction of amorphous phases and to understand the impact of the TGA analysis on the desulphurization. Gaining knowledge of the microstructure of the ash is relevant to understand the ash packing density within the DPF and to improve the regeneration of the filter [82].

Table 3.9 Peaks of the diffractogram obtained by XRD analysis on the ash of the sample "pipe 8-cylinder"

Index	Position [2θ]	Intensity [counts]
1	9,3	9305,9
2	10,9	7557,6
3	13,6	5503,8
4	17,1	4328,4
5	21,8	2694,0
6	25,9	2309,6
7	26,6	2127,5
8	27,9	2701,3
9	30,1	1990,8
10	31,2	2787,4
11	31,7	1730,7
12	32,6	1710,4
13	33,2	1726,4
14	34,5	2274,4

Index	Position [2θ]	Intensity
15	35,5	2052,0
16	36,2	1570,3
17	41,3	1362,0
18	41,9	1333,6
19	43,1	1297,3
20	44,8	1284,5
21	47,3	1446,8
22	48,3	1348,7
23	48,6	1338,9
24	53,4	1434,4
25	57,0	1776,2
26	62,5	2679,5
27	63,9	2413,9

3.4.4 Ash composition discussion

In this section, the results of the research are compared with findings present in the literature in order to highlight differences and similarities. *Table 3.**10*** compares the literature results, previously reported in *Table 1.**5*** and *Table 1.*6 and presented as relative elemental mass content, with the EDS results obtained in this research and summarized from *Table 3.**6***. The results are offered as the range between the minimum and maximum value obtained during the research and are divided between those obtained through extraction and those collected from the 8-cylinder engine for easier comparison. Results from J. A. Mcgeehan [59] [63], are obtained via EDS on ash samples collected from DPF of heavy-duty vehicles. A. Liati [61] found the results also with EDS on ash collected from the central part of the DPF, but on light-duty trucks. Meanwhile, the outcomes reported by S. Bagi [82] were derived from ICP analysis, which compares the elemental composition of DPF ash obtained from a fresh lubricant oil (first column) with that of a DPF sample collected after 60,000 miles of vehicle operation (second column).

The comparison in *Table 3.10* reveals some substantial differences between the results of this research and those reported in literature. First of all, the range of obtained values is highly variable if compared to literature, however, the latter often fall within such a range. This shows

the high heterogeneity of collected ash, which is likely to be minimized when the ash accumulates in the DPF. This is in line with A. G. Sappok [44], who infers, after analyzing with Scanning Transmission Electron Microscopy (STEM) the PM collected during an ongoing operation on a paper filter, that the distribution of phosphorous and of the metallic elements in ash were highly heterogeneous.

Table 3.10 Comparison of mass ratios of ash elements in ongoing research and literature review results

			EDS			ICP	
Ratio [wt/wt]	**Extracted**	**8-cylinder**	**J. A. Mcgeehan** [59]	**J. A. Mcgeehan** [63]	**A. Liati** [61]	**S. Bagi** [82]	**S. Bagi** [82]
Zn/P	-	0.84-3.23	1.10, 1.09	1.44	1.04	1.14	1.13
Ca/S	2.49-7.98	2.82-15.57	0.83, 1.36	1.42	0.85	0.68	1.09
Ca/Zn	-	0.77-5.06	2.34, 2.94	2.21	1.03	1.86	2.11
P/S	0.01-0.11	0.75-6.34	0.32, 0.42	0.45	0.80	0.32	0.46

A closer look at *Table 3.10* allows to observe that the ratio Ca/S resulted significantly lower if compared to all the literature findings. The low amount of sulfur detected can be due to the TGA that ash withstands before being analyzed. TGA is not an ideal representation of the environment that the ash would face in the DPF during its regeneration, and desulfurization might occur [44]. Additionally, the improvements in terms of sulfur reduction in fuel and lubricant oils might have led to the reduction of its presence in ash analyzed during this research. The ratio Ca/Zn in terms of mass was equal to 3.85 during the ICP analysis presented in *Table 3.7*, therefore higher than the review in *Table 3.10* but within the range presented for the EDS analysis.

Despite the potential to establish a correlation between the present research and other studies through *Table 3.10*, drawing quantitative, definitive comparisons is considered unrealistic. The composition of ash particles is significantly impacted by the additives present in the lubricating oil utilized during operation, rather than to operational conditions [44] [80]. Consequently, distinct oil compositions may yield different post-combustion products. Nonetheless, evaluating the composition of ash particles remains an interesting prospect, as it presents an opportunity to estimate the ash fraction and quantify its amount through the integration of ICP, XRD, and other analytical techniques.

The combined results from XRD, EDS, and ICP suggest that the majority of ash from diesel exhaust PM is likely to be in an amorphous phase. However, further XRD measurements are required to test such hypothesis since the small amount of sample and the important effect of the background noise might have also played a role.

3.5 Evaluation of the ash fraction within the PM composition

3.5.1 Estimated ash fraction

The ratio between ash and soot was assessed only for few samples due to several investigation and equipment-related limitations. The weight loss curve for each sample, as shown in *Figure 3.17* was divided into three regions to obtain results: volatile organic fraction (VOF), representing the fraction lost during conditioning; soot, representing the fraction burned during oxidation; and ash, representing the fraction remaining after oxidation.

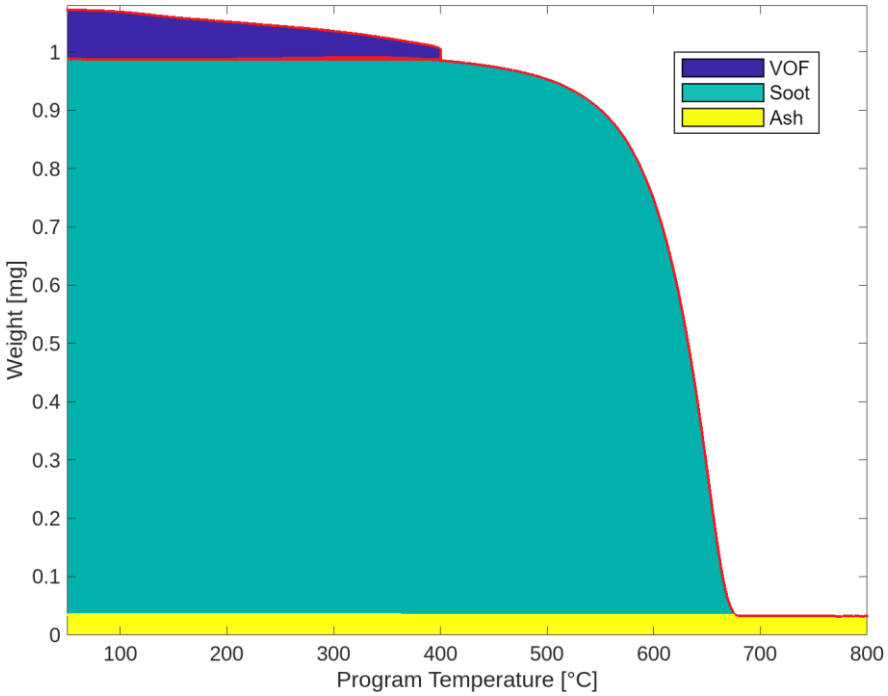

Figure 3.17 Weight loss curve for sample "STD5" with the division into areas corresponding to VOF, soot, and ash for compositional analysis

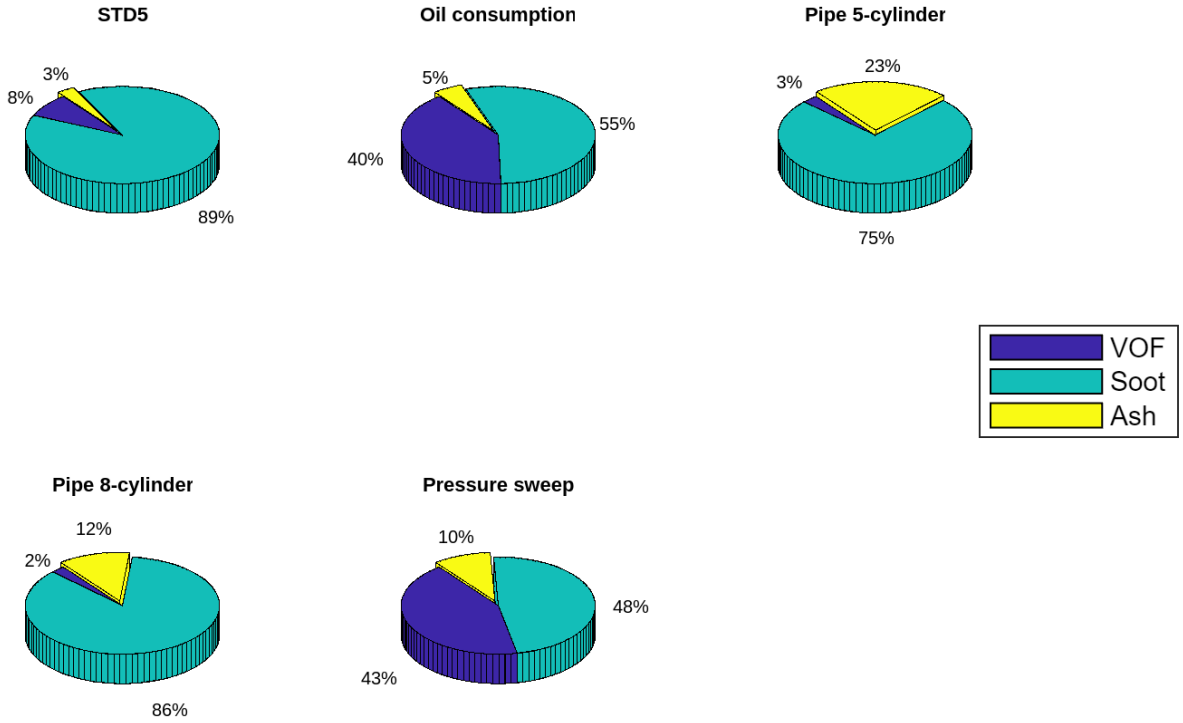

Figure 3.18 Particulate matter weight composition for the sample "STD5", "oil consumption", "pipe 5-cylinder", "pipe 8-cylinder" and "pressure sweep (Teflon)" obtained from the analysis of weight loss curves

Figure 3.18 depicts the constitution of the examined samples. Every sample presents specific peculiarities, for example in the "STD5" and "oil consumption" samples the VOF might result altered from the extraction procedure. Therefore, it results more interesting to look at the fraction between ash and soot, as shown in *Table 3.11*. A direct comparison of those two samples, though, reveals a probable impact of biodiesel on sample's "oil consumption" VOF. The VOF is reported to increase when biodiesel is utilized [66].

When the samples from the silencers are compared, a larger fraction of ash is evident in "pipe 5-cylinder" as probably effect of the longer time within the aftertreatment system.
The sample "pressure sweep" presented in *Figure 3.18* was scraped from the Teflon filer. Therefore, the depicted ash fraction was greater than the actual amount due to Teflon fiber contaminations. The results should only be interpreted as an indication for an upper limit of the ash fraction in this sample.

Table 3.11 compares to the previously discussed results, also the evaluation of the ash fraction from the ICP test, discussed in Section 4.7.

Table 3.11 Ash fraction in the analyzed samples, different calculation methods

Sample	Ash fraction [% mass]	Ash/soot* [% mass]	Calculation method
STD5	2.98 %	3.3 %	From mass loss curves (TGA)
Oil consumption	5.02 %	9.1 %	From mass loss curves (TGA)
Pipe 5-cylinder	22.79 %	30.6 %	From mass loss curves (TGA)
Pipe 8-cylinder	12.03 %	14.1 %	From mass loss curves (TGA)
Pressure sweep ICP	11.00 %	12.0 %**	Extrapolated from ICP results
Pressure sweep Teflon	9.66 %	20.3 %	Scraped from Teflon filter, analyzed from mass loss curves (TGA)

*soot is assumed as the fraction that burns during the oxidation step in thermogravimetric analysis

**the sample was not conditioned before ICP, therefore this fraction does not take in account the fraction of volatiles

3.5.2 Ash fraction discussion and comparison with literature

Comparing the results presented in *Table 3.11* with the research in this area, has shown that the ash fraction determined during the ongoing research resulted generally higher than the results proposed by the literature, summarized in *Table 3.12*. The results presented by M. Zhang [46] were also obtained throughout an extraction procedure and in different operative conditions.

Even if the EDS analysis conducted on extracted samples did not indicate any contamination from fiberglass, it remains plausible that some degree of contamination was present. Nevertheless, the findings of S. Bagi [45] reveal that an ash fraction greater than 1% can be observed under certain operational conditions, aligning with the results obtained in the current study.

Table 3.12 Comparison of the PM composition with the focus on the ash fraction between different literature researches

	A. Sappok [44]	**S. Bagi** [45]	**M. Zhang** [46]	
Operative mode	(1682 rpm, 25% load) and (1682 rpm, 75% load)	Sum of long-haul, regional delivery and city service	Low speed High load	High speed High load
Ash [%wt]	0.5	3.12	>0.5	1
Carbonic fraction [%wt]	87.5	-	91	92
VOF [%wt]	12.4	-	9	7

3.6 Extraction procedure: gas chromatography of the extraction solvent

Liquid GC showed that the extraction favored the separation of several hydrocarbons from the PM to the extracting solvent. The comparison of different chromatograms revealed that the solvents from the extraction of different samples contain the same hydrocarbons. This result was inferred also for the samples that do not share the same fuel during the operating conditions as showed in *Figure 3.19*, where the sample "STD5" is compared with the sample "oil consumption". Those compounds, shared by all the extracted samples, and not present in the pure solvent, are presented in *Table 3.13* and result different from the constituents of the fuels, as showed more in detail in the Appendix C.

Low weight PAH are likely to be soluble in the employed solvent, cyclohexane [84]. However, only benzene and 1,4-Di-tetr-butylphenol were the only detected aromatic compounds. The list of PAH commonly identified within the PM can be found in the work of V. K. Yadav [85] and comprehend a large amount of high molecular weight aromatics.

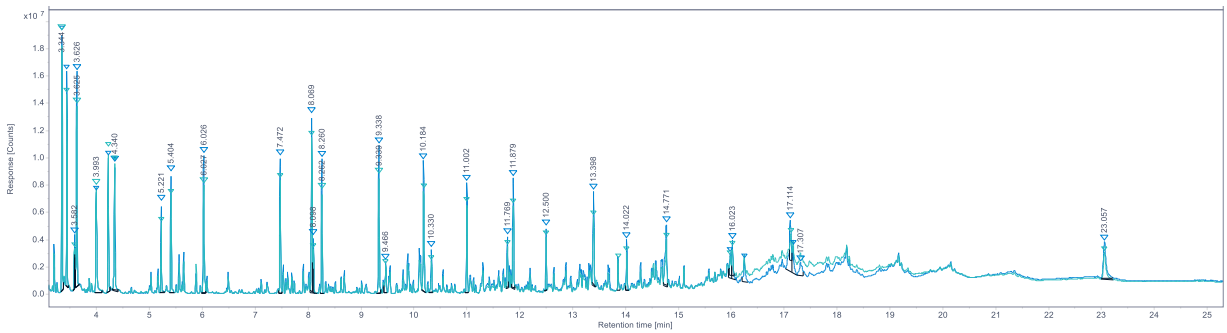

Figure 3.19 Comparison between the extraction solvent of the sample STD5 (aquamarine chromatogram) and oil consumption (blue chromatogram)

Eventual comparisons with chromatographic analyses from the literature are challenging due to different experimental conditions: the heating rate and the choice of solvent will have a major impact on the elution time. Different solvents will have different affinities for the compounds present on the PM.

K.E. Voss [86] performed a GC on the soluble organic fraction (SOF) extracted with Soxhlet procedure from PM collected at low speed and high load conditions, showing that the predominant amount of SOF is due to lubricant oil elements, which show a broad area towards high elution times. On the other side, the results of this research show that a significant fraction of the absorbed compounds were of aliphatic nature and only a limited amount were aromatic. This can also be motivated by the choice of extraction solvent.

Table 3.13 Liquid GC compounds from the extraction in cyclohexane of the samples from the 6-cylinder engine

Compound	Retention time [min]	Area [%]	Start time [min]	End time [min]	Probability [%]
Undecane	6.0	4.5	6.0	6.1	14
Dodecane	7.5	4.1	7.4	7.5	45
Benzene	8.1	5.5	8.0	8.1	76
Pentadecane	8.3	3.7	8.2	8.3	10
Tetradecane	9.3	4.5	9.3	9.4	37
Hexadecane	10.2	4.7	10.1	10.2	8
1,4-Di-tetr-butylphenol	10.3	1.4	10.3	10.4	51
Hexadecane	11.0	3.2	11.0	11.0	29
Heptadecane	11.8	1.6	11.7	11.8	18
Heneicosane	11.9	3.9	11.9	11.9	10
Eicosane	12.5	1.7	12.5	12.5	25
Tetracosane	13.4	3.6	13.4	13.4	13
Octadecanal	14.0	1.5	14.0	14.1	33
Pentacosane	14.8	3.4	14.7	14.8	15
Tetratriacontane	16.0	1.5	16.0	16.0	11
Phenanthrenecarboxylic acid	23.1	3.5	23.0	23.2	10

3.7 Samples handling discussion

The present study has revealed a number of pertinent issues that should be addressed to facilitate future research in this field. Specifically, attention should be given to the challenges associated with sample handling, potential contaminations, and the potential impact of other manipulations on the outcome of the analysis.

The first challenge is addressed to the PM collection method. The first attempt to collect the exhaust particulate was performed by using fiberglass filters coated with PTFE as accomplished by s. Bagi [45]. Nevertheless, even a delicate scraping of the upper layer of particulate revealed some filter fiber contaminations as evident in *Figure 3.20*, where a cluster of PM containing some white fiber filters can be observed. A similar procedure using pure Teflon filters yielded similar results. The use of quartz filters would inevitably result in contamination due to the brittle nature of silica dioxide (SiO_2) fibers.

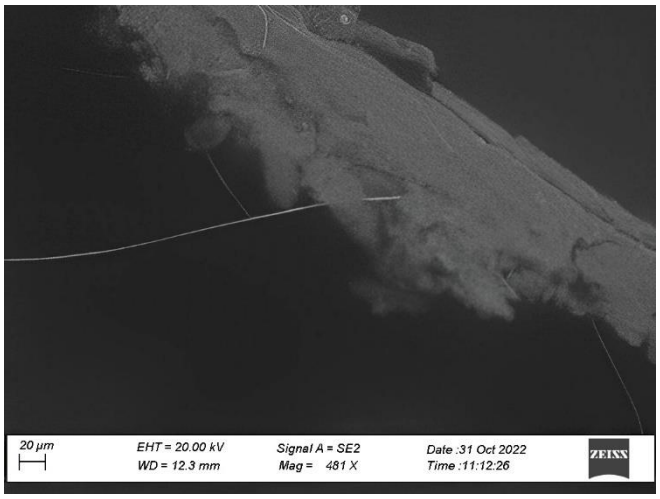

Figure 3.20 SEM: detail on fiber glass contamination on PM scraped from Pallflex TX40HI20 filter

The discovery of the contamination led to the conception of an extraction method for more precise determination of the ash percentage and ash composition using samples obtained on fiber glass filters. According to Appendix C, several solvents underwent testing. Additionally, it was thought that using ultrasounds would help remove the PM from the filter. *Figure 3.21* illustrates significant PM contaminations as a result of enhanced filter deterioration caused by the use of ultrasounds. Therefore, it is not recommended to use ultrasounds.

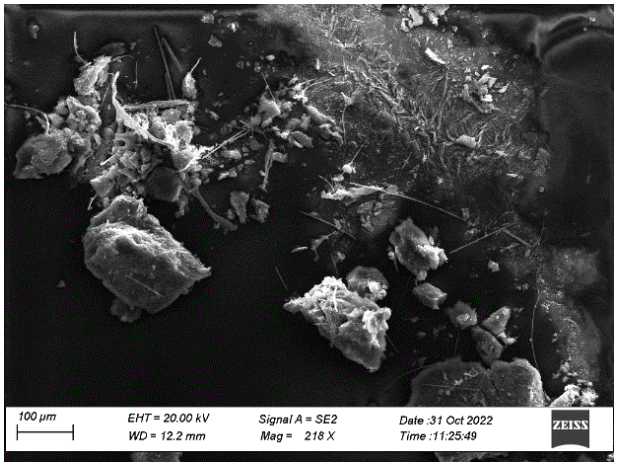

Figure 3.21 PM presenting severe fiber contamination extracted from Pallflex TX40HI20 filter and subjected to ultrasounds as part of the extraction procedure

During thermogravimetric analysis, the presence of quartz fibers will not spoil kinetic studies, as discussed previously. Though, the presence of these fibers will increase the incombustible fraction when estimating the ash fraction. Future studies should focus on determining the amount and impact of these contaminations on the analysis results. Pure silica (quartz) fiber contamination will not pose a problem for ash composition estimation via EDS, unlike borosilicate fiber glass filters, which can contain elements like Na, K, Al and eventual impurities that can also be present in ash compounds.

Quartz filters have the added advantage of being quasi-pure silica, making them suitable for ICP analysis. Pure Teflon filters can also be used for this characterization. ICP analysis provides high-precision analysis of small amounts of metals and is useful for ash composition studies. Estimating the ash fraction can be particularly challenging, but coupling ICP with XRD can enhance the knowledge in this topic.

Chapter 4
Conclusions

This work aimed to investigate an uncovered section of the worldwide scientific research, by trying to estimate the ash fraction produced during ongoing engine operations. It also poses a critical look on the limitations and potential problems that might arise during the study of the soot oxidation kinetics and ash fraction. Part of the study focused on the research of the more suitable filters and analysis of the influence they might have on the results. The following main conclusions, relative to the key research questions can be drawn.

1. The ash to soot ratio for heavy-duty diesel engines resulted incredibly hard to estimate with accuracy due to intrinsic limitation of different collection methods. Contaminations from filters are likely to occur and have been observed. The ash to soot fraction was estimated to lie between 3 and 31 percent in weight and it was detected to be higher in the samples scraped from the silencers. Probably, as effect of ash accumulation, whereas part of the soot reacts within the system. Compared to existing literature on ongoing operations, this result is higher. However, it is lower than the estimations performed during certification cycles.

   The influence of different operative conditions on the ash production resulted difficult to assess due to the high number of variables between the collected samples. The effect of the use of biodiesel was designed as the most likely reason for a greater VOF fraction in the sample "oil consumption" when compared to "STD5". The aging effect might have been the cause from a bigger ash fraction in the sample "pipe 5-cylinder" when compared with "pipe 8-cylinder", since the latter sample was deposited on the silencer inlet from a briefer time.

   The establishment of a soot-to-ash ratio range provides valuable insights into the ash fraction present in engines and obtained under analyses that ought to minimize filter contamination. This finding represents a positive outcome with important implications for the future of DPF modelling: by investigating a range of real-world driving cycles, beyond those typically employed for emission control, this study expands our understanding of particulate emissions under various conditions.

2. Soot showed similar morphological characteristics and, more interestingly, very similar activation energies (138-164 kJ/mol), by comparing completely different samples, from different engines, with different fuels and collected in diverse ways. The similar reactivity can also be inferred by the values of $MLRT_{max}$, which have been reported to be comparable for all the samples in analysis. This result opens up new possibilities for employing diverse types of soot in the research phase of diesel particulate filter modelling, with the potential to more accurately reflect real-world road conditions. In addition, this finding is relevant for enhancing our understanding of the properties of soot that accumulates in the DPF and optimizing its regeneration strategies.

3. The characterization of ash composition proved to be challenging due to the limited amount of ash available on the filters used for sample collection, as well as the potential for contamination from external agents and the filters used for the sample collection. Therefore, a variety of techniques were employed to evaluate the ash composition and to assess the reliability of the results, including a review of pertinent scientific literature and a comparison among different methods.

3.1 EDS is frequently used in literature for ash composition analyses, however, in this, as well as in other researches, the composition appear to be wildly variable from sample to sample. Whereas Ca has been stated as the main constituent, an unexpectantly high concentration of Na was detected in all samples.

3.2 Several samples were extracted by using cyclohexane in order to reduce filter contaminations which are likely to be unavoidable by scaping the PM from the filter surface. Though, by critically looking into the EDS results it can be inferred that the extraction procedure might have affected the ash composition. The extracted samples, presented a small or not detectable fraction of Mg, P and Zn during EDS.

3.3 ICP allowed only a partial evaluation of the sample since multiple elements that are expected to be present, were below the detection threshold. Nevertheless, the amounts of Ca, Zn and Cu were successfully detected. This allowed to assess a partial comparison between the "pressure sweep 1h" sample analyzed with ICP and with EDS showing similarities in results.

3.4 XRD analysis might be an effective tool to detect the composition of the ash samples, though, the limited amount of sample influenced the result: only $Zn_3(PO_4)_2$ and $Zn_3Mg(PO_4)_2$ were sensed. The absence of peaks identifying $CaSO_4$ suggests the presence of a significant fraction of ash compounds in an amorphous phase, consistent with previous findings in the literature.

Overall, EDS was found to be the more suitable method as it allowed the largest number of samples to be analyzed. The use of other analyses was limited by the small amount of ash available. XRD can be interesting because it allows to look into compounds rather than elements, but sample size limitations make it arduous to employ for ash collected during engine operation. Employing multiple analysis techniques in parallel can enhance the comprehension of ash composition and contribute to achieving greater levels of validation.

4. Every collection method that involves filters will inevitably bring some sort of contamination to the sample and can make some analyses unsuitable or meaningless.

4.1 Quartz filters are the most suitable for kinetic studies since they are inert in the soot oxidation temperatures range. However, they result being brittle and therefore would spoil the results when ash fraction estimation is the target.

4.2 When Teflon is contained within the filters (pure Teflon fibers or fiber glass coated with Teflon), it will spoil TGA results, making the weight loss curve not significative. Furthermore, the thermogravimetric analysis performed just on the filter has shown that for both kind of filters, residues will be present at the end of the heating program. Therefore, if filter contaminations are present, the ash fraction estimation, obtained by weighting the sample after the TGA, will be increased by the contaminations and thus inaccurate. and the ash composition analysis, for example performed with EDS, will be spoiled.

4.3 The advantage of fiber glass filters over the quartz filters is that they are less brittle, therefore if the ash fraction is the target, the use of this filter can be coupled with an extraction procedure in order to get rid of the filter without damaging it and thus

creating contaminations. The extraction procedure can be successful in minimizing filter contaminations prior to TGA: EDS of the extracted samples has shown that the identifying components of the fiber glass filters were not present, contrary to when the PM was scraped from the filter. However, low extraction rates are a limiting factor for the procedure. The use of an extraction procedure have to further be investigated since it might have effect of the ash composition, as presented in the results of the EDS.

4.4 The samples scraped from the inlets of the silencers had a larger fraction of ash if compared to samples collected from ongoing cycles.

Recommendations for future work

With the study´s findings in mind, the following ideas and recommendations for future work, that aim to deepen and confirm the results relative to the areas covered by the research questions, are provided:

1. In order to improve the understanding of the ash fraction in the on-going operation of heavy duty CI engines, it is critical to improve the particulate collection methods as they lead to the underlying issues for any subsequent PM characterization. Exploring alternatives to filter collection, such as the use of impactors, is a possible avenue of investigation. Additionally, this research project was constrained by the limited number of samples and the high number of parameters varying among them. The subsequent investigation ought to prioritize the development of reliable and reproducible tests. This requires first of all the availability of test cells to tailor in a more focused way the experiments: changing one characteristic per time and study its impact. The analysis of different steady state conditions would be would be a noteworthy endeavor to correlate the ash fraction to different engine operations.

2. The results of the soot oxidation kinetic study had shown similar reactivities among all the samples in analysis. This study employed a non-isothermal isoconversional multiple-ramp rates method and the kinetic parameters were estimated by applying the Flynn-Wall-Ozawa method coupled with the Doyle´s approximation. A follow-up investigation could compare different approximation techniques from the literature to assess any significant changes in the results. More accurate results in terms of kinetic might be obtained through isothermal runs. However, those require a high number of samples to be analyzed. As previously noted, some diffusion limitations might have occurred during the TGA of samples analyzed on quartz filters. A future study could compare the activation energies of commonly known soot, such as Printex-U, obtained through thermogravimetric runs of the soot in powder and deposited on quartz filters.
   To get deeper insights into the reactivity, a quantitative analysis of the primary particles and agglomerates dimension could be performed. For instance, transmission electron microscopy (TEM) could facilitate a more comprehensive analysis by enabling the detection of morphological structures with increased resolution.

3. Ash samples collected from running engines, before reaching the DPF filter where it will accumulate, are small in quantity and this renders them particularly difficult to analyze. Several characterization techniques have been proposed to characterize the ash samples in terms of composition. The limiting factor is the small amount of ash in each sample, which limits the use of some characterization techniques, such as XRD. In addition, the reduced amount is more likely to be contaminated, both from the environment and from the filters on which the PM is commonly collected. For this reason, a combination of techniques and approaches can be beneficial in determining whether an analysis is accurate or the results are affected by sample size or contamination. For example, FTIR can be employed to identify compounds present in the ash and compare them with the results of other analyses. Similarly, coupling EDS and ICP to compare the relative amount of different elements or to establish and compare mass balances may be a way to evaluate more reliable results in the future. This was not possible in the current study due to sample availability. In general, ICP can be a powerful technique to perform elemental analysis, however, to yield in reliable

results, it requires the study of a large number of samples, with multiple replicates for each operating condition. Each sample should be larger in amount of weight, as this research has shown that several elements present in the sample were below the detection threshold. The large variability in ash composition shown by the EDS results requires further investigation. In particular, whether the extraction process affects the ash composition needs to be assessed through further laboratory analyses. In addition, the reasons for the high amount of sodium (Na) detected in all samples may be of additional interest.

It is noteworthy to investigate the crystallinity of the ash via XRD. The presence of different ash phases can result in varying ash packing densities, and as such, this study can hold significance for the advancement of ash deposition techniques in DPF. Moreover, it can also facilitate the enhancement of filter cleaning and regeneration protocols.

4. The research on more effective methods for particulate matter collection forms the fundamental framework for any further progress in this field, as it represents the initial step that gives rise to a significant number of contaminations, limitations, and challenges for subsequent analyses. The extraction method showed to be a compelling opportunity for the ash fraction estimation, nevertheless, further research is needed to improve the extraction rate. Possible solutions might be use different solvents or to remove the particulate from different filters, for example Teflon filters. An example of different solvent to investigate can be dichloromethane.

References

[1] B. Giechaskiel *et al.*, "Assessment of a Euro VI Step E Heavy-Duty Vehicle's Aftertreatment System," *Catalysts*, vol. 12, no. 10, Art. no. 10, Oct. 2022, doi: 10.3390/catal12101230.

[2] R. Andersson and B. Andersson, "The effect of exhaust gas composition on the kinetics of soot oxidation and diesel particulate filter regeneration," *Fuel*, vol. 220, pp. 453–463, May 2018, doi: 10.1016/j.fuel.2018.02.037.

[3] *Commission Regulation (EU) No 582/2011 of 25 May 2011 implementing and amending Regulation (EC) No 595/2009 of the European Parliament and of the Council with respect to emissions from heavy duty vehicles (Euro VI) and amending Annexes I and III to Directive 2007/46/EC of the European Parliament and of the Council (Text with EEA relevance)Text with EEA relevance*. 2011. Accessed: Jan. 16, 2023. [Online]. Available: https://eur-lex.europa.eu/legal-content/EN/TXT/?uri=CELEX%3A02011R0582-20221210

[4] O. US EPA, "Evolution of the Clean Air Act," May 29, 2015. https://www.epa.gov/clean-air-act-overview/evolution-clean-air-act (accessed Mar. 27, 2023).

[5] *Council Directive 93/59/EEC of 28 June 1993 amending Directive 70/220/EEC on the approximation of the laws of the Member States relating to measures to be taken against air pollution by emissions from motor vehicles*, vol. 186. 1993. Accessed: Mar. 27, 2023. [Online]. Available: http://data.europa.eu/eli/dir/1993/59/oj/eng

[6] *Directive 94/12/EC of the European Parliament and the Council of 23 March 1994 relating to measures to be taken against air pollution by emissions from motor vehicles and amending Directive 70/220/EEC*, vol. 100. 1994. Accessed: Mar. 27, 2023. [Online]. Available: http://data.europa.eu/eli/dir/1994/12/oj/eng

[7] *Directive 98/69/EC of the European Parliament and of the Council of 13 October 1998 relating to measures to be taken against air pollution by emissions from motor vehicles and amending Council Directive 70/220/EEC*, vol. 350. 1998. Accessed: Mar. 27, 2023. [Online]. Available: http://data.europa.eu/eli/dir/1998/69/oj/eng

[8] "Emission Standards: Europe: Heavy-Duty Truck and Bus Engines." https://dieselnet.com/standards/eu/hd.php#stds (accessed Mar. 27, 2023).

[9] "EU: Heavy-duty: Emissions | Transport Policy." https://www.transportpolicy.net/standard/eu-heavy-duty-emissions/ (accessed Sep. 08, 2022).

[10] "Proposal for a REGULATION OF THE EUROPEAN PARLIAMENT AND OF THE COUNCIL on type-approval of motor vehicles and engines and of systems, components and separate technical units intended for such vehicles, with respect to their emissions and battery durability (Euro 7) and repealing Regulations (EC) No 715/2007 and (EC) No 595/2009." EUROPEAN COMMISSION, Nov. 10, 2022.

[11] "Control of Air Pollution From New Motor Vehicles: Heavy-Duty Engine and Vehicle Standards." US Environmental Protection Agency, 2023. [Online]. Available: https://www.govinfo.gov/content/pkg/FR-2023-01-24/pdf/2022-27957.pdf

[12] "news: Scania unveils Euro VI engines." https://dieselnet.com/news/2011/04scania.php (accessed Dec. 30, 2022).

[13] J. Merkisz and J. Pielecha, *Nanoparticle Emissions From Combustion Engines*, vol. 8. in Springer Tracts on Transportation and Traffic, vol. 8. Cham: Springer International Publishing, 2015. doi: 10.1007/978-3-319-15928-7.

[14] P. Eastwood, *Particulate emissions from vehicles*. Chichester: J. Wiley & Son, 2008.

[15] G. A. Merkel, W. A. Cutler, and C. J. Warren, “Thermal Durability of Wall-Flow Ceramic Diesel Particulate Filters,” presented at the SAE 2001 World Congress, Mar. 2001, pp. 2001-01–0190. doi: 10.4271/2001-01-0190.
[16] Y. Wang, “The origin, transport, and evolution of ash in engine particulate filters,” *Appl. Energy*, p. 26, 2020.
[17] S. Mohankumar and P. Senthilkumar, “Particulate matter formation and its control methodologies for diesel engine: A comprehensive review,” *Renew. Sustain. Energy Rev.*, vol. 80, pp. 1227–1238, Dec. 2017, doi: 10.1016/j.rser.2017.05.133.
[18] R. Khobragade *et al.*, “Chemical composition of diesel particulate matter and its control,” *Catal. Rev.*, vol. 61, no. 4, pp. 447–515, Oct. 2019, doi: 10.1080/01614940.2019.1617607.
[19] A. K. Agarwal, A. Dhar, N. Sharma, and P. C. Shukla, Eds., *Particle number and particulate mass emissions of heavy duty vehicles in real operating conditions*. in Energy, Environment, and Sustainability. Singapore: Springer Singapore, 2019. doi: 10.1007/978-981-13-3299-9.
[20] L. Rymaniak, A. Ziolkowski, and D. Gallas, “Particle number and particulate mass emissions of heavy duty vehicles in real operating conditions,” *MATEC Web Conf.*, vol. 118, p. 00025, 2017, doi: 10.1051/matecconf/201711800025.
[21] H. E. Institute, “Diesel Exhaust: Critical Analysis of Emissions, Exposure, and Health Effects,” *Health Effects Institute*, Apr. 01, 1995. https://www.healtheffects.org/publication/diesel-exhaust-critical-analysis-emissions-exposure-and-health-effects (accessed Nov. 02, 2022).
[22] A. Sappok, I. Govani, C. Kamp, Y. Wang, and V. Wong, “In-Situ Optical Analysis of Ash Formation and Transport in Diesel Particulate Filters During Active and Passive DPF Regeneration Processes,” *SAE Int. J. Fuels Lubr.*, vol. 6, no. 2, pp. 336–349, Apr. 2013, doi: 10.4271/2013-01-0519.
[23] M. Lapuerta, F. Oliva, J. R. Agudelo, and A. L. Boehman, “Effect of fuel on the soot nanostructure and consequences on loading and regeneration of diesel particulate filters,” *Combust. Flame*, vol. 159, no. 2, pp. 844–853, Feb. 2012, doi: 10.1016/j.combustflame.2011.09.003.
[24] H. Wihersaari *et al.*, “Particulate emissions of a modern diesel passenger car under laboratory and real-world transient driving conditions,” *Environ. Pollut.*, vol. 265, p. 114948, Oct. 2020, doi: 10.1016/j.envpol.2020.114948.
[25] “Exhaust Gas Sampling and Conditioning.” https://dieselnet.com/tech/measure_sample.php (accessed Jan. 09, 2023).
[26] W. Sun, Q. Wang, L. Guo, P. Cheng, D. Li, and Y. Yan, “Influence of biodiesel/diesel blends on particle size distribution of CI engine under steady/transient conditions,” *Fuel*, vol. 245, pp. 336–344, Jun. 2019, doi: 10.1016/j.fuel.2019.01.101.
[27] J. Wei and Y. Wang, “Effects of biodiesels on the physicochemical properties and oxidative reactivity of diesel particulates: A review,” *Sci. Total Environ.*, vol. 788, p. 147753, Sep. 2021, doi: 10.1016/j.scitotenv.2021.147753.
[28] F. S. Hirner, J. Hwang, C. Bae, C. Patel, T. Gupta, and A. K. Agarwal, “Nanostructure characterization of soot particles from biodiesel and diesel spray flame in a constant volume combustion chamber,” *Fuel*, vol. 235, pp. 130–149, Jan. 2019, doi: 10.1016/j.fuel.2018.07.092.
[29] H. Chen, B. Xie, J. Ma, and Y. Chen, “NOx emission of biodiesel compared to diesel: Higher or lower?,” *Appl. Therm. Eng.*, vol. 137, pp. 584–593, Jun. 2018, doi: 10.1016/j.applthermaleng.2018.04.022.

[30] J. Nuszkowski, K. Flaim, and G. Thompson, “The Effect of Cetane Improvers and Biodiesel on Diesel Particulate Matter Size,” *SAE Int. J. Fuels Lubr.*, vol. 4, no. 1, pp. 23–33, Apr. 2011, doi: 10.4271/2011-01-0330.
[31] “VERT: Curtailing Emissions of Diesel Engines in Tunnel Sites.” https://dieselnet.com/papers/9804mayer/ (accessed Jan. 23, 2023).
[32] G. Karavalakis, T. D. Durbin, J. Yang, L. Ventura, and K. Xu, “Fuel Effects on PM Emissions from Different Vehicle/Engine Configurations: A Literature Review,” presented at the WCX World Congress Experience, Apr. 2018, pp. 2018-01–0349. doi: 10.4271/2018-01-0349.
[33] Y. Wang, H. Yang, X. Liang, H. Song, and Z. Tao, “Effect of metallic lubricant additives on morphology, nanostructure, graphitization degree and oxidation reactivity of diesel particles,” *Chemosphere*, vol. 306, p. 135588, Nov. 2022, doi: 10.1016/j.chemosphere.2022.135588.
[34] M. J. Payne, “Using Lubricant Technology to Drive Down Particulate and CO2 Emissions in Diesel Engines,” *EngineExpo 2006*, May 2006.
[35] N. R. Abdullah, R. Mamat, P. Rounce, A. Tsolakis, M. L. Wyszynski, and H. M. Xu, “Effect of Injection Pressure with Split Injection in a V6 Diesel Engine,” presented at the 9th International Conference on Engines and Vehicles, Sep. 2009, pp. 2009-24–0049. doi: 10.4271/2009-24-0049.
[36] D. B. Kittelson, “Engines and nanoparticles: a review,” *J. Aerosol Sci.*, vol. 29, no. 5, pp. 575–588, Jun. 1998, doi: 10.1016/S0021-8502(97)10037-4.
[37] M. N. Ess *et al.*, “Reactivity and structure of soot generated at varying biofuel content and engine operating parameters,” *Combust. Flame*, vol. 163, pp. 157–169, Jan. 2016, doi: 10.1016/j.combustflame.2015.09.016.
[38] J. P. Soussi, R. Demarco, J. L. Consalvi, F. Liu, and A. Fuentes, “Influence of soot aging on soot production for laminar propane diffusion flames,” *Fuel*, vol. 210, pp. 472–481, Dec. 2017, doi: 10.1016/j.fuel.2017.08.086.
[39] S. Vyazovkin *et al.*, “ICTAC Kinetics Committee recommendations for collecting experimental thermal analysis data for kinetic computations,” *Thermochim. Acta*, vol. 590, pp. 1–23, Aug. 2014, doi: 10.1016/j.tca.2014.05.036.
[40] M. Lapuerta, J. Rodríguez–Fernández, and J. Sánchez-Valdepeñas, “Soot reactivity analysis and implications on diesel filter regeneration,” *Prog. Energy Combust. Sci.*, vol. 78, p. 100833, May 2020, doi: 10.1016/j.pecs.2020.100833.
[41] C. D. Doyle, “Estimating isothermal life from thermogravimetric data,” *J. Appl. Polym. Sci.*, vol. 6, no. 24, pp. 639–642, 1962, doi: 10.1002/app.1962.070062406.
[42] H. N. Sharma, L. Pahalagedara, A. Joshi, S. L. Suib, and A. B. Mhadeshwar, “Experimental Study of Carbon Black and Diesel Engine Soot Oxidation Kinetics Using Thermogravimetric Analysis,” *Energy Fuels*, vol. 26, no. 9, pp. 5613–5625, Sep. 2012, doi: 10.1021/ef3009025.
[43] J. Rodríguez-Fernández, F. Oliva, and R. A. Vázquez, “Characterization of the Diesel Soot Oxidation Process through an Optimized Thermogravimetric Method,” *Energy Fuels*, vol. 25, no. 5, pp. 2039–2048, May 2011, doi: 10.1021/ef200194m.
[44] A. G. Sappok and V. W. Wong, “Detailed Chemical and Physical Characterization of Ash Species in Diesel Exhaust Entering Aftertreatment Systems,” presented at the SAE World Congress & Exhibition, Apr. 2007, pp. 2007-01–0318. doi: 10.4271/2007-01-0318.
[45] S. Bagi, C. J. Kamp, V. Sharma, and P. B. Aswath, “Multiscale characterization of exhaust and crankcase soot extracted from heavy-duty diesel engine and implications for DPF ash,” *Fuel*, vol. 282, p. 118878, Dec. 2020, doi: 10.1016/j.fuel.2020.118878.

[46] M. Zhang *et al.*, “An investigation into the impact of burning diesel/lubricant oil mixtures on the nature of particulate emissions: Implications for DPF ash-loading acceleration method,” *J. Energy Inst.*, vol. 93, no. 3, pp. 1207–1215, Jun. 2020, doi: 10.1016/j.joei.2019.11.004.
[47] J. Gao, C. Ma, S. Xing, L. Sun, and H. Liyong, “A review of fundamental factors affecting diesel PM oxidation behaviors,” *Sci. China Technol. Sci.*, vol. 61, Sep. 2017, doi: 10.1007/s11431-016-9117-x.
[48] J. SONG, M. ALAM, and A. L. BOEHMAN∗, “Impact of Alternative Fuels on Soot Properties and Dpf Regeneration,” *Combust. Sci. Technol.*, vol. 179, no. 9, pp. 1991–2037, Aug. 2007, doi: 10.1080/00102200701386099.
[49] J. Wei, W. Lu, Y. Zeng, H. Huang, M. Pan, and Y. Liu, “Physicochemical properties and oxidation reactivity of exhaust soot from a modern diesel engine: Effect of oxyfuel type,” *Combust. Flame*, vol. 238, p. 111940, Apr. 2022, doi: 10.1016/j.combustflame.2021.111940.
[50] J.-O. Müller, D. S. Su, R. E. Jentoft, J. Kröhnert, F. C. Jentoft, and R. Schlögl, “Morphology-controlled reactivity of carbonaceous materials towards oxidation,” *Catal. Today*, vol. 102–103, pp. 259–265, May 2005, doi: 10.1016/j.cattod.2005.02.025.
[51] C. Su, Y. Wang, A. Kumar, and P. J. McGinn, “Simulating Real World Soot-Catalyst Contact Conditions for Lab-Scale Catalytic Soot Oxidation Studies,” *Catalysts*, vol. 8, no. 6, Art. no. 6, Jun. 2018, doi: 10.3390/catal8060247.
[52] M. Kalogirou and Z. Samaras, “A thermogravimetic kinetic study of uncatalyzed diesel soot oxidation,” *J. Therm. Anal. Calorim.*, vol. 98, no. 1, pp. 215–224, Oct. 2009, doi: 10.1007/s10973-009-0110-8.
[53] C. J. Tighe, M. V. Twigg, A. N. Hayhurst, and J. S. Dennis, “The kinetics of oxidation of Diesel soots and a carbon black (Printex U) by O2 with reference to changes in both size and internal structure of the spherules during burnout,” *Carbon*, vol. 107, pp. 20–35, Oct. 2016, doi: 10.1016/j.carbon.2016.04.075.
[54] Y. Liu, S. Wu, C. Fan, X. Wang, F. Liu, and H. Chen, “Variations in surface functional groups, carbon chemical state and graphitization degree during thermal deactivation of diesel soot particles,” *J. Environ. Sci.*, vol. 124, pp. 678–687, Feb. 2023, doi: 10.1016/j.jes.2022.01.007.
[55] S. Jian *et al.*, “Kinetic analysis of morphologies and crystal planes of nanostructured CeO2 catalysts on soot oxidation,” *Chem. Eng. Sci.*, vol. 226, p. 115891, Nov. 2020, doi: 10.1016/j.ces.2020.115891.
[56] Z. Meng, D. Yang, and Y. Yan, “Study of carbon black oxidation behavior under different heating rates,” *J. Therm. Anal. Calorim.*, vol. 118, no. 1, pp. 551–559, Oct. 2014, doi: 10.1007/s10973-014-4020-z.
[57] X. Liang *et al.*, “Experimental investigation of diesel soot oxidation reactivity along the exhaust after-treatment system components,” *Fuel*, vol. 302, p. 121047, Oct. 2021, doi: 10.1016/j.fuel.2021.121047.
[58] D. Zhang, Y. Ma, and M. Zhu, “Nanostructure and oxidative properties of soot from a compression ignition engine: The effect of a homogeneous combustion catalyst,” *Proc. Combust. Inst.*, vol. 34, no. 1, pp. 1869–1876, Jan. 2013, doi: 10.1016/j.proci.2012.05.096.
[59] J. McGeehan *et al.*, “Analysis of DPF Incombustible Materials from Volvo Trucks Using DPF-SCR-Urea With API CJ-4 and API CI-4 PLUS Oils,” *SAE Int. J. Fuels Lubr.*, vol. 2, no. 1, pp. 762–780, Jun. 2009, doi: 10.4271/2009-01-1781.
[60] A. Sappok, M. Santiago, T. Vianna, and V. W. Wong, “Characteristics and Effects of Ash Accumulation on Diesel Particulate Filter Performance: Rapidly Aged and Field

Aged Results," presented at the SAE World Congress & Exhibition, Apr. 2009, pp. 2009-01–1086. doi: 10.4271/2009-01-1086.
[61] A. Liati, P. Dimopoulos Eggenschwiler, E. Müller Gubler, D. Schreiber, and M. Aguirre, "Investigation of diesel ash particulate matter: A scanning electron microscope and transmission electron microscope study," *Atmos. Environ.*, vol. 49, pp. 391–402, Mar. 2012, doi: 10.1016/j.atmosenv.2011.10.035.
[62] D. M. Young, D. L. Hickman, G. Bhatia, and N. Gunasekaran, "Ash Storage Concept for Diesel Particulate Filters," presented at the SAE 2004 World Congress & Exhibition, Mar. 2004, pp. 2004-01–0948. doi: 10.4271/2004-01-0948.
[63] J. A. Mcgeehan *et al.*, "On The Road to 2010 Emissions: Field Test Results and Analysis with DPF-SCR System and Ultra Low Sulfur Diesel Fuel," presented at the Powertrain & Fluid Systems Conference & Exhibition, Oct. 2005, pp. 2005-01–3716. doi: 10.4271/2005-01-3716.
[64] A. Liati and P. Dimopoulos Eggenschwiler, "Characterization of particulate matter deposited in diesel particulate filters: Visual and analytical approach in macro-, micro- and nano-scales," *Combust. Flame*, vol. 157, no. 9, pp. 1658–1670, Sep. 2010, doi: 10.1016/j.combustflame.2010.02.015.
[65] "Particulate Measurement: Collecting Methods." https://dieselnet.com/tech/measure_pm_col.php (accessed Apr. 28, 2023).
[66] M. Lapuerta, R. Ballesteros, and J. Rodríguez-Fernández, "Thermogravimetric analysis of diesel particulate matter," *Meas. Sci. Technol.*, vol. 18, no. 3, pp. 650–658, Mar. 2007, doi: 10.1088/0957-0233/18/3/015.
[67] "Pallflex® Filters: Emfab™, Fiberfilm™, and Tissuquartz™ Filters." [Online]. Available: https://www.newstarenvironmental.com/pub/media/wysiwyg/PDF/Pall_Filters.pdf
[68] D. Uy *et al.*, "Characterization of gasoline soot and comparison to diesel soot: Morphology, chemistry, and wear," *Tribol. Int.*, vol. 80, pp. 198–209, Dec. 2014, doi: 10.1016/j.triboint.2014.06.009.
[69] C. D. Ávila, M. L. Botero, A. F. Agudelo, and J. R. Agudelo, "An assessment on how different collection methods impact thermal properties, surface functional groups, nanostructure and morphology of diesel particulate matter," *Combust. Flame*, vol. 225, pp. 74–85, Mar. 2021, doi: 10.1016/j.combustflame.2020.10.042.
[70] J. P. A. Neeft, T. X. Nijhuis, E. Smakman, M. Makkee, and J. A. Moulijn, "Kinetics of the oxidation of diesel soot," *Fuel*, vol. 76, no. 12, pp. 1129–1136, Jan. 1997, doi: 10.1016/S0016-2361(97)00119-1.
[71] A. Sinha, G. Ischia, G. Straffelini, and S. Gialanella, "A new sample preparation protocol for SEM and TEM particulate matter analysis," *Ultramicroscopy*, vol. 230, p. 113365, Nov. 2021, doi: 10.1016/j.ultramic.2021.113365.
[72] B. Giechaskiel, "Solid Particle Number Emission Factors of Euro VI Heavy-Duty Vehicles on the Road and in the Laboratory," *Int. J. Environ. Res. Public. Health*, vol. 15, no. 2, Art. no. 2, Feb. 2018, doi: 10.3390/ijerph15020304.
[73] S. Yoon *et al.*, "Characteristics of particle number and mass emissions during heavy-duty diesel truck parked active DPF regeneration in an ambient air dilution tunnel," *Atmos. Environ.*, vol. 122, pp. 58–64, Dec. 2015, doi: 10.1016/j.atmosenv.2015.09.032.
[74] T. Selleri *et al.*, "Measuring Emissions from a Demonstrator Heavy-Duty Diesel Vehicle under Real-World Conditions—Moving Forward to Euro VII," *Catalysts*, vol. 12, no. 2, p. 184, Feb. 2022, doi: 10.3390/catal12020184.
[75] C. J. Kamp, A. Sappok, Y. Wang, W. Bryk, A. Rubin, and V. Wong, "Direct Measurements of Soot/Ash Affinity in the Diesel Particulate Filter by Atomic Force

Microscopy and Implications for Ash Accumulation and DPF Degradation," *SAE Int. J. Fuels Lubr.*, vol. 7, no. 1, pp. 307–316, Apr. 2014, doi: 10.4271/2014-01-1486.
[76] J.-Y. Park, J.-H. Lee, C.-H. Kim, and Y.-J. Kim, "Fabrication of polytetrafluoroethylene nanofibrous membranes for guided bone regeneration," *RSC Adv.*, vol. 8, pp. 34359–34369, Oct. 2018, doi: 10.1039/C8RA05637D.
[77] S. Vyazovkin, A. K. Burnham, J. M. Criado, L. A. Pérez-Maqueda, C. Popescu, and N. Sbirrazzuoli, "ICTAC Kinetics Committee recommendations for performing kinetic computations on thermal analysis data," *Thermochim. Acta*, vol. 520, no. 1, pp. 1–19, Jun. 2011, doi: 10.1016/j.tca.2011.03.034.
[78] S. Vyazovkin, "Chapter 13 - Isoconversional Kinetics," in *Handbook of Thermal Analysis and Calorimetry*, M. E. Brown and P. K. Gallagher, Eds., in Recent Advances, Techniques and Applications, vol. 5. Elsevier Science B.V., 2008, pp. 503–538. doi: 10.1016/S1573-4374(08)80016-7.
[79] Z. Zhang, R. Dong, G. Lan, T. Yuan, and D. Tan, "Diesel particulate filter regeneration mechanism of modern automobile engines and methods of reducing PM emissions: a review," *Environ. Sci. Pollut. Res.*, vol. 30, no. 14, pp. 39338–39376, Mar. 2023, doi: 10.1007/s11356-023-25579-4.
[80] M. Morcos, P. Ayyappan, and T. Harris, "Characterization of DPF Ash for Development of DPF Regeneration Control and Ash Cleaning Requirements," presented at the SAE 2011 World Congress & Exhibition, Apr. 2011, pp. 2011-01–1248. doi: 10.4271/2011-01-1248.
[81] B. D. Cullity and J. W. Weymouth, "Elements of X-Ray Diffraction," *Am. J. Phys.*, vol. 25, no. 6, pp. 394–395, Sep. 1957, doi: 10.1119/1.1934486.
[82] S. Bagi, R. Bowker, and R. Andrew, "Understanding Chemical Composition and Phase Transitions of Ash from Field Returned DPF Units and Their Correlation with Filter Operating Conditions," *SAE Int. J. Fuels Lubr.*, vol. 9, no. 1, pp. 239–259, Apr. 2016, doi: 10.4271/2016-01-0898.
[83] A. Sappok and V. W. Wong, "Lubricant-Derived Ash Properties and Their Effects on Diesel Particulate Filter Pressure-Drop Performance," *J. Eng. Gas Turbines Power*, vol. 133, no. 3, Nov. 2010, doi: 10.1115/1.4001944.
[84] A. M. Dowaidar, M. S. El-Shahawi, and I. Ashour, "Adsorption of Polycyclic Aromatic Hydrocarbons onto Activated Carbon from Non-Aqueous Media: 1. The Influence of the Organic Solvent Polarity," *Sep. Sci. Technol.*, vol. 42, no. 16, pp. 3609–3622, Dec. 2007, doi: 10.1080/01496390701626537.
[85] V. K. Yadav, S. Prasad, D. K. Patel, A. H. Khan, M. Tripathi, and Y. Shukla, "Identification of polycyclic aromatic hydrocarbons in unleaded petrol and diesel exhaust emission," *Environ. Monit. Assess.*, vol. 168, no. 1, pp. 173–178, Sep. 2010, doi: 10.1007/s10661-009-1101-8.
[86] Voss, K.E., *"Catalytic Oxidation of Diesel Particulates with Base Metal Oxides", In: Frennet A. and Bastin J.M. (editors), "Catalysis and Automotive Pollution Control III."* Amsterdam: Elsevier, 1995.

Appendix A
Samples details

Table 0.1 Detailed operative condition of the samples, duration of the sampling and sample´s weight

Sample name	Description	Sample weight	Test duration
STD5	Engine´s durability cycle. The sample was collected on 2 filters, each collection time was of 3h.	9.84 mg (on filter) 1.07 mg (for TGA)	6h
900 rpm	Alternation of engine working at 900 rpm with full load and shout downs, every few seconds.	2.04 mg (on filter)	2h
1700 rpm	Alternation of engine working at 1700 rpm with full load and shout downs, every few seconds.	1.62 mg (on filter)	2h
2300 rpm	Alternation of engine working at 2300 rpm with full load and shout downs, every few seconds.	5.02 mg (on filter)	2h
Oil consumption	Engine´s oil consumption test. The sampling lasted 4h.	6.86 mg (on filter) 0.12 mg (for TGA)	4h
Pipe 5-cylinder	Scraped deposit from the silencer´s inlet.	-	Aged sample
Pipe V8	Scraped deposit from the silencer´s inlet. The sampling was performed 3 days after cleaning the section.	-	Soot was collected 3 days after performing a cleaning on that area
Pressure sweep 1h	Gradual decrease in speed from 1800 to 860 [rpm] in 1h.	1.01 mg (on filter) 3.49 mg (for TGA, PM+filter)	1h
Pressure sweep 2h	Gradual decrease in speed from 1800 to 860 [rpm] in 2h.	- 4.06 mg (for TGA, PM+filter)	2h

Pressure sweep (warm)	Gradual decrease in speed from 1800 to 860 [rpm] in 1h. The engine was already warm when the sample was collected.	0.86 mg (on filter) 3.92 mg (for TGA, PM+filter)	0.50 min
Pressure sweep (Teflon)	Same conditions of "Pressure sweep 1h" but collected on a Teflon filter.	1.01 mg (on filter) 0.17 mg (for TGA, scraped)	1h
Soot loading	Test at 1600 [rpm] and 600 [Nm] for 1h.	11.94 mg (on filter) 3.73 mg (for TGA, PM+filter)	1h
Soot regeneration	Test at 1800 [rpm] and full load.	2.22 mg (on filter) 3.56 mg (for TGA, PM+filter)	1h

Appendix B

Experimental cycles

For the sample STD5 the operative cycle was composed by an alternation between idling for 5 minutes and full load for 20 minutes at different engine speeds. The speed varied between 900 and 2400 rpm during the various phases and the entire cycle lasted approximately one hour.

For the sample oil consumption the operative cycle was composed by a long idling and then motoring phase. It ends with a slow load increase up to 100%. During the whole cycle the speed resulted below 1100 rpm.

For the samples 900 rpm, 1700 rpm and 2300 rpm, the cycles are described respectively in *Table 0.2*, *Table 0.3* and *Table 0.4*.

Table 0.2 Operative cycle performed during the collection of the sample "900 rpm", the cycle was performed 10 times

Time [s]	Engine speed [rpm]	Engine load
170	1000	No combustion
360	900	Full
10	900	No combustion

Table 0.3 Operative cycle performed during the collection of the sample "1700 rpm",the cycle was performed 10 times

Time [s]	Engine speed [rpm]	Engine load
170	1000	No combustion
360	1700	Full
10	900	No combustion

Table 0.4 Operative cycle performed during the collection of the sample "2300 rpm ",the cycle was performed 10 times

Time [s]	Engine speed [rpm]	Engine load
170	1000	No combustion
360	2300	Full
10	900	No combustion

Appendix C

Extraction procedure

The extraction procedure was performed on the samples STD5, 900 rpm, 1700 rpm, 2300 rpm and oil consumption in the laboratory. Preliminary analyses were conducted with different solvents such as water, methanol and isopropanol, with lower extraction rates. Each sample's filter was placed in a beaker containing approximately 20 mL of cyclohexane, for 10 minutes. The extraction process was assisted by manual handling of the filter with the aid of tweezers. At the end of the process, the filter was removed from the solution while the extraction liquid and the solid particles were transferred to a centrifuge for 5 minutes at 2500 rpm. Subsequently, the liquid was separated from the solid fraction that was then dried. Additional chromatograms are displayed in *Figure 0.1, Figure 0.2* and *Figure 0.3*.**Figure 0.3** Chromatograms of pure cyclohexane (1), STD5 (2), 900rpm (3), 1700rpm (4), 2300rpm (5) and oil consumption (6)

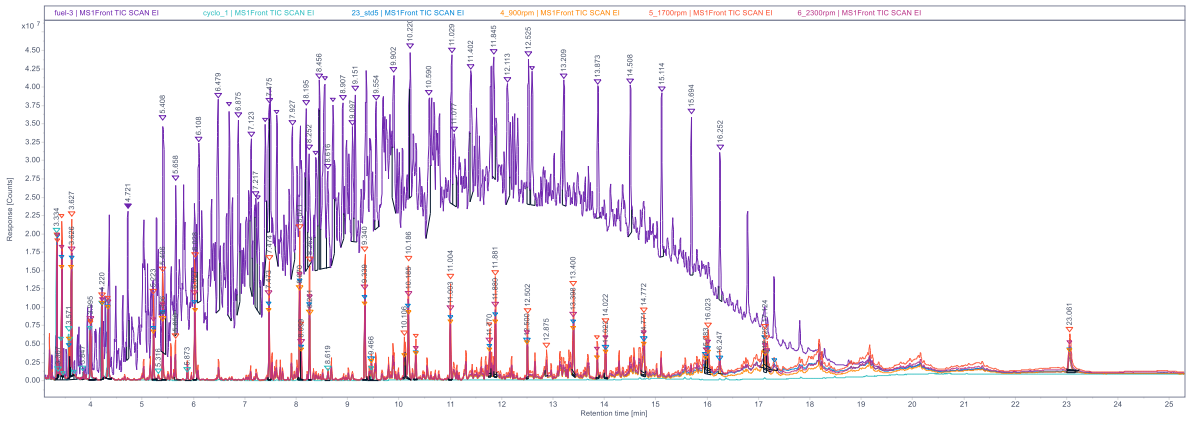

Figure 0.1 Comparison between the fuel B0 diluted in cyclohexane and the extracting solvent of the samples STD5, 900rpm,1700rpm and 2300rpm

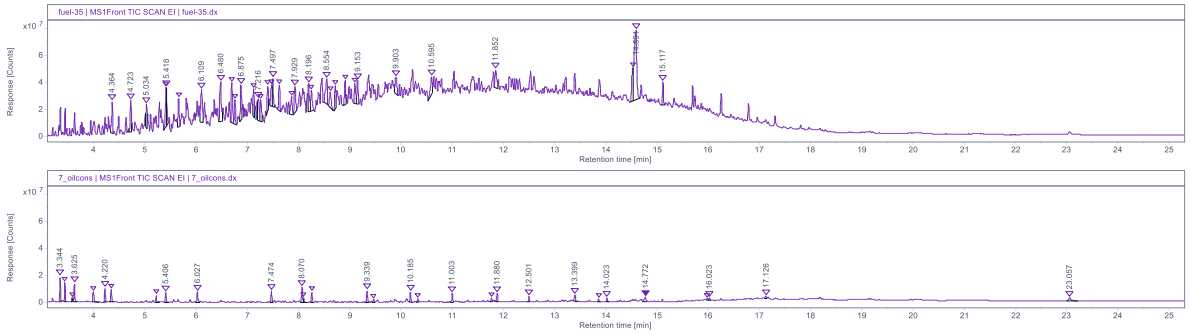

Figure 0.2 Comparison between the fuel B7 diluted in cyclohexane (top) and the extracting solvent of the sample oil consumption (bottom)

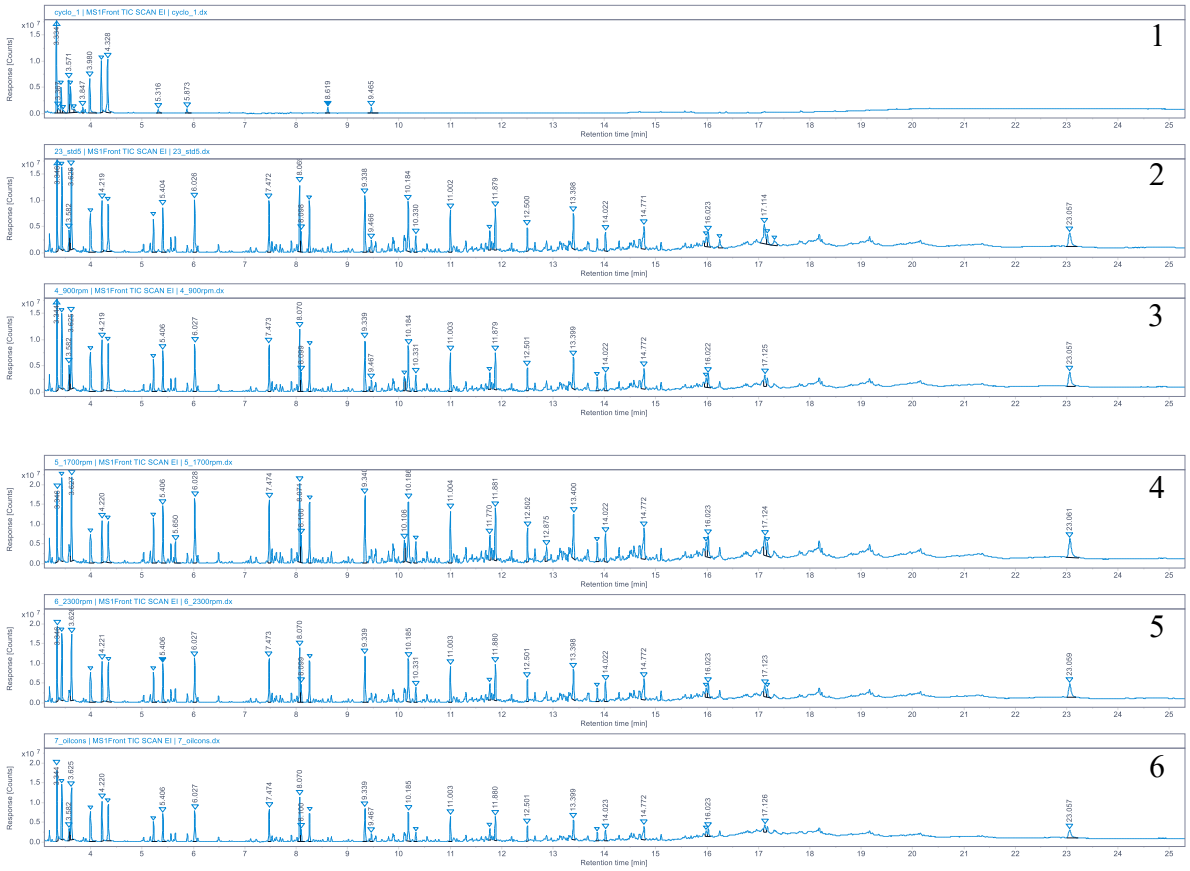

Figure 0.3 Chromatograms of pure cyclohexane (1), STD5 (2), 900rpm (3), 1700rpm (4), 2300rpm (5) and oil consumption (6)

Appendix D

SEM images

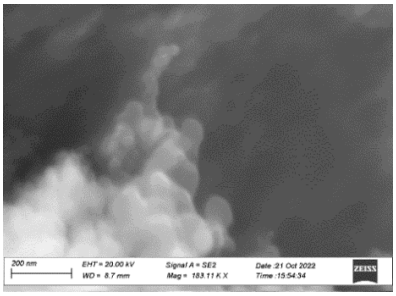

Figure 0.4 SEM image of soot of sample STD5

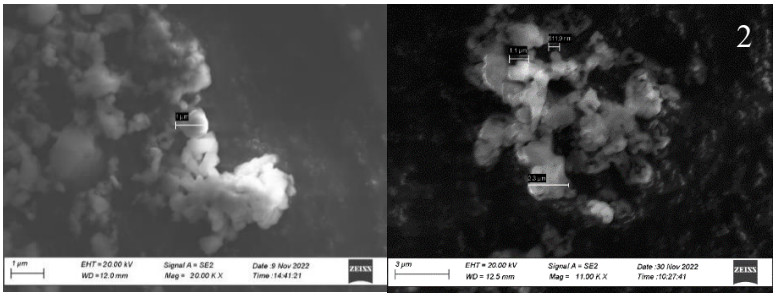

Figure 0.5 SEM images of ash of samples STD5 (1), oil consumption (2)

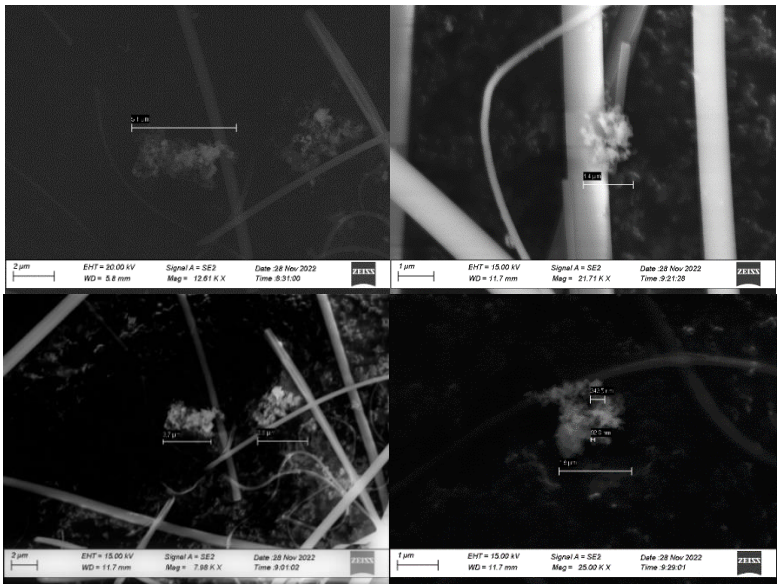

Figure 0.6 SEM images of ash of sample "pressure sweep", qualitative morphological analysis

Appendix E

Ash composition (detailed)

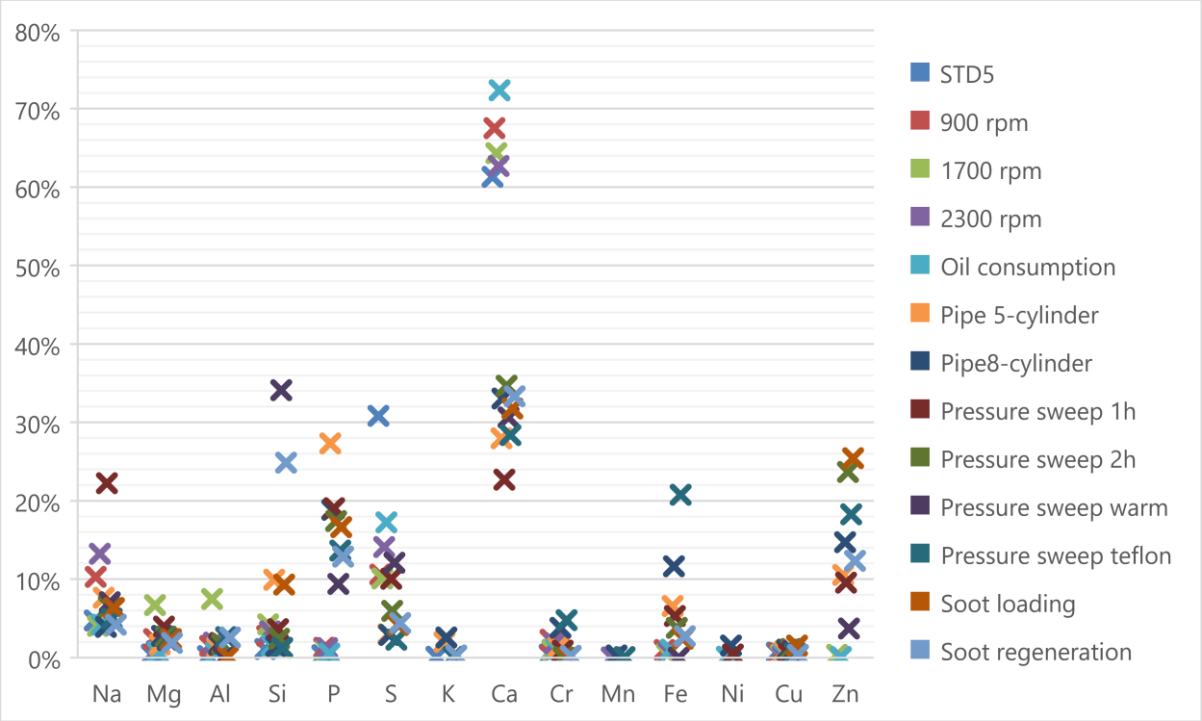

Figure 0.7 Detailed ash atomic composition [%] comparison for the tested samples, from the EDS results